



Michigan Technological University  
*Create the Future* Digital Commons @ Michigan Tech

---

Dissertations, Master's Theses and Master's  
Reports - Open

Dissertations, Master's Theses and Master's  
Reports

---

2011

## Graphite exfoliation by supercritical carbon dioxide extraction

Chaiyaporn Wattanaprayoon  
*Michigan Technological University*

Follow this and additional works at: <https://digitalcommons.mtu.edu/etds>

 Part of the [Chemical Engineering Commons](#)


Copyright 2011 Chaiyaporn Wattanaprayoon

---

### Recommended Citation

Wattanaprayoon, Chaiyaporn, "Graphite exfoliation by supercritical carbon dioxide extraction", Master's Thesis, Michigan Technological University, 2011.  
<https://doi.org/10.37099/mtu.dc.etds/8>

Follow this and additional works at: <https://digitalcommons.mtu.edu/etds>

 Part of the [Chemical Engineering Commons](#)

GRAPHITE EXFOLIATION BY SUPERCRITICAL  
CARBON DIOXIDE EXTRACTION

By  
Chaiyaporn Wattanaprayoon

A THESIS  
Submitted in partial fulfillment of the requirements for the degree of  
MASTER OF SCIENCE  
(Chemical Engineering)

MICHIGAN TECHNOLOGICAL UNIVERSITY  
2011

Copyright © Chaiyaporn Wattanaprayoon 2011

This thesis, “Graphite Exfoliation by Supercritical Carbon Dioxide Extraction,” is hereby approved in partial fulfillment of the requirements for the Degree of MASTER OF SCIENCE IN CHEMICAL ENGINEERING.

Department of Chemical Engineering

Signatures:

Thesis Advisor

\_\_\_\_\_  
Dr. Michael E. Mullins

Department Chair

\_\_\_\_\_  
Dr. Komar Kawatra

Date

\_\_\_\_\_

# Table of Contents

<b>List of Figures.....</b>	<b>v</b>
<b>List of Tables .....</b>	<b>viii</b>
<b>Acknowledgements .....</b>	<b>ix</b>
<b>Abstract.....</b>	<b>x</b>
<b>1. Introduction.....</b>	<b>1</b>
1.1 Graphite.....	1
1.2. Supercritical carbon dioxide .....	6
1.3. Graphene .....	7
1.3.1. Graphene synthesis .....	9
1.4. Other graphene synthesis methods.....	12
1.5. Co-solvents .....	17
<b>2. Hypothesis.....</b>	<b>18</b>
<b>3. Experiment .....</b>	<b>20</b>
3.1. Supercritical CO <sub>2</sub> extraction .....	20
3.2. Photon Correlation Spectroscopy (PCS).....	24
3.3. Brunauer, Emmett, and Teller (BET) analysis.....	26
3.4. Field Emission Scanning Electron Microscopy (FE-SEM) .....	27
3.5. Atomic Force Microscopy (AFM).....	28
<b>4. Results and Discussion.....</b>	<b>30</b>
4.1. Experimental conditions for Photon Correlation Spectroscopy (PCS).....	30
4.1.1. Effects of pressure and temperature of supercritical carbon dioxide (ScCO <sub>2</sub> ) on sizes and zeta potentials of graphitic flakes, using NMP as a co-solvent.....	31
4.1.2. Effects of sonication after supercritical carbon dioxide (ScCO <sub>2</sub> ) treatment on sizes and zeta potentials of graphitic flakes .....	40
4.1.3. Effects of co-solvents on sizes and zeta potentials of graphitic flakes .....	44
4.1.4. Effects of treatment times on sizes and zeta potentials of graphitic flakes ....	53
4.2. Brunauer, Emmett, and Teller (BET) analysis.....	56
4.3. FE-SEM images .....	65



4.3.1. FE-SEM images for the samples in N-methyl pyrrolidinone (NMP) without additional sonication .....	66
4.3.2. FE-SEM images for the samples in a one percent by weight solution of sodium dodecylbenzene sulfonate (SDBS) with additional one-hour sonication.....	70
4.4. AFM analysis .....	75
<b>5. Conclusion .....</b>	<b>84</b>
<b>6. Future work .....</b>	<b>86</b>
<b>References .....</b>	<b>87</b>
<b>Appendix A. PCS analysis .....</b>	<b>96</b>
A.1. Overall PCS data .....	97
A.2. Sonicated NMP-samples .....	100
A.3. Non-sonicated NMP-samples .....	104
A.4. DMF- and isopropanol-samples .....	108
A.5. Effect of treatment time on the obtained flakes .....	112
<b>Appendix B. BET analysis data .....</b>	<b>120</b>
<b>Appendix C. AFM section analysis .....</b>	<b>138</b>
C.1 Section analysis of the treated flakes at 60°C and 3000 psi .....	139
C.2 Section analysis of the treated flakes at 60°C and 2500 psi .....	141
D.3 Section analysis of the treated flakes at 60°C and 2000 psi .....	148

## List of Figures

Figure 1.1 Structure of Graphite .....	1
Figure 1.2 Synthetic graphite powder .....	2
Figure 1.3 Structures of carbon allotropes .....	8
Figure 2.1 Schematic of graphite exfoliation by supercritical carbon dioxide .....	19
Figure 3.1 The supercritical CO <sub>2</sub> extraction system .....	21
Figure 3.2 The supercritical CO <sub>2</sub> extractor .....	22
Figure 3.3 The 6-way valve diagram .....	22
Figure 3.4 The Zeta Nano Instrument (a) and the universal ‘dip’ cell (b).....	26
Figure 3.5 The ASAP 2020 analyzer .....	27
Figure 3.6 The Hitachi S-4700 FE-SEM .....	28
Figure 3.7 Veeco Dimension 3000 Atomic Force Microscope .....	29
Figure 4.1 Effect of temperature and pressure on diameter with sonication .....	32
Figure 4.2 Effect of temperature and pressure on diameter without sonication .....	33
Figure 4.3 Effect of temperature and pressure on z-average size with sonication .....	36
Figure 4.4 Effect of temperature and pressure on z-average size without sonication .....	36
Figure 4.5 Effect of temperature and pressure on zeta potential with sonication.....	38
Figure 4.6 Effect of temperature and pressure on zeta potential without sonication.....	38
Figure 4.7 Effect of sonication on diameter.....	41
Figure 4.8 Effect of sonication on z-average size.....	42
Figure 4.9 Effect of sonication on zeta potential .....	43
Figure 4.10 Effect of co-solvents on diameter with sonication .....	45
Figure 4.11 Effect of co-solvents on diameter without sonication .....	45
Figure 4.12 Effect of co-solvents on z-average size with sonication .....	47
Figure 4.13 Effect of co-solvents on z-average size without sonication .....	47
Figure 4.14 Effect of co-solvents on zeta potential with sonication.....	49
Figure 4.15 Effect of co-solvents on zeta potential without sonication.....	49
Figure 4.16 Effect of sonication on diameter with different co-solvent treated .....	51
Figure 4.17 Effect of sonication on z-average size with different co-solvent treated .....	51

Figure 4.18 Effect of sonication on zeta potential with different co-solvent treated.....	52
Figure 4.19 Effects of treatment time on diameter .....	54
Figure 4.20 Effects of treatment time on z-average size .....	54
Figure 4.21 Effects of treatment time on zeta potential.....	55
Figure 4.22 BET surface areas of various samples.....	58
Figure 4.23 BET plot with N <sub>2</sub> of different treated samples .....	58
Figure 4.24 BET plot with N <sub>2</sub> of different co-solvents treated samples .....	59
Figure 4.25 BET plot with N <sub>2</sub> and CO <sub>2</sub> of original and treated samples .....	59
Figure 4.26 BET isotherm linear plot with N <sub>2</sub> of different treated samples .....	63
Figure 4.27 BET isotherm linear plot with N <sub>2</sub> of different co-solvents treated samples ..	63
Figure 4.28 BET isotherm linear plot with N <sub>2</sub> and CO <sub>2</sub> of original and treated samples..	64
Figure 4.29 FE-SEM image of 60°C and 3000 psi treated sample in NMP .....	67
Figure 4.30 FE-SEM image of 60°C and 2500 psi treated sample in NMP .....	68
Figure 4.31 FE-SEM image of 60°C and 2000 psi treated sample in NMP .....	69
Figure 4.32 FE-SEM image of 60°C and 3000 psi treated sample in 1% SDBS .....	71
Figure 4.33 FE-SEM image of 60°C and 2500 psi treated sample in 1% SDBS .....	72
Figure 4.34 FE-SEM image of 60°C and 2000 psi treated sample in 1% SDBS .....	73
Figure 4.35 FE-SEM image of 40°C and 3000 psi treated sample in 1% SDBS .....	74
Figure 4.36 AFM 2D (a) and 3D image (b) of 60°C and 2000 psi treated sample.....	78
Figure 4.37 Horizontal (a) and vertical section analysis (b) of the flake 3.7.....	79
Figure 4.38 AFM 2D (a) and 3D image (b) of 60°C and 2000 psi treated sample.....	80
Figure 4.39 Horizontal (a) and vertical section analysis (b) of the flake 3.12.....	81
Figure A.1 PCS size of NMP-sample of 2000 psi, 60°C with sonication .....	100
Figure A.2 PCS zeta of NMP-sample of 2000 psi, 60°C with sonication .....	101
Figure A.3 PCS size of NMP-sample of 3000 psi, 40°C with sonication .....	102
Figure A.4 PCS zeta of NMP-sample of 3000 psi, 40°C with sonication. ....	103
Figure A.5 PCS size of NMP-sample of 2000 psi, 60°C without sonication .....	104
Figure A.6 PCS zeta of NMP-sample of 2000 psi, 60°C without sonication .....	105
Figure A.7 PCS size of NMP-sample of 3000 psi, 40°C without sonication .....	106
Figure A.8 PCS zeta of NMP-sample of 3000 psi, 40°C without sonication .....	107
Figure A.9 PCS size of DMF-sample of 3000 psi, 40°C with sonication .....	108

Figure A.10 PCS size of DMF-sample of 3000 psi, 40°C with sonication .....	109
Figure A.11 PCS size of isopropanol-sample of 3000 psi, 40°C with sonication .....	110
Figure A.12 PCS zeta of isopropanol-sample of 3000 psi, 40°C with sonication .....	111
Figure A.13 PCS size of 2-hour treated sample of 3000 psi, 60°C with sonication .....	112
Figure A.14 PCS zeta of 2-hour treated sample of 3000 psi, 60°C with sonication .....	113
Figure A.15 PCS size of 3-hour treated sample of 3000 psi, 60°C with sonication .....	114
Figure A.16 PCS zeta of 3-hour treated sample of 3000 psi, 60°C with sonication .....	115
Figure A.17 PCS size of 2-hour treated sample of 3000 psi, 60°C without sonication..	116
Figure A.18 PCS zeta of 2-hour treated sample of 3000 psi, 60°C without sonication .	117
Figure A.19 PCS size of 3-hour treated sample of 3000 psi, 60°C without sonication..	118
Figure A.20 PCS zeta of 3-hour treated sample of 3000 psi, 60°C without sonication .	119
Figure C.1 Horizontal (a) and vertical section analysis (b) of the flake 1.2 .....	139
Figure C.2 Horizontal (a) and vertical section analysis (b) of the flake 1.3 .....	140
Figure C.3 Horizontal (a) and vertical section analysis (b) of the flake 2.2 .....	141
Figure C.4 Horizontal (a) and vertical section analysis (b) of the flake 2.4 .....	142
Figure C.5 Horizontal (a) and vertical section analysis (b) of the flake 2.6 .....	143
Figure C.6 Horizontal (a) and vertical section analysis (b) of the flake 2.8 .....	144
Figure C.7 Horizontal (a) and vertical section analysis (b) of the flake 2.9 .....	145
Figure C.8 Horizontal (a) and vertical section analysis (b) of the flake 2.13 .....	146
Figure C.9 Horizontal (a) and vertical section analysis (b) of the flake 2.14 .....	147
Figure C.10 Vertical section analysis of the flake 3.1 (a) and 3.2 (b) .....	148
Figure C.11 Horizontal (a) and vertical section analysis (b) of the flake 3.3 .....	149
Figure C.12 Horizontal (a) and vertical section analysis (b) of the flake 3.8 .....	150
Figure C.13 Horizontal (a) and vertical section analysis (b) of the flake 3.9 .....	151
Figure C.14 Horizontal (a) and vertical section analysis (b) of the flake 3.11 .....	152
Figure C.15 Horizontal (a) and vertical section analysis (b) of the flake 3.12 .....	153

## List of Tables

Table 1.1 Interesting properties of graphite.....	4
Table 1.2 Critical temperature, pressure, and density of different fluids .....	6
Table 1.3 Properties of NMP, DMF, and isopropanol.....	17
Table 4.1 Matrix of experimental conditions for PCS analysis .....	31
Table 4.2 Effect of temperature and pressure on size and zeta potential.....	32
Table 4.3 Effect of co-solvents on size and zeta potential.....	44
Table 4.4 Effect of treatment time on size and zeta potential.....	53
Table 4.5 BET experimental analysis .....	57
Table 4.6 BET surface areas of various samples .....	57
Table 4.7 Experimental analysis for FE-SEM. ....	66
Table 4.8 Experimental analysis for AFM.....	76
Table 4.9 Horizontal and vertical sizes of the flakes from AFM analysis.....	77
Table A.1 Overall PCS data of flakes obtained from different treatment conditions.....	97
Table A.2 Overall PCS data of flakes obtained from different co-solvents treatment .....	98
Table A.3 Overall PCS data of flakes obtained from different treatment time .....	99
Table B.1 Data of $P/P_0$ and $1/[Q(P_0/P - 1)]$ of each sample .....	121
Table B.2 Data of $P/P_0$ and quantity absorbed (mmol/g) of each sample .....	124

## **Acknowledgements**

I would like to thank my fantastic advisor, Dr. Michael Mullins, who was involved in every part of in this thesis, for his persistent support. Also, I would like to give my thanks to Dr. David Chesney, who let me use the supercritical carbon dioxide extractor, fluorescent spectroscopy, and utilities in his lab; and provided technical instruction as well. In addition, I would like to say thank you to Dr. Bahne Cornilson for his help with Raman spectroscopy. Appreciation is extended to Dr. Tony Rogers, Dr. John Jaszczak, and Dr. Wenzhen Li for serving as my committee members. The last but not least, I would like to express my appreciation to Mr. Owen Mills, Ms. Cho Hui Lim, Ms. Qiaoyu Lu, and Ms. Wen Nee Yeo for their great collaboration in FE-SEM, PCS, and BET analysis. Besides, all friends and colleagues at Michigan Technological University deserve my thanks for their kindness and friendship. Finally, I would like to thank my family, including my fiancéé, for their great fulfillment and mental support that encouraged me to break through all of the obstacles. Above all, to his majesty the King Bhumibol Adulyadej of Thailand, who is the soul of our nation, for my inspiration and spiritual encouragement.

## Abstract

Supercritical carbon dioxide is used to exfoliate graphite, producing a small, several-layer graphitic flake. The supercritical conditions of 2000, 2500, and 3000 psi and temperatures of 40°, 50°, and 60°C, have been used to study the effect of critical density on the sizes and zeta potentials of the treated flakes. Photon Correlation Spectroscopy (PCS), Brunauer-Emmett-Teller (BET) surface area measurement, field emission scanning electron microscopy (FE-SEM), and atomic force microscopy (AFM) are used to observe the features of the flakes. N-methyl-2-pyrrolidinone (NMP), dimethylformamide (DMF), and isopropanol are used as co-solvents to enhance the supercritical carbon dioxide treatment. As a result, the PCS results show that the flakes obtained from high critical density treatment (low temperature and high pressure) are more stable due to more negative charges of zeta potential, but have smaller sizes than those from low critical density (high temperature and low pressure). However, when an additional 1-hour sonication is applied, the size of the flakes from low critical density treatment becomes smaller than those from high critical density treatment. This is probably due to more CO<sub>2</sub> molecules stacked between the layers of the graphitic flakes. The zeta potentials of the sonicated samples were slightly more negative than non-sonicated samples. NMP and DMF co-solvents maintain stability and prevented reaggregation of the flakes better than isopropanol. The flakes tend to be larger and more stable as the treatment time increases since larger flat area of graphite is exfoliated. In these experiments, the temperature has more impact on the flakes than pressure. The BET surface area results show that CO<sub>2</sub> penetrates the graphite layers more than N<sub>2</sub>. Moreover, the negative surface area of the treated graphite indicates that the CO<sub>2</sub> molecules may be adsorbed between the graphite layers during supercritical treatment. The FE-SEM and AFM images show that the flakes have various shapes and sizes. The effects of surfactants can be observed on the FE-SEM images of the samples in one percent by weight solution of SDBS in water since the sodium dodecylbenzene sulfonate (SDBS) residue covers all of the remaining flakes. The AFM images show that the vertical thickness of the graphitic flakes can range from several nanometers (less than ten layers

thick), to more than a hundred nanometers. In conclusion, supercritical carbon dioxide treatment is a promising step compared to mechanical and chemical exfoliation techniques in the large scale production of thin graphitic flake, breaking down the graphite flakes into flakes only a few graphene layers thick.



# 1. Introduction

## 1.1 Graphite

Graphite is a carbon allotrope which has a 3D-planar structure with a hexagonal (honeycomb) lattice structure in each plane<sup>1</sup>. Different from ideal graphene, which consists of a single layer sheet of carbon, graphite is a multi-layer carbon sheet with the distance between layers of approximately 0.335 nm<sup>2</sup>. In other words, graphite is a multi-layer carbon sheet which consists of many layers of graphene, a single-layer carbon sheet. These single sheets are held together by van der Waals forces which are weak enough to separate to some degree by simple mechanical exfoliation<sup>3</sup>. The structure of graphite and synthetic graphite powder from Aldrich Chemical Company, Inc. are shown in Figure 1.1 and 1.2, respectively.

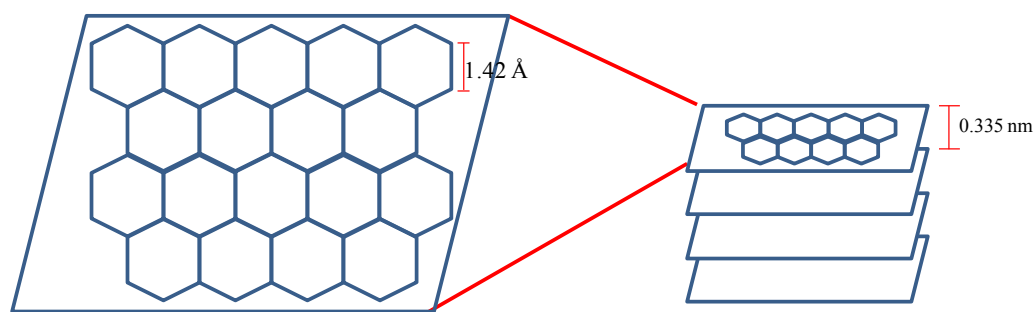


*Figure 1.1 Graphite is a multi-layer carbon material with 0.335 nm interlayer spacing. It consists of a single layer hexagonal planar of carbon (graphene) with 1.42 Å c-c bond distance (inspired by Geim et al.<sup>1</sup>).*

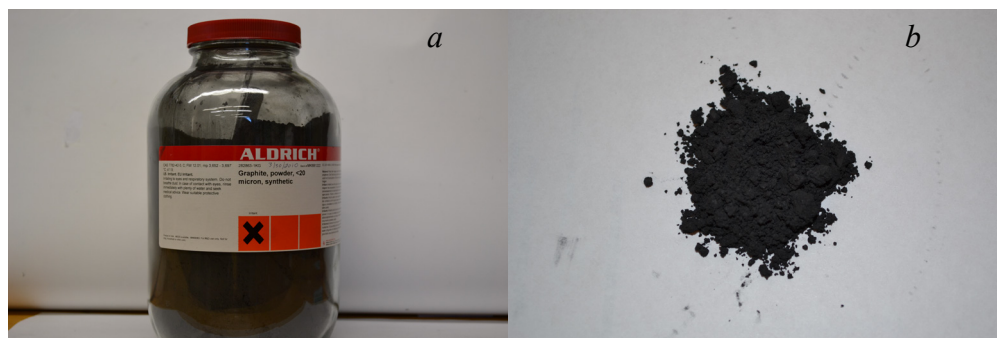


*Figure 1.2 The synthetic graphite powder with the size less than twenty microns from Aldrich Chemical Company, Inc (a,b), which is used in this experiment.*

Typically, graphite is black and soft, so it is applied in many ways such as pencil, coating, etc. It is one of the most stable substances due to its high melting point and resistance to acid and chemical reactions. In the world market, natural graphite is classified into three types that are used in different kinds of applications. Amorphous graphite (microcrystalline graphite) is created from the metamorphism of coal. Amorphous graphite is the finest of the graphite classes and is used in applications including lubrication, coatings, and high thermal shock resistance. Lump graphite (vein graphite) is a class of pure coarse-grained graphite that can be discovered as a part of metamorphic rocks. It is used in casting, batteries, powder metal industries, etc. The last class of natural graphite is crystalline flake graphite. This graphite occurs disseminated in the metamorphic rock, and occurs often less than the other classifications, making the price the highest. Its application is mostly in applications that require high performance and quality of graphite such as medical treatment, fuel cells, computer circuit, etc<sup>4</sup>.

Synthetic graphite can be made by from precursors of carbon such as petroleum coke, pitch coke, carbon black, coal tar-based cokes, etc. In the synthesizing process, these materials are mixed and heated at temperatures above 2500°C in the absence of oxygen conditions<sup>5</sup>. At a result, the carbon precursors are decomposed and crystallized as crystalline graphite. From this process, high purity synthetic graphite is produced. Eventually, crushing and ball milling processes are applied to control the size of the synthetic graphite powder<sup>6</sup>. The purity of synthetic graphite depends on the type of the raw materials and the purifying processes. With high-purity precursors, 99.9% pure

graphite can be made<sup>7</sup>. In this experiment, synthetic graphite powder from Aldrich Chemical Company, Inc.<sup>8</sup>, as shown in Figure 1.2, was used.

As mentioned previously, graphite is one of the most inert materials since it has a high melting point and high thermal and acid resistivity<sup>4</sup>. Moreover, other properties such as high thermal and electrical conductivity, high compressive strength, high resistance to erosion, corrosion from chemicals, low friction, etc., make graphite a versatile material which is applied in many fields. Some general properties are shown in Table 1.1<sup>9</sup>.

From Table 1.1, graphite is a  $sp^2$  carbon allotrope with 1.412 Å carbon distance. The electrical resistivities perpendicular to and parallel to c-axis are  $9.8 \times 10^{-6}$  and  $4.1 \times 10^{-5}$  ohm·m, respectively. The thermal conductivities (at 273K) perpendicular and parallel to c-axis are 250 and 80 W/m·K, respectively. The linear thermal expansion coefficient ( $\alpha$ ) of a-axis is 1.2, while that of c-axis is 25.9 at 293K. This coefficient increases when temperature increases (the overall value increases from 7.8 at 293K to 8.9 at 500K). The bulk modulus for a single crystal is 34 Gpa with the hardness approximately 1 to 2 in Mohs scale. Since it has a negative magnetic susceptibility, graphite is one of the strongest diamagnetic.

**Table 1.1**Some interesting properties of graphite<sup>9</sup>

Property		Reference
Formular	C	
Unit Cell	a=2.4612 Ang., c=6.7079 Ang.	
Crystal Class and Space Group	6/m 2/m 2/m and P6 <sub>3</sub> /mmc	
Formula Units per Unit Cell	trigonal planar (sp <sup>2</sup> )	
Bonding	with -C-C- 1.412 Ang.	
JCPDS	25-284 for 2H (26-1079 for 3R)	
Polymorphs	Diamond, Chaoite, Graphite 3R	
<b>Conductivity</b>		
<b><i>Electical Resistivity (ohm.m)</i></b>		
perpendicular to c-axis	9.8×10 <sup>-6</sup>	10
parallel to c-axis	4.1×10 <sup>-5</sup>	
natural	1.2×10 <sup>-6</sup>	
<b><i>Thermal (Watts/m·K at 273K)</i></b>		
perpendicular to c-axis	250	10
parallel to c-axis	80	
natural	160	
<b>Thermal</b>		
Linear Thermal Expansion	Coeff. Alpha(×10 <sup>-6</sup> K <sup>-1</sup> )	10
overall	7.8 (at 293K); 8.9 (at 500K)	
a-axis	-1.2 (at 293K); 0.7 (at 500K)	
c-axis	25.9 (at 293K); 28.2 (at 500K)	
<b>Optical</b>		
Bireflectance and reflection	o-vibration: higher reflectance and	11
pleochroism	yellow or brownish tint	
	e-vibration: bluish-grey tint	
<b>Mechanical</b>		
Bulk Modulus (single xtl)	34 Gpa	12,13
Bulk Modulus (polycrystal)	7.3-10.7 Gpa (non-irradiated, uncoated)	14
	2.5-7.3 Gpa (non-irradiated, coated)	
	14.0-16.9 Gpa (irradiated, uncoated)	
	7.8-8.4 Gpa (irradiated, coated)	
Mohs Hardness	1 to 2	
Specific Gravity	2.2	
<b>Magnetic</b>		
Magnetic Susceptibility	strongly diamagnetic	15
(pyrolitic)	-450×10 <sup>-6</sup> perpendicular to c-axis	
(pyrolitic)	-85×10 <sup>-6</sup> parallel to c-axis	
(rod)	-160×10 <sup>-6</sup>	

Graphite is normally used as a conductive substance in the cathode of alkaline batteries, due to its low electrical resistivity, and high resistance to heat and chemical corrosion<sup>7,8</sup>. Moreover, graphite layers can exchange lithium ions between themselves so it is also popularly used in rechargeable lithium-ion batteries<sup>7,8</sup>. Recently, graphene, a new allotrope of carbon, was introduced. In the case of electrical characteristics, the Dirac cones<sup>16</sup> are created due to the conduction and valence bands of graphene. This causes the other phenomena of graphene such as the abnormal quantum Hall effect (QHE) and nonzero Berry's phase, etc<sup>17</sup>. These phenomena make for unique properties of graphene, especially in electronics<sup>18</sup>. Due to high electron mobility (excess  $15,000 \text{ cm}^2\text{V}^{-1}\text{s}^{-1}$ )<sup>1</sup> and low resistivity ( $10^{-6} \text{ ohm}\cdot\text{m}$ <sup>19</sup>), less than silver, graphene is expected to replace graphite in electrode and battery applications.

Wang C et al.<sup>20</sup> studied the electrochemical properties of graphene paper electrodes used in lithium batteries. The graphene paper was made by chemical exfoliation<sup>3</sup>. As a result, the graphene paper could provide a discharge capacity of  $582 \text{ mA h g}^{-1}$  (to the cut off voltage of 2.0V), better than that of graphite ( $298 \text{ mA h g}^{-1}$ ), with a specific energy density of  $1162 \text{ W h kg}^{-1}$ . This points out that the graphene paper cathode and lithium anode battery has the potential to replace traditional graphite battery due to its higher performance. However, the performance of the graphene paper was decreased by the oxide group contained in the graphene paper due to the production method.

Due to the promising properties of graphene, especially in electrical energy storage<sup>21</sup>, many new synthesizing methods have been introduced. However, current production methods do not produce significant amounts of pure graphene<sup>3</sup>. Therefore, the motivation of this thesis is to synthesize high yields of few-layer graphenic materials without destroying its unique properties, for applications in electrodes and batteries applications.

## 1.2. Supercritical carbon dioxide

Supercritical is a condition that occurs when the temperature and pressure of the fluid are higher than its critical temperature and pressure, respectively. The point that the temperature and pressure of any fluid becomes supercritical is called the “critical point”. At this point, fluid that reaches its critical condition will show both gas and liquid properties at the same time. On the other hand, the critical fluid can show the ability to diffuse and dissolve like gas and liquid<sup>21,22</sup>. Moreover, the combination of gas and liquid properties, brings about a homogeneous fluid phase without surface tension between the two phases<sup>23</sup>. Therefore, critical fluid is applied in many applications, such as extraction, cleaning, dyeing, drying, refrigeration, deposition, etc. The critical properties of several substances are shown in Table 1.2<sup>24</sup>.

**Table 1.2**

Critical temperature, pressure, and density of different fluids<sup>24</sup>

Substance	Molecular Weight g/mol	Critical Temperature K (°C)	Critical Pressure MPa (psi)	Critical Density kg/m <sup>3</sup>
Carbon dioxide (CO <sub>2</sub> )	44.01	304.10 (30.95)	7.38 (1070.38)	469
Water (H <sub>2</sub> O)	18.015	647.10 (373.95)	22.06 (3200.11)	322
Methane (CH <sub>4</sub> )	16.04	190.40 (-82.75)	4.60 (667.17)	162
Ethane (C <sub>2</sub> H <sub>6</sub> )	30.07	305.30 (32.15)	4.87 (706.33)	203
Propane (C <sub>3</sub> H <sub>8</sub> )	44.09	369.80 (96.65)	4.25 (616.41)	217
Ethylene (C <sub>2</sub> H <sub>4</sub> )	28.05	282.40 (9.25)	5.04 (730.99)	215
Propylene (C <sub>3</sub> H <sub>6</sub> )	42.08	364.90 (91.75)	4.60 (667.17)	232
Methanol (CH <sub>3</sub> OH)	32.04	512.60 (239.45)	8.09 (1173.36)	272
Ethanol (C <sub>2</sub> H <sub>5</sub> OH)	46.07	513.90 (240.75)	6.14 (890.53)	276
NMP (C <sub>5</sub> H <sub>9</sub> NO) <sup>25</sup>	99.13 <sup>25</sup>	724.15 (451.00) <sup>26</sup>	4.52 (655.57) <sup>27</sup>	319 <sup>27</sup>
DMF (C <sub>3</sub> H <sub>7</sub> NO) <sup>28</sup>	73.09 <sup>28</sup>	922.75 (649.60) <sup>24</sup>	4.42 (641.07) <sup>24</sup>	279 <sup>29</sup>
Isopropanol (CH <sub>3</sub> ) <sub>2</sub> CHOH <sup>30</sup>	60.09 <sup>30</sup>	526.35 (253.20) <sup>31</sup>	4.76 (691.00) <sup>31</sup>	273 <sup>32</sup>

The solubility of chemicals in supercritical fluids is a function of the supercritical density. This density depends on temperature and pressure set to create the supercritical condition. Therefore, the solubility and the density can be altered by adjusting the temperature and pressure<sup>23</sup>.

Among supercritical fluids, supercritical CO<sub>2</sub> is one of the most commonly used because of its low critical pressure (7.38 MPa (1070.38 psi)), low critical temperature (304.1K (31°C)) and high solvating potential<sup>24</sup>. Moreover, CO<sub>2</sub> is abundant, and its low toxicity makes less impact on humans and the environment. For these reasons, supercritical CO<sub>2</sub> is a widely used fluid in many applications<sup>21,22,33</sup>.

### 1.3. Graphene

Carbon is one of the most common elements on the earth's surface. It exists in many forms in the environment due to different kinds of structures that it can form. In terms of crystallography, pure carbon has several interesting forms or allotropes. The allotropes are not only different in appearances, but also in properties. Diamond and graphite, for example, are carbon allotrope which have been familiar to humans for centuries. These allotropes are arranged in three-dimensions (3D). For the next generation, nanotubes and fullerene were introduced several decades ago (1990s). Their structures are one-dimensional (1D) and zero-dimensional (0D), respectively<sup>1,3</sup>.

Graphene is the most recently discovered carbon allotrope. Its structure is two-dimensional (2D) with aromatic lattices of carbon atom<sup>1</sup>. Since it is a two-dimensional structure (2D), it is only one carbon-atom thick, and with 1.42 Å for the carbon-bond distance<sup>1,34</sup>. Therefore, it appears like a carbon net that contains many hexagonal holes. This newly discovered material is present in graphite (the multi-layer carbon sheet) with the layer-layer distance approximately 0.335 nm<sup>2</sup>. However, this thickness can increase due to disorder such as rotation and twist of the layers<sup>34</sup>. The structures of graphene and other carbon allotropes are shown in figure 1.3<sup>1,3</sup>.

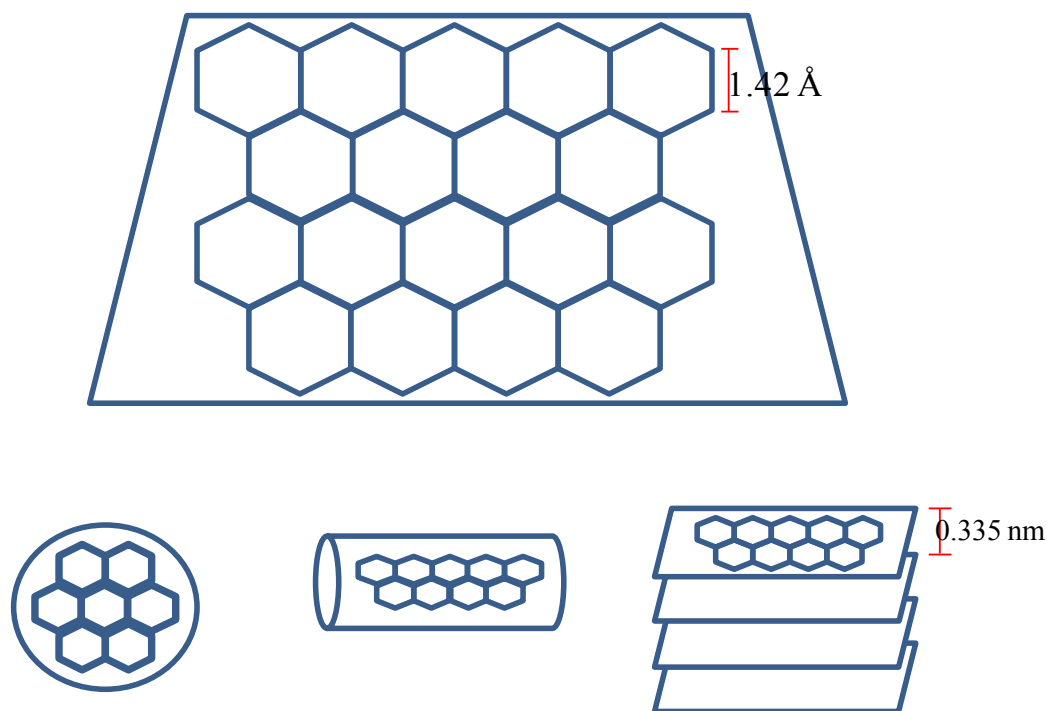


*Figure 1.3 Carbon structures of carbon allotrope (inspired by Geim et al.<sup>1</sup>). From the figure, graphene is a fundamental form of other allotropes.*

As a 2D structure, graphene is theoretically expected to have many excellent properties in terms of electronics<sup>35</sup>, mechanics<sup>36</sup>, thermals<sup>37</sup>, etc. Consequently, many scientists try to study and discover its properties as well as utilize this promising material for many applications such as transistors<sup>38,39</sup>, electrodes<sup>40</sup>, ultracapacitors<sup>41</sup>, biodevices<sup>42,43</sup>, etc. However, the biggest challenge is its production in commercially useful quantities and preservation of high quality. Current production methods do not produce pure graphene, are slow, and have poor yields or high disorder. Moreover, they often degrade some of the properties that pure graphene is expected to have<sup>3</sup>.

Theoretically, the melting point of any substance decreases dramatically when the thickness of that substance decreases. Therefore, a one-atom thick plane or the two-dimensional material might be unable to exist<sup>1</sup>. Moreover, scientists such as Landau<sup>44</sup> and Peierls<sup>45</sup> stated 70 years ago that a 2D material could not be stable due to thermal fluctuations. Therefore, the 2D plane was only known as a basic part of 3D material. This belief continued until the success of Aundrey Geim and his colleague, Konstantin Novoselov, at the University of Manchester, in extracting the 2D graphene from 3D



graphite by a “Scotch tape method”<sup>38,46</sup>. Together they won the Nobel Prize in Physics in 2010 for this discovery.

The “Scotch tape method” is the simplest way to extract the 2D material or graphene. Since the graphite layers are held together by weak van der Waals forces, the force which is required to separate (exfoliate) the graphite layers is around  $300 \text{ nN}/\mu\text{m}^2$ <sup>3,47</sup>. This intensity of force could be easily achieved by a mechanical exfoliation or Scotch tape method as mentioned above. Geim and Nevoselov utilized this method by sticking the tape to graphite flakes and peeling the tape multiple times<sup>38,46</sup>. After observing by optical microscopy, they placed the residuals on the oxidized silicon wafer ( $\text{SiO}_2$ ) by lightly applying and removing the peeled tape. The residuals were examined by optical microscopy. This shows graphene-silicon interaction which leads to different contrast in terms of different flake colors. Since then, several other methods of synthesizing graphene have been introduced. They are discussed further in the next sections.

### **1.3.1. Graphene synthesis**

Mechanical exfoliation or the “Scotch tape method” can synthesize graphene<sup>38,46</sup>, but it is not suitable for large scale production. Moreover, the quality of the graphene from this method is highly variable. Therefore, researchers have been trying to find a way to produce graphene precisely and productively<sup>3</sup>. New methods have been introduced, several of which are very promising are mentioned.

#### **1.3.1.1. Growth of graphene**

Graphene can be grown in metals and carbide substrates. The one method is chemical vapor decomposition (CVD) which is a technique used to produce a thin film on a substrate<sup>3,48,49</sup>. In this technique, a substrate is exposed to a vapor or volatile substrate which can react with or attach on the substrate itself. As a result, a thin film is created. Another technique is using heat to decompose metal and carbide substrates. For both techniques, substrates and growth conditions are specified for the graphene production.

Kim KS et al.<sup>16</sup> tested the electronic properties of graphene synthesized by CVD on nickel substrate with 300 nm thickness. SEM, TEM, Raman spectroscopy, and AFM were used to characterize the graphene. As a result, the grown graphene had very low resistance between the layers (approximately 280 ohm per unit area), high yield transparent layers (approximately eighty percent yield), and high electron mobility (more than  $3,700 \text{ cm}^2\text{V}^{-1}\text{s}^{-1}$ ). Moreover, the electron mobility was almost identical with that of graphene from mechanical exfoliation. Therefore, CVD is a good method to synthesize graphene which can preserve the electronic properties for electrode applications.

Lee Y et al.<sup>49</sup> produced large flakes of graphene by transferring graphene to a polymer substrate. This graphene was produced by CVD on a metal substrate, such as Ni or Cu. Then, an etching process by  $\text{FeCl}_3$  was applied to remove the metal layer before transferring it to the polymer substrate. This method reduced the limits of the metal substrate on size of the growth graphene by CVD. As a result, a 3-in graphene film was created with high electron mobilities.

Shi Y et al.<sup>50</sup> tested electrode properties of graphene which were synthesized by chemical vapor deposition (CVD). The chemical doping of graphene covered by metal ions such as Au, was tested and compared with traditional graphene (without chemical doping). In this way, graphene was grown as a film and dispersed into  $\text{AuCl}_3$  solution. Then, the Au particle would cover the graphene surface due to surface interactions with the metal ions. This phenomenon maintained the stability of the graphene film. As a result, a maximum power conversion efficiency (PCE) reached 0.08 percent which was forty times greater than that without chemical doping.

Although grown graphene has a high quality structure compared with pure graphene, this method still has some disadvantages. By interaction with the substrate, grown graphene has a carrier mobility five times less than that of pure graphene<sup>3</sup>. Moreover, the lateral size is limited due to this substrate interaction<sup>3</sup>. Therefore, additional methods are required to improve the properties of this growth<sup>34</sup>. Nickel is the best substrate to increase the lateral size of grown graphene<sup>3</sup>. This substrate can dissolve in hydrochloric acid

solution so the deposited graphene is transferred from the metal substrate to a polymer covering<sup>16,51,52</sup>. A polymer film is formed at this point. With this technique, the lateral size of grown graphene depends on the crystal size of the nickel substrate. Moreover, the mobility is doubled compared to traditionally grown graphene<sup>53,54</sup>. In conclusion, these methods make a high quality graphene, however, special conditions are required, which means additional cost. Grown graphene is suitable for high performance applications that need high quality graphene<sup>3</sup>.

### **1.3.1.2. Graphene oxide**

Another method of producing graphene is “chemical exfoliation”. The key is to oxidize a graphite layer using chemical substances<sup>3,53,54</sup>. Since the graphite layers are connected to each other by a weak van der Waals force, this oxidation exfoliates a single sheet in the form of graphene oxide<sup>3</sup>. Graphite, sodium nitrate, and sulfuric acid are mixed together in an ice bath, and then potassium permanganate is slowly added. The reaction is stirred at room temperature for an hour. Then, water is added and the temperature is set at 45°C. The reaction is continued for another half an hour. Next, hydrogen peroxide and additional water are added slowly. Finally, the mixture is filtered and washed until a pH of six is reached. The graphite oxide is separated out at this point<sup>40</sup>. It remains stable for around six months. To exfoliate a single sheet, a thermal treatment is applied to produce CO<sub>2</sub> between layers. This inter-generated CO<sub>2</sub> will expand the graphite layer. Then, the single layer graphite oxide sheet (graphene oxide) is exfoliated. Typically, the temperature that is used to generate the CO<sub>2</sub> is 1050°C (with a heating rate of more than 200°C/min). To obtain good quality graphene oxide flake, the additional treatment such as sonication may be required<sup>55</sup>.

However, due to the effects of the chemical treatment, the obtained graphene oxide loses some of its desirable properties compared with that of graphene from mechanical exfoliation. The structure of graphite is changed dramatically during the chemical reactions<sup>56,57</sup>. Moreover, the chemicals can revert the single layer (graphene) into the multi-layers (graphite). Therefore, to restore the properties, additional treatments, such as

hydrazine vapors ( $\text{NH}_2\text{-NH}_2$ ) or hydrogen plasma, are required to change the product from graphene oxide to graphene, making the process more complex and expensive<sup>58,59</sup>. Moreover, the identification of graphene oxide in graphene is still problematic in the final product.

#### **1.4. Other graphene synthesis methods**

Jiang et al.<sup>17</sup> studied the electronic properties of graphene using infrared spectroscopy. In the case of electrical characteristics of graphene, the Dirac cones<sup>16</sup> are created due to the conduction and valence bands of graphene. This causes the other electrical phenomena of graphene, such as the abnormal quantum Hall effect (QHE) and nonzero Berry's phase, etc. The infrared spectroscopy together with a magnetic field can reveal the Landau Level (LL) spectrum of graphene. In this task, the magnetic field was set at 6 Tesla, 12.1 Tesla, and 18 Tesla. As a result, the transition energies were approximately equal to the square root of the magnetic field. Moreover, the LL transitions were shown to result with no exact pattern among different transitions. This was because of the effects of a large amount of the observed particles.

Pu NW et al.<sup>21</sup> exfoliated graphene sheets from graphite powder using a supercritical  $\text{CO}_2$  technique. The natural graphite powder was put into the cell and the supercritical  $\text{CO}_2$  was set to flow through the cell for thirty minutes. The products were collected by passing the output  $\text{CO}_2$  gas into water with sodium dodecyl sulfate (SDS) surfactant to prevent reaggregating of the expanded sheets. Transmission electron microscopy (TEM), atomic force microscopy (AFM), field-emission scanning electron microscopy (FESEM) were used to observe the products and showed that multi layers graphenic materials (~10 layers) were produced.

Malesevic A et al.<sup>48</sup> synthesized graphene using the microwave plasma-enhanced chemical vapor deposition technique. The obtained graphenes were observed by electron microscopy, x-ray diffraction, Raman spectroscopy and scanning tunneling microscopy.

As a result, the flakes which were approximately six-layer thick, appear in a vertical direction, perpendicular to the substrate surface.

Shen J et al.<sup>53</sup> synthesized graphene from graphene oxide. First, the reaction between graphite and benzoyl peroxide (BPO) was used to produce graphene oxide. Then, the graphene oxide sheet was converted to graphene using its *in situ* reduction. CO<sub>2</sub> was also used to expand the distance between graphite layers. Thermogravimetric analysis, Raman spectroscopy, and Fourier transform infrared spectroscopy showed the completion of graphene oxide production. TEM and AFM were used to compare graphene oxide with obtained graphene (from graphene oxide) in a final state. The result showed that the graphene oxide with a single layer could be produced by this technique.

Wu ZS et al.<sup>54</sup> studied the effect of the lateral size and the crystallinity of the graphite, which was used as a reactant on the graphene product. Graphene oxide, also referred to as chemical exfoliation mean, was used to synthesize the graphene. Four kinds of graphite which were artificial graphite, flake graphite powder, Kish graphite, and natural flake graphite were used as reactants. As a result, the highest yield of monolayer graphenes was produced when artificial graphite was used as a reactant. These graphenes also were found to have high quality and electrical conductivity ( $\sim 1 \times 10^3$  S/cm).

Lotya M et al.<sup>60</sup> made graphene by dispersing graphite in a water-based surfactant (sodium dodecylbenzene sulfonate (SDBS)). The solution was sonicated for thirty minutes in a sonication bath. Transmission electron microscopy, atomic-resolution TEM, Raman and IR spectroanalysis, and X-ray photoelectron spectroscopy were used to examine the product. Moreover, the stability of the exfoliated flake was also observed in terms of Coulomb repulsion. As a result, more than forty percent of the product had less than five layers (approximately three percent were monolayer). Those flakes lacked any defects and oxides with high stability and had a semitransparent appearance.

Ferrari AC et al.<sup>61</sup> studied the Raman spectra of graphene which was influenced by its number of layers. The increasing number of layers affected the topography (shape and

size) of the flake. This also affected the D peak second order (2D) in the Raman spectrum of graphene because of double resonance in the Raman process. The G peak, which was slightly changed, represented no defect or impurity in the graphene flakes.

Rangappa D et al.<sup>62</sup> exfoliated graphene using the supercritical fluid exfoliation method of graphite crystals. N-methyl-pyrrolidone (NMP), dimethylformamide (DMF), and ethanol were used as supercritical solvents due to their high solubilities. In preparation, graphite crystals were dispersed in the solutions and sonicated for ten minutes. Then, the sonicated crystals were put into the pressure vessel and the supercritical conditions were set within 300-400 °C and 38-40 MPa for 15-60 minutes. The process was completed after the vessel was placed in an ice bath. The collection was done by removing the residues, washing and centrifuging them, then drying them overnight in a vacuum oven at 100 °C. Raman spectroscopy, high resolution transmission electron microscopy (HR-TEM), AFM, and X-ray diffraction (XRD) were used to characterize the obtained flakes. Most of the flakes (ninety to ninety five percent) were found to be less than eight layers. Moreover, monolayer flakes were found approximately comprise six to ten percent.

Woods HM et al.<sup>63</sup> studied materials under supercritical carbon dioxide. The study was separated into three tasks: applied surfactant in the supercritical CO<sub>2</sub> as a new material synthesizing method, the effect of the supercritical CO<sub>2</sub> on polymer processing, and the supercritical CO<sub>2</sub> in biomedical applications. In conclusion, the supercritical CO<sub>2</sub> was an effective tool to create a new interesting feature and property of the product, which was hard to reveal from other means.

Kaschak DM et al.<sup>64</sup> expanded graphite using oxidizing solutions which were nitric acid based. Moreover, additional treatment by supercritical water, carbon dioxide, and helium was used to exfoliate graphite. The conditions below supercritical and near supercritical for each fluid were also examined. As a result, the graphite flakes with fifty micron thickness were created. This might be due to the reaggregation of a few layers of the graphite flakes.

Green AA and Hersam MC<sup>65</sup> made graphene using solution dispersion and controlled the thickness using gradient ultracentrifugation (DGU). This method began by dispersing graphite in sodium cholate surfactant, which was amphiphilic. Then, horn ultrasonication was used to exfoliate the graphene flakes. These exfoliated flakes were stable because of the amphiphilic molecules of sodium cholate that covered the surface area of the flakes. Then, the solution was centrifuged by gradient ultracentrifugation to separate the desired thickness of the graphene flakes due to different density. The separated graphene flakes were placed on a SiO<sub>2</sub> substrate for AFM and Raman spectroscopy observation. As a result, different shades of density occurred in the centrifuge tube. These shades contained different thicknesses of graphene flakes. The shade became darker as the thickness (density) of the contained flakes increased.

Ghosh A et al.<sup>66</sup> measured H<sub>2</sub> and CO<sub>2</sub> adsorption of graphene at 1 atm with 77 and 195 K, respectively, using a Quantacrome instrument. The surface areas of graphene were also measured by using Brunauer-Emmett-Teller (BET). The graphenes were prepared from the method of graphene oxide<sup>29,30</sup> and nanodiamond transformation<sup>30,31</sup>. As a result, the H<sub>2</sub> adsorption of graphene was 1.7 weight percent while the CO<sub>2</sub> adsorption was 35 weight percent. Moreover, for the single layer graphene the H<sub>2</sub> adsorption was more than three weight percent and might be approximately 7.7 weight percent. These adsorptions changed proportionally with the surface areas, but inversely with the number of layers.

Behabtu N et al.<sup>67</sup> studied the graphite dispersion in chlorosulphonic acid with 2 mg-carbon/mL-acid concentration. From this method, graphite was exfoliated to single layer graphene without additional treatments or solvents to produce single layer flakes, recovered some properties of the flakes, and maintained the stability of those flakes. Three kinds of graphite (expanded, microcrystalline, and highly ordered pyrolytic) were compared with each other. Raman spectroscopy, TEM and HR-TEM, X-ray photoelectron microscopy (XPS), and AFM were used to examine the obtained graphene. As a result, the liquid-phase graphene was produced with a concentration of approximately 20-30 mg/L. Moreover, eighty percent of the crystalline flakes were transparent.

Subrahmanyam KS et al.<sup>68</sup> studied and compared the characteristics of graphene which were synthesized from different methods. Graphene produced from pyrolysis of camphor, graphitic oxide exfoliation, and conversion of nanodiamond, were used in this task. X-ray diffraction (XRD), TEM, AFM, Raman spectroscopy, magnetic measurement, and Brunauer-Emmett-Teller (BET) were used to characterize the obtained graphenes. As a result, exfoliated graphene showed the smallest size, the least number of layers, and the best crystalline graphene with minimum defects. Moreover, it also showed the highest surface area and the highest weight percent of hydrogen and carbon dioxide adsorptions.

Kozhemyakina NV et al.<sup>69</sup> studied the electronic characteristics of graphene-perylen bisimide (PBI) interaction in N-methylpyrrolidone (NMP). The graphene was made by dispersion of turbostratic graphite in NMP. The solution was stirred for five days and then centrifuged to separate single-layer and few-layer graphene. Perylene bisimide was also dispersed in NMP. To study the interaction of these two materials (graphene and perylene bisimide), the sample was prepared by dropping both dispersed solutions on a silicon substrate with 300 nm SiO<sub>2</sub> coating. Raman spectroscopy and fluorescence spectroscopy were used after evaporation of the solvent. As a result, the Raman spectra of graphene at 532 nm excitation was interfered by those of perylene bisimide, although the D-band, 2D-band, and G-band were still seen. However, the spectra at 633 nm showed graphene-like spectra, since perylene bisimide was not activated by this wavelength. As for fluorescent spectroscopy, both graphene and bisimide were fluoresced by green light (545 nm wavelength) and emitted from 605 nm. Graphene showed a blue contrast while perylene bisimide showed various colors (red, yellow, and light blue) in the fluorescent micrograph.

Li Q et al.<sup>70</sup> studied the solubility of 2-naphthol and anthracene in supercritical CO<sub>2</sub>. Acetone, ethanol, and cyclohexane were used as co-solvents. The process was run at temperatures between 308.1 K and 328.1 K, and pressures between 10 MPa and 30 MPa. The solubility of both solid materials was measured by making equilibrium flow between



two phases (fluid and solid), and applying the gravimetric analysis method. As a result, when the temperature or pressure increased, the solubility of both solids was increased. Moreover, the non-polar co-solvent (cyclohexane) could increase the solubility of both materials in supercritical CO<sub>2</sub> better than the polar solvent (ethanol and acetone) could do.

## 1.5. Co-solvents

Due to lack of polarity of the supercritical carbon dioxide, co-solvents are used to increase its polarity. This increases the solubility power of the supercritical carbon dioxide<sup>70</sup>. Moreover, another function of co-solvent is to make more comfortable and effective way in collecting the samples since the treated flakes are dispersed in exiting drops of co-solvent. In this experiment, three solvents, N-methyl pyrrolidinone (NMP), dimethylformamide (DMF), and isopropanol, were used as co-solvents. Some of the properties are shown in Table 1.3.

**Table 1.3**

Some properties of N-methyl pyrrolidinone (NMP), dimethylformamide (DMF), and isopropanol.

Solvent	NMP <sup>71</sup>	DMF <sup>28</sup>	Isopropanol <sup>30</sup>
Formular	C <sub>5</sub> H <sub>9</sub> NO	C <sub>3</sub> H <sub>7</sub> NO	(CH <sub>3</sub> ) <sub>2</sub> CHOH
Molecular Weight (g/mol)	99.13	73.09	60.09 <sup>26</sup>
pH	7.7 to 8.0	6.0 to 8.0	N/A
Vapor Pressure (×10 <sup>-5</sup> MPa at 293.15K)	0.29-0.32	3.68	33.00
Melting Point (K(°C))	249.15(-24)	212.15(-61)	184.15(-89)
Boiling Point (K(°C))	457.15(202)	426.15(153)	355.45(82.3)
Critical Temperature (K(°C))	724.15(451.00) <sup>26</sup>	922.75(649.60) <sup>24</sup>	526.35(253.20) <sup>31</sup>
Critical Pressure (MPa(psi))	4.52(555.57) <sup>27</sup>	4.42(641.07) <sup>24</sup>	7.76(691.00) <sup>31</sup>
Dielectric constant (at 293.15°C)	33 <sup>72</sup>	36.7 <sup>73</sup>	19.26 <sup>74</sup>

## 2. Hypothesis

Graphite is a carbon allotrope that is a multi-layer stacking of hexagonal network planes<sup>1</sup>. The distance between carbon atoms in the same plane is 1.42 Å<sup>34</sup>. In other words, graphite consists of a single-atom-layer material (graphene) attached together by a van der Waals force that is weak enough to allow graphite to be exfoliated by normal method, such as pressing and peeling an adhesive tape (Scotch tape method)<sup>1,3</sup>. However, the percent yield is the main problem of a few-layer production<sup>3</sup>. Other methods, such as chemical vapor deposition (CVD) and thermal decomposition of metal on carbide substrate<sup>3,48,49</sup>, and chemical exfoliation<sup>3,53,54,55</sup>, are also invented by many groups of people as mentioned previously. However, those methods also bring about some unfavorable results of the product, such as the lack of some properties, defects, etc., due to chemical interactions and treatment of the process<sup>3</sup>. Therefore, more processes are required to recover those loosen properties<sup>3</sup>. This means more time, labors, and funds are consumed in the production. At this point, supercritical CO<sub>2</sub> is considered as a promising way to exfoliate graphite.

As mentioned previously, the distance between layers is approximately 0.335 nm, but can be increased due to rotation and twisting of the layers<sup>2,3</sup>. As for the carbon dioxide, the vertically molecular size of carbon dioxide is approximately 0.33 nm<sup>75</sup>. Moreover, due to the high kinetic energy of carbon dioxide and its polarizability, carbon dioxide has the potential to pass between the graphite layers since its molecular size is approximately smaller than the layer-layer distance<sup>76</sup>. In addition, when the supercritical condition is applied, the diffusivity and dissolvability of the fluid are enhanced<sup>36</sup>. Together with added co-solvents (N-methylpyrrolidone, dimethylformamide, and isopropanol), which can increase the polarity and the fluid-solid interaction<sup>36</sup>, the graphite layers are expected to be expanded and exfoliated at this point. The exfoliated pieces will come out with the output fluid and can be collected in a u-tube. In conclusion, supercritical carbon dioxide might be an effective and productive method to synthesize a few-layer graphenic material via the exfoliation of graphite. A schematic of this hypothesis is shown in Figure 2.1.

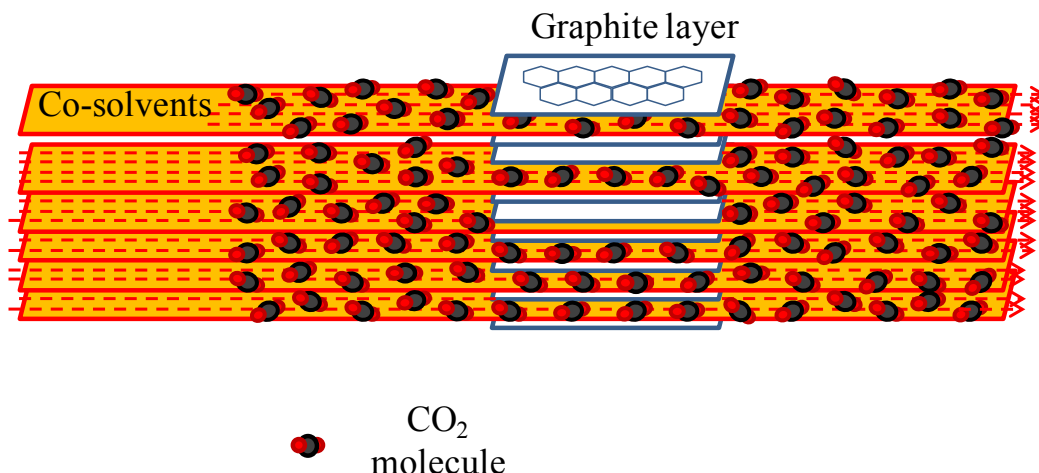


*Figure 2.1 A schematic of graphite exfoliation by supercritical carbon dioxide. The carbon dioxide molecule is small enough to pass through the layer-layer space of graphite. Moreover, the supercritical condition increases the diffusivity and dissolvability of the fluid. Co-solvents are used to increase the polarity of the supercritical carbon dioxide and the interaction between fluid and solid phase. A few-layer graphite is expected to exfoliated at this point.*

From Figure 2.1, when graphite is treated by supercritical carbon dioxide, its layers are expanded because of carbon dioxide molecules that pass between the graphite layers. Co-solvents are injected to maintain the expanded distances between the graphite layers. The graphite layers are also exfoliated into smaller flat pieces under the supercritical treatment. The degree of exfoliation depends on the supercritical density of the treatment. In other words, higher supercritical density treatment can exfoliate and break down the graphite layers into smaller sizes while lower supercritical density treatment cannot exfoliate and break down the graphite layers as completely as higher supercritical density treatment. Instead, it expands the graphite layers which loose the force held between the layers.

### 3. Experiment

#### 3.1. Supercritical CO<sub>2</sub> extraction

The supercritical CO<sub>2</sub> extractor system consists of a pump, a pressure cell, a heating unit, and a release valve. The procedure begins when the carbon dioxide, which is stored as a liquid in a cylinder tank, is pumped into the extraction cell with a high-pressure syringe pump. In this tube, the supercritical pressure is set by the pump. Then, this CO<sub>2</sub> is released to the pressure cell which contains the material or substance that is to be extracted. The pressure cell is a cylindrical stainless steel tube with two hexagonal stainless steel caps. The inner diameter of the tube is 1 cm and the outer diameter is 1.2 cm. The length of the tube including caps is 12.2 cm. The volume is approximately 9.582 cm<sup>3</sup>. It can contain approximately 2.8 grams of graphite powder (without applying force). This cell is placed in the controlled temperature oven, and set to the desired supercritical temperature. The supercritical conditions are held until the extraction process is complete, which is normally ten to sixty minutes, depending on the extracted material. The sample is collected into a collection vessel, often a glass U-tube by opening the needle valve at the extraction cell exit, and reducing the pressure to subcritical levels. The supercritical CO<sub>2</sub> flashes into a gas and passes through the tube, whereas the co-solvent and graphenic materials are condensed and collected. This collection method is very effective in collecting fine shape and small piece of products since the pressure cell has 0.5 micron filters at end each. Therefore, large and rough pieces are filtered out. Moreover, the U-tube can collect pieces which come out with the fluid, along with the co-solvent because it creates a phase separation between the supercritical fluid and co-solvent. The released CO<sub>2</sub> gas will flow in to the U-tube and flow out of the other side, while the co-solvent stays in the curve of the tube. The extracted material, which comes out with the supercritical fluid, will be collected in the liquid phase of co-solvent. The flow of the outlet is controlled by a release valve (needle valve). The schematic of the supercritical CO<sub>2</sub> system and a photo of the supercritical CO<sub>2</sub> extractor (Varian Aerograph Series 1400) used in this experiment are shown in Figure 3.1 and 3.2, respectively.

Co-solvent can be injected into the pressure cell using a 6-way valve system which can be rotated to select the path of injection to the pressure cell. Once the path is changed from CO<sub>2</sub> to co-solvent, the co-solvent is injected into the pressure cell before shifting back to the CO<sub>2</sub>. It is necessary to momentarily reduce the inside pressure in the pressure cell by opening the release valve. Consequently, the co-solvent can flow into the pressure cell because the pressure inside the cell is released and less than that in the injection tube. The schematic of the 6-way valve system, which is used to inject the co-solvent, is shown in Figure 3.3.

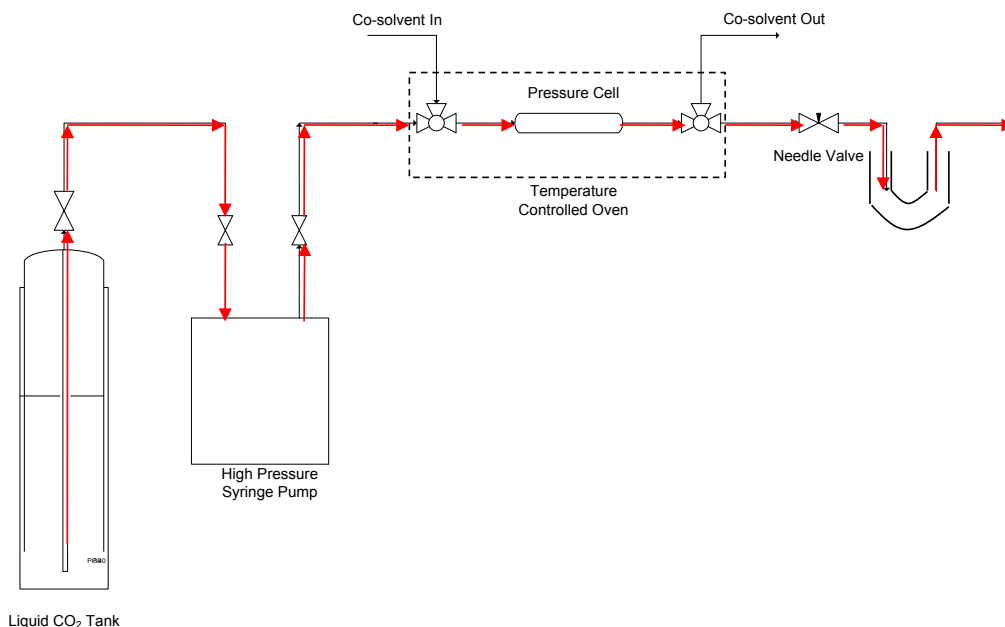


*Figure 3.1 The supercritical CO<sub>2</sub> extraction system. This system consists of a liquid CO<sub>2</sub> tank, high-pressure syringe pump, pressure gauge, thermocouple, pressure cell, 6-way valve release needle valve, and U-tube. The red arrow line shows the CO<sub>2</sub> path.*



*Figure 3.2 The supercritical CO<sub>2</sub> extractor Series 1400 from Varian Aerograph (a), pressure vessel (b), and syringe pump controller model REV D 260d from ISCO, Inc. (c).*

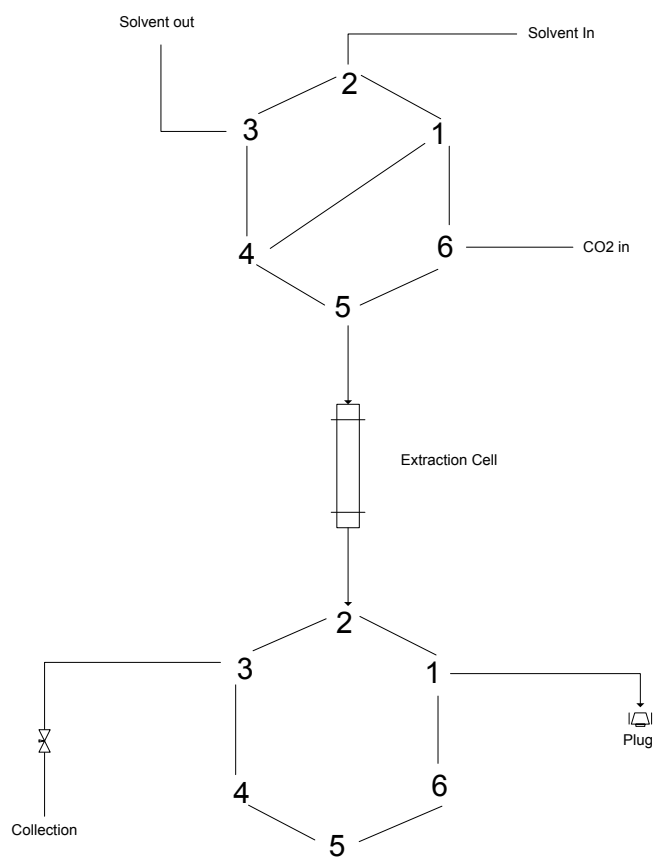


*Figure 3.3 The 6-way valve diagram. The valve can be rotated to select whether the supercritical CO<sub>2</sub> path or co-solvent path goes to the pressure cell.*

The synthetic graphite powder (Aldrich Chemical Company, Inc.) was filled into the pressure cell until it is full (approximately 2.8 grams) without applying any pressure when filling, then close both sides with filter caps. Then, the pressure cell was installed in the supercritical CO<sub>2</sub> extractor (Series 1400 from Varian Aerograph) by screwing on and tightening both sides with the plastic fittings. The temperature can be set by the

temperature control box, to 40°C, then close the oven door, turn on the oven fan and then the oven heater. In the case of pressure setting, open the main valve on the CO<sub>2</sub> tank and turn on the syringe pump controller (model REV D 260d from ISCO, Inc.). Open the CO<sub>2</sub> inlet valve, fill the syringe pump by pushing the “refill” button, and close the CO<sub>2</sub> inlet valve when the pump is full. Then, set the pressure as 2000 psi and push the “run” button. To inject CO<sub>2</sub> into the system, open the CO<sub>2</sub> outlet valve to pressurize the cell and check for leaks.

Co-solvent (N-methyl-pyrrolidone (NMP)) was inject by moving the injection valve fully clockwise (arm up), filling Luer-lok syringe with NMP; attaching the syringe to the injection valve, depressing the syringe plunger to push solvent through the injection valve loop, moving injection valve counter-clockwise to put loop into high pressure line, bleeding off CO<sub>2</sub> pressure with outlet valve; close valve, and move the injection valve back into the load position (arm up), respectively. Inject the NMP two times (approximately 0.3 mL) every three minutes for one and half hours to ensure the co-solvent pass through all of the graphite powder in the cell.

The 0.5 mg/mL sodium dodecylbenzene sulfonate (SDBS) surfactant was prepared<sup>60</sup> by mixing 125 mg of SDBS salt technical grade (Aldrich Chemical Company, Inc.) into 250 mL of water. The mixture was stirred overnight in an oil bath at a temperature of forty degrees Celsius, then pipet 10 mL of the surfactant into small bottles.

Before collecting a sample, the U-tube was rinsed with ten milliliters of the SDBS surfactant. The metal tube connected to the release needle valve was placed inside the U-tube and the release valve was opened slowly to let the drops of the exiting NMP fall into the U-tube for ten minutes (gathering approximately three milliliters).

The process was shut off by closing the CO<sub>2</sub> outlet valve, depressurized system by opening the release needle valve completely, turned the oven heater and oven fan off, removed the cell, turned off the pump and closed the CO<sub>2</sub> tank main valve. Removed the powder from inside the cell and place it into a bottle for further analysis.

The process was repeated three times to collect three sets of samples for all temperature (40°, 50°, and 60°C) and pressures (2000, 2500, 3000 psi).

### **3.2. Photon Correlation Spectroscopy (PCS)**

The Zetasizer Nano Particle Analyzer is the instrument to measure the net charge (zeta potential), size, and molecular weight of dispersed particles<sup>77</sup>. In this experiment, the net charge and size measurement are considered. As for zeta potential theory<sup>77</sup>, when particles are dispersed in solution, the net charges on the surface of the particles will attach to opposite charges in solution. This creates a double-charge layer. The inner region will have higher concentration of ions which are tightly attached together while the outer region has lower concentration and less tight attaching. This outer charge is called the “zeta potential” of the colloid particle. This parameter shows the stability of the colloid particle. Normally, the particle is considered stable if its zeta potential is more positive or more negative than +30 mV or -30 mV<sup>77</sup>, respectively. This means the particle tends to repulse each other since it has the same strong charge. The zeta potential can be measured using the folded capillary cell or the dip cell in the glass square cuvette.

In the case of size measurement<sup>77</sup>, the Zetasizer software simulates the particle size by measuring laser scattering and its correlating change due to Brownian motion. When a light source, such as a laser, is applied, the light is scattered due to the particles. The detector screen detects this scattered light which is shown as a bright-dark pattern. The bright regions are from the light scattering reaching the detector screen, while the dark region shows that no light is detected because it is blocked by the particle. Due to the Brownian theory, the particles always move because of the collision between molecules. Therefore, the light scattered pattern is unstable both in position and intensity. The Zetasizer Nano System measures this rate of change and uses it for calculating the size of the particle. As a result, the intensity contribution of the size is shown.



The Zetasizer Nano Particle Analyzer (Nano ZS model ZEN3500, Malvern Instruments Ltd.) and the DTS (Nano) software<sup>77</sup> were used to measure sizes and zeta potentials of the dispersed graphenic flakes in the SDBS solution. Before the analysis, the system needs to be warmed up for thirty minutes. For the sizing analysis, the sample (in the SDBS solution) was rinsed into the glass square cuvette until it reaches a ten millimeter height and placed in the Zetasizer Nano Particle Analyzer then close the lid. The analysis was begun by selecting the “size” measurement, “graphene” material, “water” dispersion, and “PCS1115 Glass cuvette with square aperture” cell in the DTS (Nano) software. The data were collected when the analysis was complete. In the case of zeta potential analysis<sup>77</sup>, the universal dip cell was applied into the glass square cuvette before placing both of them in the analyzer. In the software, the option of “zeta potential” measurement, “graphene” material, “water” dispersion, and “DTS1070 – Zeta dip cell” were selected before starting the analysis. The data were collected when the analysis was complete.

Sonication was applied after the supercritical treatment to study its effects on the obtained flaked. The sonication was done in a sonication bath (Branson 3510). 30% volume of ethanol (Pharmco-AAPER, ACS/USP Grade) was added in the sample. In this experiment, 7 mL of suspended sample was mix with 3 mL of ethanol in small tube. The sample tube was place in the sonication bath covered by water. The sonication was run without heat for one hour before doing the PCS analysis.

After analysis, the glass square cuvette and the bottom of the universal dip cell were rinsed with deionized (DI) water, and put into the sonication bath (Branson 3510) to be sonicated for 15 minutes<sup>77</sup>. They were cleaned with DI water and ethanol (Pharmco-AAPER, ACS/USP Grade) and dried by applying air under chemical hood.



*Figure 3.4 The Zeta Nano Instrument: ZS model ZEN3500 with a 532 nm green laser, Marvern Instruments Limited (a) and the universal 'dip' cell and the glass square cuvette (b). The instrument is located in the Chemical Science and Engineering Building, Michigan Technological University, USA.*

### **3.3. Brunauer, Emmett, and Teller (BET) analysis**

Before doing the analysis, the sample was degassed to make sure that no other gas came out from sample during analysis at low-pressure conditions. The sample weighted approximately 0.0555 grams and was put into the sample tube. Liquid nitrogen was filled to approximately 2/3 of the BET degas tank. An O-ring (with some vacuum sealer) and metal knob were place on the sample tube. The sample tube was attached and tightened to the BET degas port by screwing on the metal knob. Then, the heater pad was applied to the bottom of the sample tube with the metal clip. The instrument was started by turning on the machine, vacuum pump, and nitrogen-, helium-, and carbon dioxide tanks. The degas condition of 210°C, which is higher than boiling point of NMP, DMF, and isopropanol (Table 3), with a holding time 360 minutes and an increasing rate of 10°C per minute was set in the ASAP2000 software. The sample tube was removed from the degas port after the process was complete<sup>78</sup>.

The BET process measurement was operated with the degassed sample. The BET tank was filled by liquid nitrogen (until it reaches a marker level to determine the amount needed). Plastic sleeve, metal knob and O-ring (with some vacuum sealer) were placed on the sample tube. Then, the sample tube was attached and tightened to the BET port by screwing on the metal knob. The weight of the sample and adsorptive gases (N<sub>2</sub> and CO<sub>2</sub>) were filled and selected in the ASAP2000 software. The sample was removed from the

port when the analysis was complete. The untreated and treated graphite were analyzed with both of  $N_2$  and  $CO_2$  adsorption<sup>78</sup>.

For cleaning, a solution of 50 mL (10%) of Micro-90 (item#M-9031-12) in warm water was used. The solution was rinsed in a sonication bath (Branson 3510). After removal of sample, the sample tube was placed into the sonication bath by letting the water cover all of the tube with no air inside it. The sonication was applied for 15 minutes. Then, the sample tube was removed from the bath and rinsed with isopropanol. A metal tube connecting to nitrogen tank was inserted into the sample tube to dry out the interior of the tube. After it dried, the sample tube was baked in the oven at 110 °C for two hours<sup>78</sup>.



*Figure 3.5 The ASAP 2020 analyzer from Micromeritics Instrument Corporation, located in the Chemical Science and Engineering Building, Michigan Technological University, USA.*

### **3.4. Field Emission Scanning Electron Microscopy (FE-SEM)**

The FE-SEM was used to observe the characteristics of flakes obtained. To avoid residual surfactant (SDBS), the samples for FE-SEM were prepared by using the flakes in NMP directly obtained from the supercritical extractor. Another way was prepared by using the flakes in one percent of weight of SDBS in weight of water (9.94 mg SDBS/mL water). The one percent weight by SDBS to weight of water was prepared by mixing 2.4846 grams of SDBS in 245.98 grams (250 mL) of water, then the mixture was stirred overnight at 40°C. The sample was dropped on the sample holder, which is aluminum, until all of surface was covered. The prepared sample holder was left for two days under

a chemical hood (Labconco – Protector Laboratory Hood); or until it was the solution was completely evaporated. The process was repeated three times for the same sample holder. The analysis was done using Hitachi S-4700 FE-SEM with a working distance of five millimeters and five kilo-electron volts (keV) at various magnifications for each sample.



*Figure 3.6 The Hitachi S-4700 FE-SEM located in Material Science and Engineering Building, Michigan Technological University, USA.*

### **3.5. Atomic Force Microscopy (AFM)**

Veeco Dimension 3000 Atomic Force Microscopy was used to construct topographic and 3D images, and analyze the horizontal and vertical sizes of flakes obtained. AFM samples were prepared from the flakes in the NMP co-solvent, which were obtained directly from the exit of the supercritical extractor. The sample was dropped directly on a silicon substrate until the solution covered all surface of the substrate. The deposited substrate was left to dry for two days under a chemical hood (Labconco – Protector Laboratory Hood); or until the solution completely evaporated<sup>62</sup>. A tapping mode, 1:1 aspect ratio, 1 Hz scan rate, and 5 and 50 micrometer scan sizes were set for the AFM operation.



*Figure 3.7 Veeco Dimension 3000 Atomic Force Microscope and Control Center. The instrument is located in the Materials Science and Engineering laboratory at Michigan Technological University.*

## **4. Results and Discussion**

### **4.1. Experimental conditions for Photon Correlation Spectroscopy (PCS)**

In this study, the flakes obtained from several different processing conditions using supercritical CO<sub>2</sub> treatment were analyzed. Temperatures of 40°, 50°, and 60°C and pressures of 2000, 2500, and 3000 psi were used in this experiment to study effects of supercritical density on the flakes obtained. NMP was used as a main co-solvent due to its high solubility, polarity (Table 3) and ability to dissolve in supercritical CO<sub>2</sub><sup>19</sup>. Therefore, it was expected to be the best co-solvent to exfoliate and maintain stability of the flakes. DMF and isopropanol, which has a high dielectric constant and a different polarity range, respectively, were used in some experiments to study the effects of co-solvents on the flakes obtained. The PCS samples were prepared by collecting the exiting co-solvent suspensions into a 0.5 mg/mL SDBS solution. This water-based surfactant served to maintain the stability of the suspensions for a short period during the PCS analysis without damaging the instrument from organic solvents (NMP and DMF). The majority of treatments were run for one hour. However, to study the effect of treatment time on the flakes obtained, the treatment at 60°C and 3000 psi was run for 2 and 3 additional hours with NMP as a co-solvent. The experiments for PCS are shown in Table 4.1.

**Table 4.1**

Matrix of experimental conditions for PCS analysis. a = NMP, b = DMF, c = isopropanol, 2 = two hour treatment with NMP as co-solvent, and 3 =three hour treatments with NMP as co-solvent.

Condition	Pressure (psi)	40°C	50°C	60°C
Sonication	2000	a	a	a
	2500	a	a	a
	3000	a,b,c	a,b,c	a,b,c, 2,3
Non-Sonication	2000	a	a	a
	2500	a	a	a
	3000	a,b,c	a,b,c	a,b,c, 2, 3

The analysis were separated into studying effects of temperatures, pressures, co-solvents, times, and additional sonication to diameters, z-average sizes, and zeta potentials of obtained flakes. All of the raw data for all experiment runs is in the appendix A.

#### **4.1.1. Effects of pressure and temperature of supercritical carbon dioxide ( $ScCO_2$ ) on sizes and zeta potentials of graphitic flakes, using NMP as a co-solvent**

##### **4.1.1.1. Effects of pressures and temperatures of supercritical carbon dioxide ( $ScCO_2$ ) on diameters of flakes obtained**

Table 4.2 shows the PCS results of each individual experimental condition with NMP as a co-solvent. The PCS analysis can obtain the mean diameter, which is the highest intensity size of the flakes obtained; the z-average size, which is the log mean size of the flakes obtained; and the zeta potential, which is the charge that covers the outer surface of the flakes obtained<sup>68</sup>.

**Table 4.2**

Sizes and zeta potentials of graphitic flakes after supercritical CO<sub>2</sub> treatment at different temperatures (40°, 50°, and 60°) and pressures (2000, 2500, and 3000 psi) with and without additional one-hour sonication. NMP was used as a co-solvent.

Parameter	Pressure (psi)	Sonication			Non- Sonication		
		40°C	50°C	60°C	40°C	50°C	60°C
Diameter (nm)	2000	153.80	117.50	78.66	157.30	143.20	175.70
	2500	144.60	122.22	85.28	155.90	122.30	207.10
	3000	130.90	121.10	105.10	151.90	160.90	215.20
Z-average size (nm)	2000	142.90	100.90	82.15	148.30	158.40	167.10
	2500	136.80	107.40	96.86	163.80	161.80	167.80
	3000	111.40	102.70	85.58	121.10	175.40	133.60
Zeta potential (mV)	2000	-56.90	-41.20	-27.80	-33.30	-29.10	-32.20
	2500	-57.80	-42.40	-28.50	-32.10	-29.20	-20.20
	3000	-43.50	-39.10	-32.20	-56.40	-44.10	-40.80

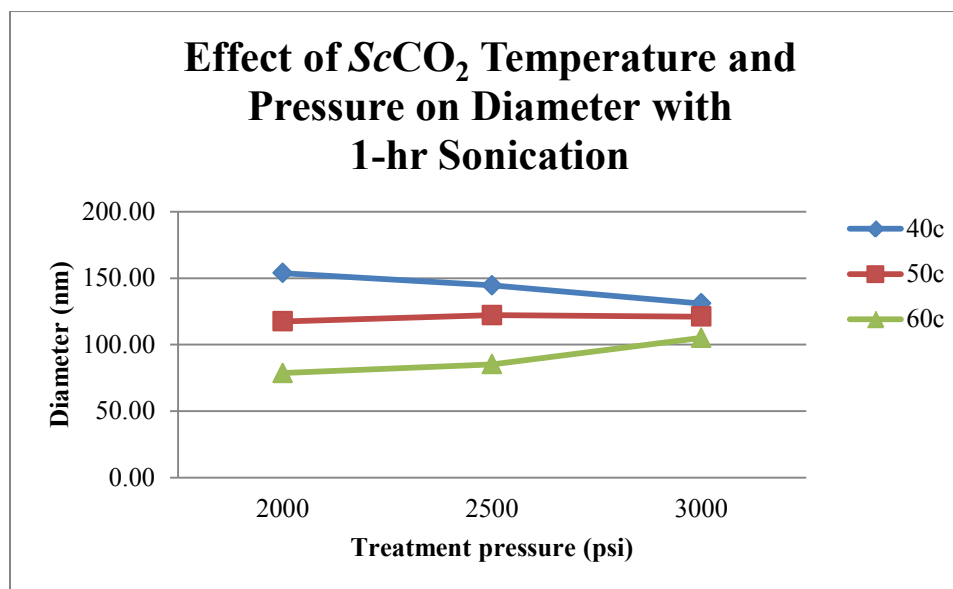


Figure 4.1 The diameter (nm) of the graphitic flakes at different treatment temperatures (°C) and pressures (psi) with additional one-hour sonication. NMP was used as a co-solvent.



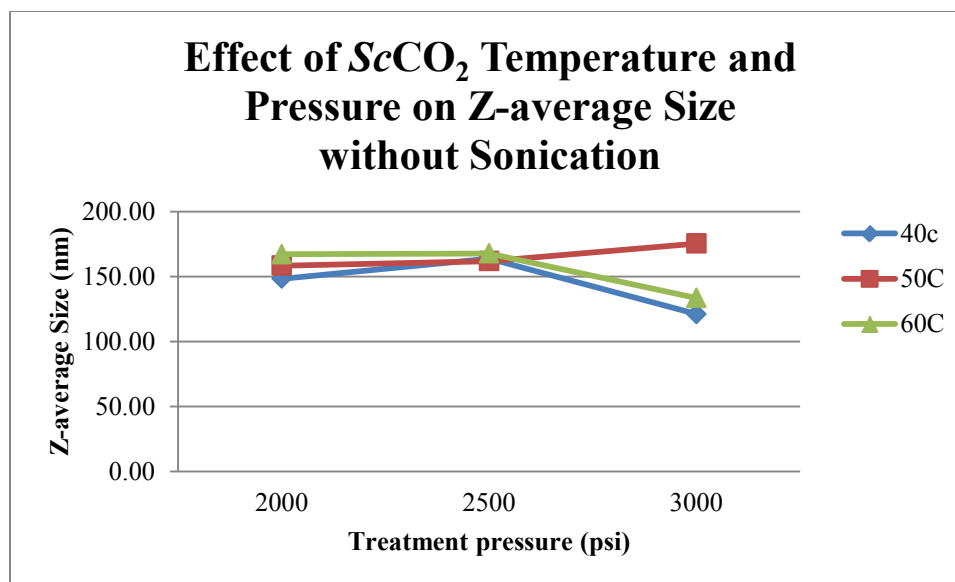


Figure 4.2 The diameter (nm) of the graphitic flakes at different treatment temperatures ( $^{\circ}\text{C}$ ) and pressure (psi) without additional sonication. NMP was used as a co-solvent.

From Table 4.2 and Figure 4.1, in the case of the additional one-hour sonication, the diameters of the flakes are clearly affected by the temperature of the supercritical carbon dioxide. In the case of sonication at  $60^{\circ}\text{C}$ , flakes show the smallest sizes, 78.66 nm, while at  $40^{\circ}\text{C}$ , the flakes are the largest, 153.80 nm, in comparison to other temperatures at the same pressures. The effects of pressure are less obvious. Although the pressure changes, the diameters of the flakes at the same temperature are relatively close to each other. At  $60^{\circ}\text{C}$ , diameter tends to increase when the pressure increases (78.66 nm, 85.28 nm, and 105.10 at the pressures of 2000 psi, 2500 psi, and 3000 psi, respectively). The diameters are almost constant at  $50^{\circ}\text{C}$  (117.50 nm, 122.22 nm, and 121.10 nm at the pressures of 2000 psi, 2500 psi, and 3000 psi, respectively). In contrast, the diameter tends to decrease when the pressure rises at the pressure for  $40^{\circ}\text{C}$  (153.80 nm, 144.60 nm, and 130.90 nm at the pressures of 2000 psi, 2500 psi, and 3000 psi, respectively).

For the non-sonicated data in Table 4.2 and Figure 4.2, the results are different from those of the sonicated samples in terms of the order of the temperature which affects the diameter of the flake. At  $60^{\circ}\text{C}$ , the diameters of the flakes are the largest compared with those of other temperatures at the same pressure. However, the diameters of flakes at

50°C at the pressures of 2000 psi and 2500 psi (143.2 nm and 122.3 nm, respectively) are lower than at 40°C (157.3 nm and 155.9 nm, respectively). The largest diameter for the non-sonicated samples is 215.2 nm, at 60°C and the pressure of 3000 psi while the smallest diameter is 122.3 nm at 50°C and the pressure of 2500 psi.

For the supercritical condition, the critical point of carbon dioxide is 304.1K and 7.38 MPa (30.95°C and 7070.38 psi; Table 1.2). However, the supercritical density of the carbon dioxide depends on the temperature and pressure used to create the supercritical condition<sup>23</sup>. For carbon dioxide, the supercritical density is high when the temperature is slightly higher than its critical temperature and when the pressure is much higher than its critical pressure. Therefore, in this case the supercritical density is the highest at 40°C and 3000 psi, but is the lowest at 60°C and 2000 psi. The data shown in Table 4.2, and Figures 4.1 and 4.2 indicates that the temperature has more of an effect on the flake diameter than the pressure does. For the sonicated samples, the diameter increases when the temperature decreases. This trend is the same for all pressures presented in this experiment. In contrast, the diameters of the non-sonicated samples increase when the temperature increases. This is because when the temperature increases, the supercritical density of carbon dioxide decreases. The carbon dioxide molecules per unit area decreased. Therefore, at 40°C and 3000 psi, the supercritical fluid has the highest yield of the carbon dioxide molecules per unit area. Consequently, the graphitic flakes are intercalated by a large number of the supercritical CO<sub>2</sub> molecules. However, the ability to absorb the molecule per unit area of the graphite surface is limited. As a result, the graphite layers are exfoliated and broken up into small flakes. When sonication is applied after the supercritical carbon dioxide treatment, the diameter of the flake decreases less than the low-critical density treated samples because the high-critical density treated flakes are already exfoliated and broken up to small pieces. This is why the differences between the diameter of the sonicated sample and non-sonicated sample at the high critical density (40°C and 3000 psi) are less than that of the low critical density (60°C and 2000 psi).

In the case of the effect of the temperatures on the diameters of non-sonicated samples, the high critical density at 40°C creates the smallest flakes diameters for non-sonicated samples, followed by those of temperature at 50° and 60°C. However, the data shown in Table 4.2 and Figure 4.2 show some differences. The diameters of the non-sonicated flakes at the temperature of 50°C at pressures of 2000 psi (143.2 nm) and 2500 psi (122.3 nm) are less than those of 40°C (157.3 nm and 155.9 nm, respectively) which has higher critical density at the same pressures. This is not statically significant due to high deviation of the sample sizes obtained.

In the case of the effect of the temperature, the smallest diameters are created by the temperatures of 60°C, followed by those of 50° and 40°C, respectively. These are the inverse of the data set for the non-sonicated samples where the lower temperatures can make smaller flakes in terms of the diameters. This is because in the supercritical treatment, the carbon dioxide molecules pass through and are adsorbed between the layers of graphite. This can cause exfoliation via expansion, due to the carbon dioxide molecules are stacked between the graphite layers. For the high supercritical density treatment (low temperature), the graphite layers are already exfoliated more completely than low supercritical density treatment (high temperature), which the layers are expanded and loosen. Therefore, applying energy to the treated graphite by sonication breaks down these expanded and loosen layers. This is why the sonicated flakes sizes are relatively smaller than those of non-sonicated flakes. Pressure do not affect the diameter of the flakes as much as the temperatures do since we cannot see the exact trend of the pressure. This may be because high deviation of obtained sample sized that may interfere the trend of pressure effects.

#### **4.1.1.2. Effects of pressure and temperature of supercritical carbon dioxide (ScCO<sub>2</sub>) on z-average sizes of flakes obtained**

The z-average size is another method to calculate the size of a flake. This parameter is a log mean size of suspended particle<sup>77</sup>. However, it is also based on Brownian motion and laser scattering of particles<sup>77</sup>. Therefore, z-average sizes have the same inclinations as the

diameter sizes of various temperatures and pressures and sonicated and non-sonicated samples as shown in Table 4.2 and Figure 4.3 and 4.4.

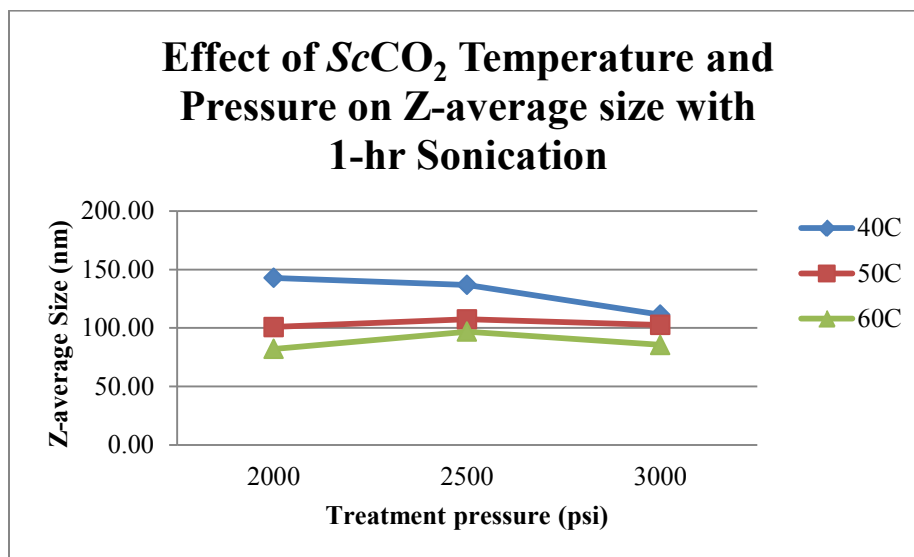


Figure 4.3 The z-average size (nm) of graphitic flakes at different treatment temperatures (°C) and pressures (psi) with additional one-hour sonication. NMP was used as a co-solvent.

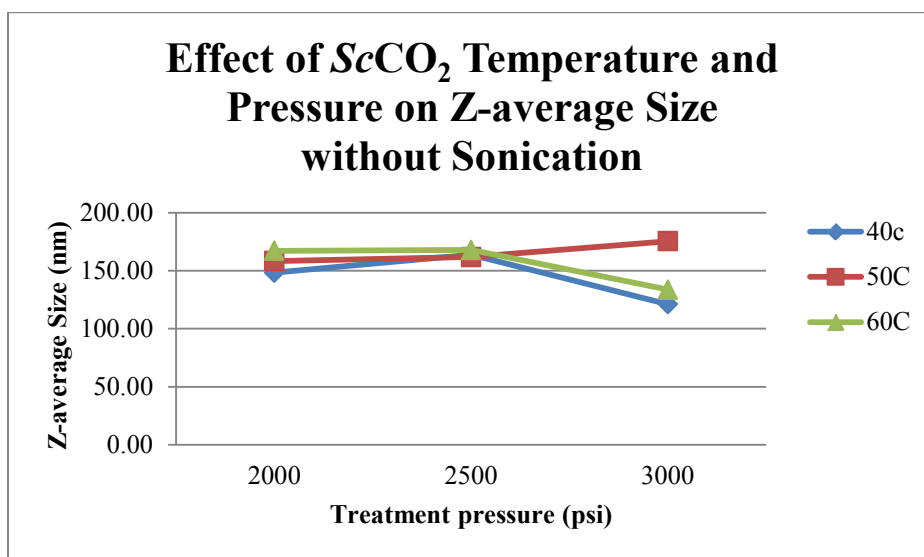


Figure 4.4 The z-average size (nm) of the graphitic flakes at different treatment temperatures (°C) and pressures (psi) without additional sonication. NMP was used as a co-solvent.

In the case of the effects of temperature for the sonicated samples, at the same pressure, the temperature of 60°C creates the smallest z-average size, followed by 50° and 40°C, respectively. For non-sonicated samples, the smallest z-average sizes are created by 40°, 50°, and 60°C, respectively. These can be explained in the same way as with the diameters. Repeatedly, at lower temperatures, the supercritical density of carbon dioxide is lower than it is at higher temperatures. Therefore, the lower temperatures can break the graphite more completely than higher temperatures, due to high amounts of the carbon dioxide molecule per unit area of the layer surface. In contrast, at higher temperature, the graphite flakes are not completely exfoliated but expanded due to carbon dioxide molecules that go inside and be stacked more between the graphite layers. As a result, the lower temperatures make a smaller z-average size for non-sonicated sample but larger z-average sizes for sonicated samples since the expanded layers of graphite are broken up further by sonication. These make the z-average size differences between sonicated and non-sonicated samples of the higher temperatures larger than those of the lower temperatures. However, for non-sonicated samples, the z-average size at 50°C (161.80 nm) is smaller than at 40°C (163.80 nm) and 2500 psi; and the z-average size at 50°C and 3000 psi is the largest (175.40 nm).

For the effects of pressure on the z-average size, higher pressure yields higher critical density. When pressure increases, the z-average size should be decreased for non-sonicated samples but increased for sonicated samples. However, these inclinations are not clear, as shown in Table 4.2 and Figures 4.3 and 4.4. This might be due to the error of high deviation of obtained sample. Moreover, they are close to each other if the temperatures are the same. In this case, the effects of pressure on the z-average size are minor, while temperature is a main factor that has more impact on the z-average size.

#### **4.1.1.3. Effects of pressure and temperature of supercritical carbon dioxide (ScCO<sub>2</sub>) on zeta potentials of flakes obtained**

The zeta potential is the outer charge that covers the surface of dispersed particles in a solution. These outer charges belong to the solution charges which are attracted by the opposite charges on the dispersed particle surfaces<sup>77</sup>. To maintain the stability of the

suspended particles, the zeta potential has to be as negative or positive as much as possible<sup>60,77</sup>. Normally, dispersed particles with a zeta potential less than -30 mV or more than +30 mV are considered to be highly stable due to high repulsive forces between the particles in solution, which prevent reaggregation<sup>60,77</sup>.

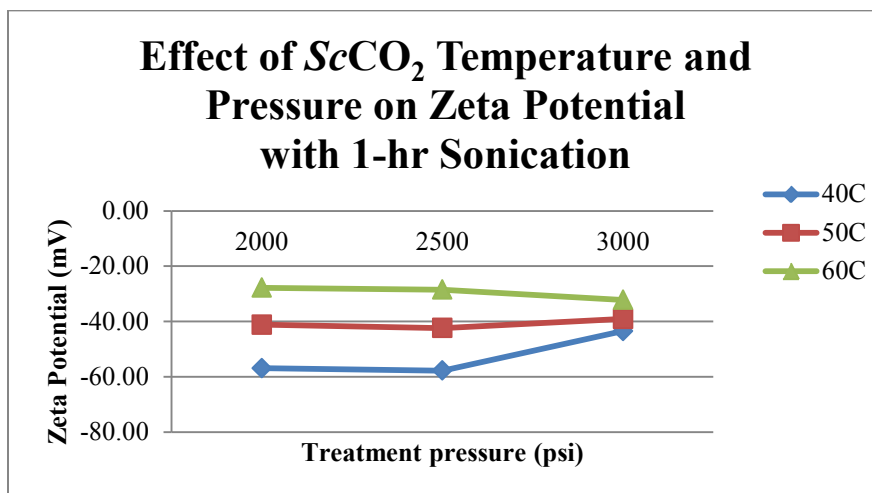


Figure 4.5 The zeta potential (mV) of the graphitic flakes at different treatment temperatures ( $^{\circ}\text{C}$ ) and pressures (psi) with additional one-hour sonication. NMP was used as a co-solvent.

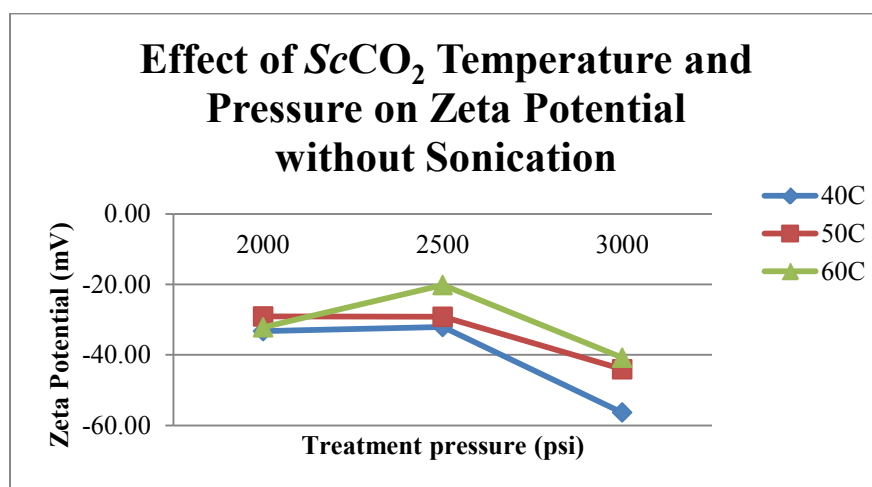


Figure 4.6 The zeta potential (nm) of the graphitic at different treatment temperatures ( $^{\circ}\text{C}$ ) and pressures (psi) without additional sonication. NMP was used as a co-solvent.

Table 4.2 and Figure 4.5 show the zeta potentials of the sonicated samples at various temperatures and pressures used in the supercritical carbon dioxide treatment. The data show that at 40°C, where the critical density is the highest, the zeta potential is lowest, followed by 50° and 60°C, respectively. In this case, the zeta potentials at 40°C are much lower than -30 mV, especially at 2000 psi (-56.90 mV) and 2500 psi (-57.80 mV), while the zeta potentials at 60°C fluctuated close to -30 mV (-27.80, -28.50, and -32.20 mV at 2000, 2500, and 3000 psi, respectively). These show that flakes at 40°C are more stable than at 50° and 60°C, respectively. This is due to the high critical density of supercritical CO<sub>2</sub> at 40°C, which can expand the graphite layers more completely. The lower critical densities at 60°C do not break the graphite layers as much. However, the carbon dioxide molecules can be adsorbed without complete exfoliation or expansion. Although sonication is applied and breaks up more flakes after the supercritical treatment, some partly expanded flakes still exist with carbon dioxide molecules still adsorbed between the layers. In this case, the Van der Waals forces which hold the layers together are weaker than in the original graphite, due to the increased distances between the layers. Therefore, the stability of the dispersed flakes in terms of zeta potential is small due to excess carbon dioxide absorption on the surface of the flake layers, thus leading to a high degree of reaggregation.

For the non-sonicated sample data in Table 4.2 and Figure 4.6, the trends are the same as that of the sonicated samples. The zeta potentials are the lowest at 40°C, followed by 50° and 60°C. Except for at 2000 psi, where the zeta potential at 60°C (-32.20 mV) is lower than that of at 50°C (-29.10 mV). However, they are close enough that this difference is not statistically significant since they are very comparable. This may be due to error from high dispersity in zeta potential of the suspended flakes.

In the case of the effects of pressure on the zeta potential, the trends are once again not as clearly distinguished as those of temperatures. At 3000 psi when the critical density is highest, the zeta potential should show the most stability. This feature can be seen for the non-sonicated samples that, at the same temperature, 3000 psi creates the lowest zeta potentials (-56.40 nm, -44.10 nm, and -40.80 nm at 40°, 50°, and 60°C, respectively).

However, this is not the case for the sonicated samples since only those at 60°C follow this hypothesis. Although the stability of the flakes cannot be related clearly to the pressure, the zeta potentials are very close at the same temperature. In conclusion, for diameters and z-average sizes data, the effect of supercritical pressure is not as important as temperature.

#### **4.1.2. Effects of sonication after supercritical carbon dioxide ( $\text{ScCO}_2$ ) treatment on sizes and zeta potentials of graphitic flakes**

##### **4.1.2.1. Effects of sonication after supercritical carbon dioxide ( $\text{ScCO}_2$ ) on diameters of flakes obtained**

Table 4.2 and Figure 4.7 show the comparison of the diameters between sonicated and non-sonicated samples. The relationship shows that at the same temperatures and pressures, the sonicated diameters are always less than those of non-sonicated samples. This is because sonication applies energy to the sample through vibration. As a result, the flakes are broken up into small pieces depending on how loosely they are stacked with the high critical density treatment (40°C, 3000 psi), the flakes are already extensively exfoliated by the attack of the carbon dioxide molecules. Although sonication is applied, the differences of the diameter before and after doing sonication are not large as those at low critical density (60°C, 2000 psi). This is because at low critical density the flakes and layers are not as completely expanded due to a lower concentration of carbon dioxide molecules between the flakes. Instead, they stack together loosely as large chunks. When sonication is applied, these flakes are loosen and broken up vertically and hexagonally into much small pieces, even smaller than those processed at a high critical  $\text{CO}_2$  density.



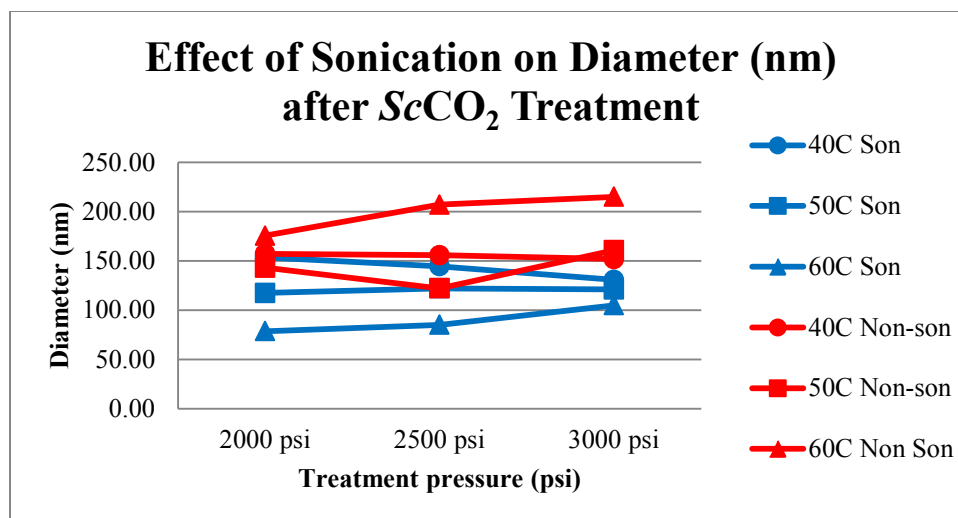


Figure 4.7 The diameters (nm) of sonicated and non-sonicated samples after supercritical(Sc) CO<sub>2</sub> treatment at different temperatures and pressures. NMP was used as a co-solvent.

In addition, sonication also brings about homogeneity in terms of the size and stability of the dispersed flakes in the solution. This can be observed from the zeta analysis software shown in appendix A. Some of the results of the size analysis of the samples show the message “Refer to quality report”. This is due to high heterogeneity in the sizes and reaggregation of the dispersed flakes, resulting in a high Poly Dispersity Index (PDI). In contrast, all the results for sonicated samples are labeled “good” quality (appendix A) since sonication can break down the loosely-bonded flakes from the supercritical treatment more completely into small pieces in the same size range. These small flakes are separated more thoroughly from each other, so reaggregation is more difficult compared to those without additional sonication.

The flake diameter shows no clear trend with changing pressure. In contrast, the diameters of the flakes are clearly different at different treatment temperatures. If temperature increases, the diameter decreases for non-sonicated samples, but increases for sonicated samples. This shows that treatment temperature has a more significant effect on the diameter of the flakes.

#### 4.1.2.2. Effects of sonication after supercritical carbon dioxide ( $\text{ScCO}_2$ ) treatment on z-average sizes of flakes obtained

Table 4.2 and Figure 4.8 show the comparison of the z-average size between sonicated and non-sonicated samples. In the same way, the sonicated samples have lower z-average size than that of non-sonicated samples due to the destruction of flakes from sonication. Moreover, the z-average size difference between the sonicated and non-sonicated samples at a high critical density temperature at  $40^\circ\text{C}$  is the smallest, followed by  $50^\circ$  and  $60^\circ\text{C}$ , respectively. This is due to the density of the carbon dioxide molecules at the treatment conditions and the absorption capacity of the graphite flakes. Temperature is still a major factor, and the effect of pressure is relatively minor.

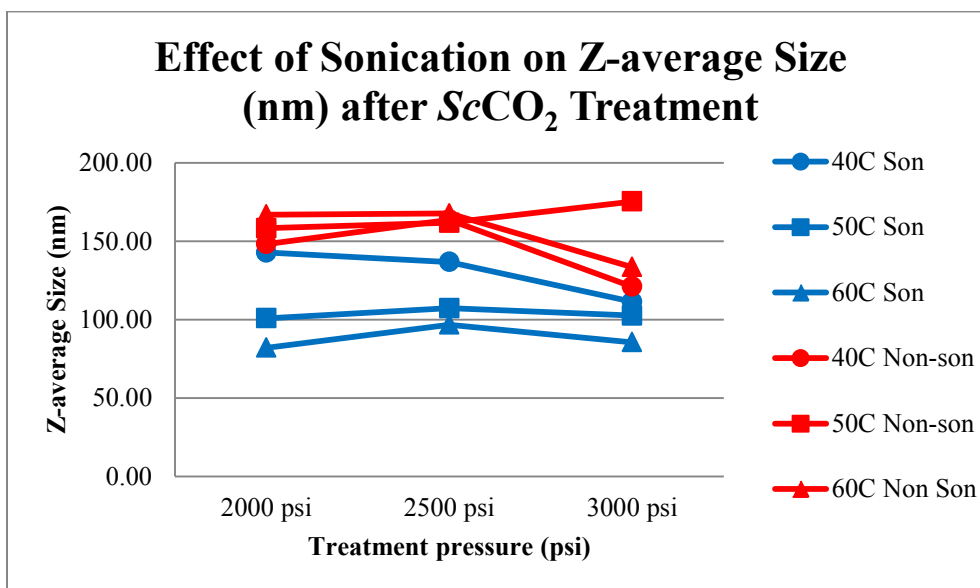


Figure 4.8 The z-average sizes (nm) of sonicated and non-sonicated samples after supercritical( $\text{Sc}$ )  $\text{CO}_2$  treatment at different temperatures and pressures. NMP was used as a co-solvent.

Similar to the diameter results, the zeta analyzer software shows “good” result quality for sonicated samples, but often displays “referring to quality report” for non-sonicated samples (appendix A). This is because additional sonication makes the particle sizes more homogeneous and stable. This can be explained for the same reasons as supercritical treatment, which does not completely exfoliate and break down the flakes

the first time, so the layers of the treated flakes may be partly expanded and still be loosely bonded together by Van der Waals forces. Applying sonication provides energy to these expanded flakes, which are then the flakes are cracked and broken up into small pieces. In the case of the flakes that already broken into the small pieces by the supercritical treatment, although sonication is applied, the differences in sizes are not as significant. That is why the differences between the z-average size and the diameter of the sonicated and non-sonicated samples at the high critical density are less than those treated at the low critical density.

#### 4.1.2.3. Effects of sonication after supercritical carbon dioxide ( $\text{ScCO}_2$ ) treatment on zeta potentials of flakes obtained

Since sonication can break the loosely stack flakes into smaller flakes, the sonicated flakes should be more stable than non-sonicated flakes. The data in Table 4.2 and Figure 4.9 show that the zeta potentials of the sonicated flakes have more negative charges than that of non-sonicated flakes at the same temperature and pressure. Although, at 3000 psi, the zeta potentials of the non-sonicated are less than that of sonicated flakes at the same temperature, they are close enough not to be statically different.

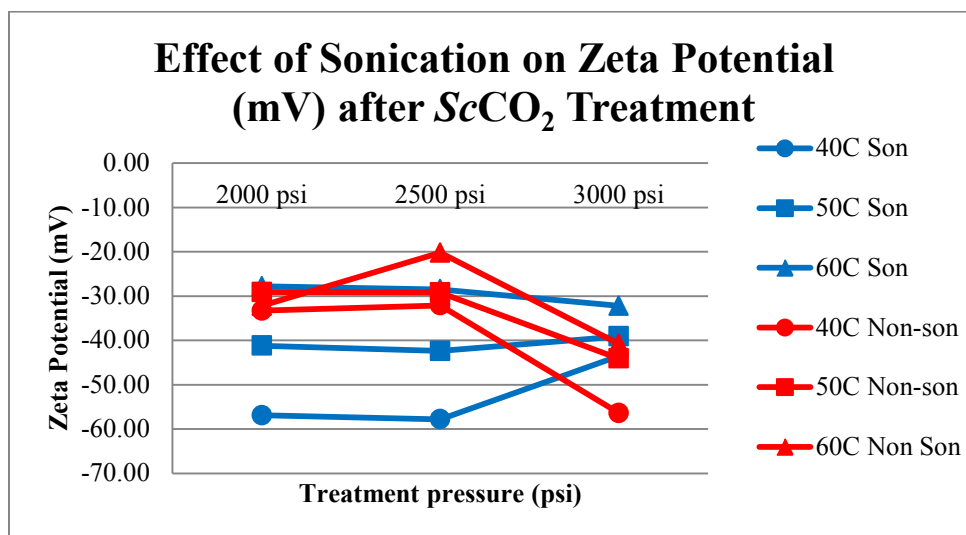


Figure 4.9 The zeta potentials (mV) of sonicated and non-sonicated samples after supercritical( $\text{Sc}$ )  $\text{CO}_2$  treatment at different temperatures and pressures. NMP was used as a co-solvent.

### 4.1.3. Effects of co-solvents on sizes and zeta potentials of graphitic flakes

#### 4.1.3.1. Effects of co-solvents of supercritical carbon dioxide ( $\text{ScCO}_2$ ) treatment on diameters of flakes obtained

Co-solvents were used to increase the solvating power of the supercritical  $\text{CO}_2$ <sup>59</sup>. Moreover, they also served to disperse the treated flakes and carry them out of the pressure cell through the pressure release valve. NMP, DMF and isopropanol were used due to their range of polarities to study the effect of co-solvents on the supercritical processing. The PCS results show the diameter, z-average size, and zeta potential of the flakes obtained from each experimental condition in Table 4.3.

**Table 4.3**

Sizes and the zeta potentials of graphitic flakes after the supercritical  $\text{CO}_2$  treatment with different co-solvents. The processes were run at different temperatures (40°, 50° and 60°C) and 3000 psi with and without additional one-hour sonication.

Parameter	Co-solvent	Sonication			Non- Sonication		
		40°C	50°C	60°C	40°C	50°C	60°C
Diameter (nm)	NMP	130.9	121.1	105.1	151.9	160.9	215.2
	DMF	191.2	153.6	82.27	253.7	178.9	277.5
	Isopropanol	290.1	314.9	291.5	231.6	236.8	217.8
Z-average size (nm)	NMP	111.4	102.7	85.58	121.1	175.4	133.6
	DMF	181.2	123.1	81.87	198.2	122.1	197.9
	Isopropanol	202.2	262.7	247.1	226.2	243.9	218.2
Zeta potential (mV)	NMP	-43.5	-39.1	-32.2	-43.5	-39.1	-32.2
	DMF	-47.1	-63.6	-60.5	-47.1	-63.6	-60.5
	Isopropanol	-25.4	-28.5	-29.1	-25.4	-28.5	-29.1

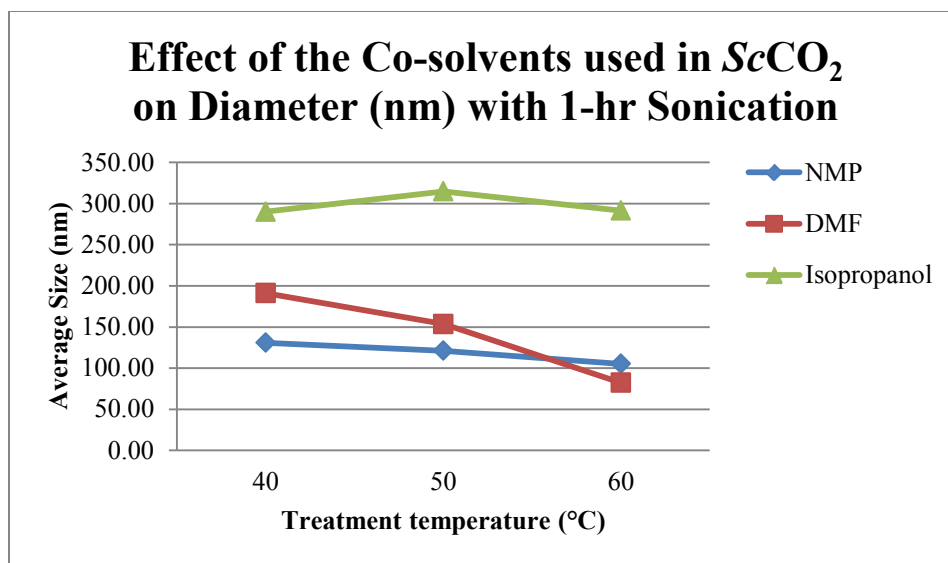


Figure 4.10 The diameter (nm) of graphitic flakes with different co-solvents used and treatment temperature (°C) at 3000 psi with additional one-hour sonication.

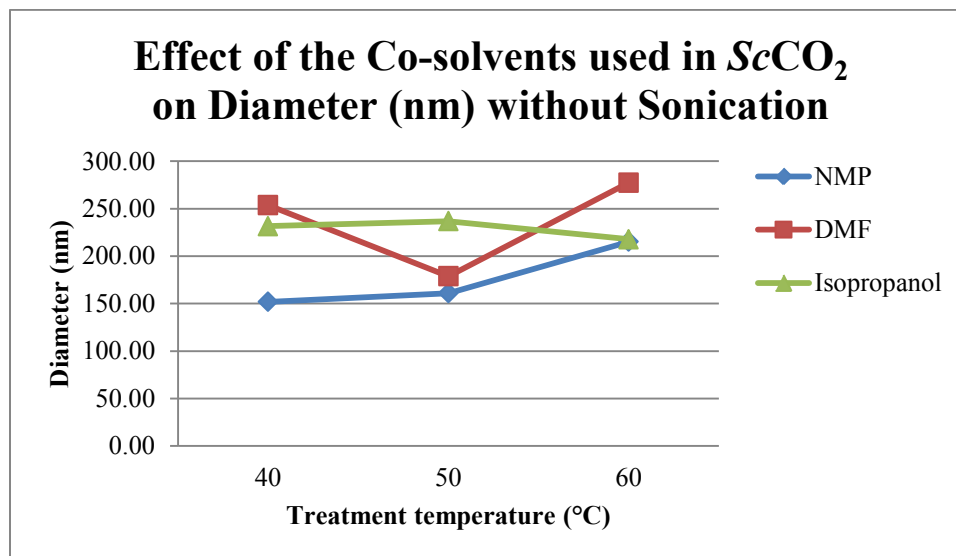


Figure 4.11 The diameter (nm) of graphitic flakes with different co-solvents used and treatment temperature (°C) at 3000 psi without sonication.

For non-sonicated samples (Table 4.3 and Figure 4.11) the N-methyl pyrrolidinone (NMP) flakes are the smallest. For the isopropanol- and dimethylformamide (DMF) – flakes, the diameters trends are unclear: the isopropanol diameters are smaller at 40° and 60°C but larger at 50°C. Moreover, the diameter of the NMP for non-sonicated sample at

60°C (215.20 nm) is very close to that of the isopropanol (217.80 nm). This case of the effects of temperature, the relationship between diameters and temperatures are unclear.

As for the diameters of the sonicated samples (Table 4.3 and Figure 4.10), the NMP-diameters are the smallest, followed by the DMF- and isopropanol-diameters, respectively, at the same treatment temperatures and 3000 psi. However, at 60°C, the diameter of the DMF-sample (82.27 nm) is the smallest, and smaller than that of the NMP-sample (105.10 nm). Moreover, the diameters of the flakes tend to decrease when the temperature increases for NMP and DMF, but for the isopropanol-flakes, the trend is not clear (290.10 nm, 314.90 nm, and 291.50 nm at 40°, 50°, and 60°C, respectively). This might be due to reaggregation. Obviously, the isopropanol-diameters are much larger than those of NMP- and DMF-diameters which are close to each other. This also might be due to reaggregation of the flakes. Since isopropanol has a low dielectric constant (Table 3), it cannot maintain the stability of the flakes. Consequently, those smaller flakes become reaggregated after sonication. This occurs less in the organic solvents with high dielectric constant like NMP and DMF (Table 1.3).

In conclusion, NMP and DMF which have high dielectric constants, can maintain the stability of the flakes by preventing reaggregation better than isopropanol, which has a low dielectric constant. As a result, the diameters of the NMP- and DMF-flakes are smaller than those of the isopropanol-flakes. This can be observed clearly in sonicated samples (Figure 4.10) since sonication breaks the graphitic flakes into smaller pieces after supercritical treatment. Those small and sonicated flakes are less stable than the flakes before sonication.

#### **4.1.3.2. Effects of co-solvents of supercritical carbon dioxide (ScCO<sub>2</sub>) treatment on z-average sizes of flakes obtained**

Table 4.3 and Figures 4.12 and 4.13 show the data of the z-average size (nm) of the flakes obtained at 3000 psi with various temperatures (40°, 50°, and 60°C, respectively) for sonicated and non-sonicated samples. The effects of different co-solvents (NMP,

DMF, and isopropanol) used in the supercritical carbon dioxide treatment on the z-average sizes, are observed and compared to each other. The results show the same trends as the diameters sizes. For the non-sonicated samples, the NMP- and DMF-flakes have the smallest z-average ranges followed by the isopropanol-flakes. However, the relationship between the z-average sizes of each co-solvent and the temperature is not clear. These might be due to high polydispersity index (PDI) of the sample (Appendix A).

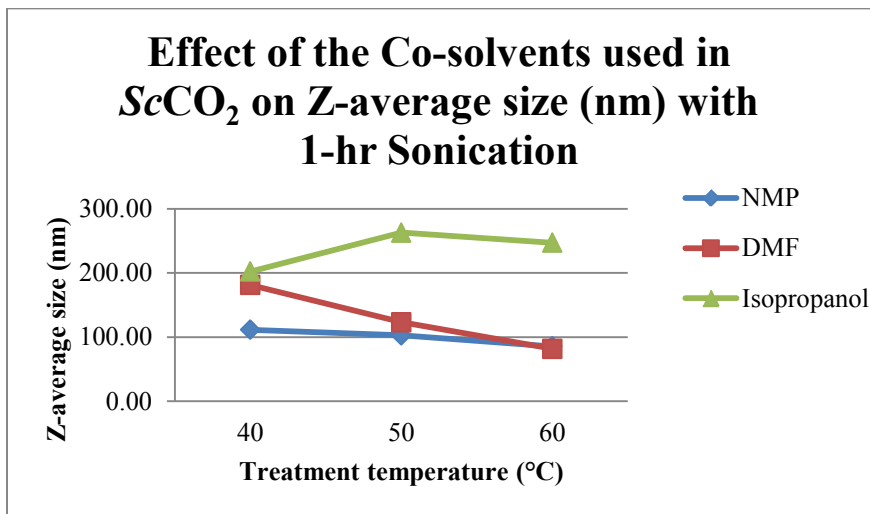


Figure 4.12 The z-average sizes (nm) of graphitic flakes with different co-solvents used and treatment temperature (°C) at 3000 psi with additional one-hour sonication.

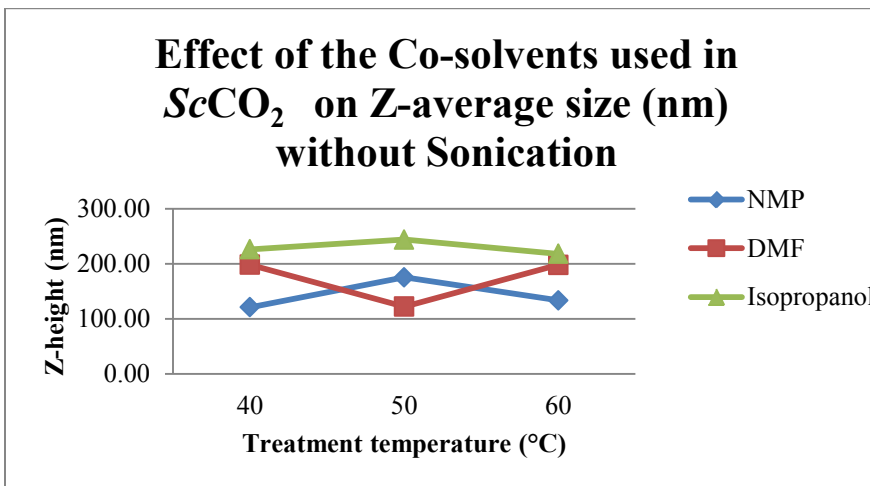


Figure 4.13 The z-average sizes (nm) of graphitic flakes with different co-solvents used and treatment temperature (°C) at 3000 psi without sonication.

In the case of the sonicated flakes, the NMP- diameters are the smallest, followed by the DMF- and Isopropanol, respectively, except at 60°C, for which the DMF-flakes (81.87 nm) is are comparable to the NMP-flakes (85.58 nm). Both of these organic solvents have high dielectric constants. The relationship between the temperatures and the z-average sizes for these two solvents show that when temperature increases, the z-averages of each co-solvent tend to decrease due to the sonication effects on the low critical density of the supercritical treatment. However, for isopropanol, no clear trend is observed.

These results can be explained in the same way as the differences in diameters were. NMP and DMF are the best co-solvents for dissolving in the supercritical carbon dioxide in order to exfoliate the graphite layers into the smallest flakes, and maintaining the stability of those flakes after the treatment due to their high dielectric constant. Isopropanol cannot prevent flake reaggregation due to its low dielectric constant. Therefore, the z-average sizes of the isopropanol-flakes are larger than those of the NMP- and DMF- flakes for both sonicated and non-sonicated samples.

#### **4.1.3.3. Effects of co-solvents of supercritical carbon dioxide (ScCO<sub>2</sub>) treatment on the zeta potentials of obtained flakes**

For the non-sonicated samples (Table 4.3 and Figure 4.15), the NMP- and DMF treated flakes are stable since their zeta potentials are much less than -30 mV. Although the zeta potentials of the DMF treated flakes are somewhat less than that of the NMP treated flakes, in general, they are comparable to each other. For the isopropanol treated flakes, the zeta potentials have very small negative charges (-8.52, -13.80, and -12.00 mV for 40°, 50°, and 60°C, respectively), and much smaller than -30 mV. This means the isopropanol treated flakes are much more likely to experience reaggregation due to small repulsive force of the same charge.

The trend is the same in the sonicated sample (Table 4.3 and Figure 4.14), the DMF-flakes should be most stable since they have the highest negative charges. This is due to DMF, which has the highest dielectric constant compared to those of NMP and isopropanol. However, the NMP-flakes should also be stable since the zeta potential is



lower than -30 mV. In the case of isopropanol, although the zeta potentials are higher, the zeta potentials do not exceed the stable ranges (more than +30 mV or less than -30 mV)<sup>77</sup>. Therefore, the isopropanol treated flakes are not stable in suspension.

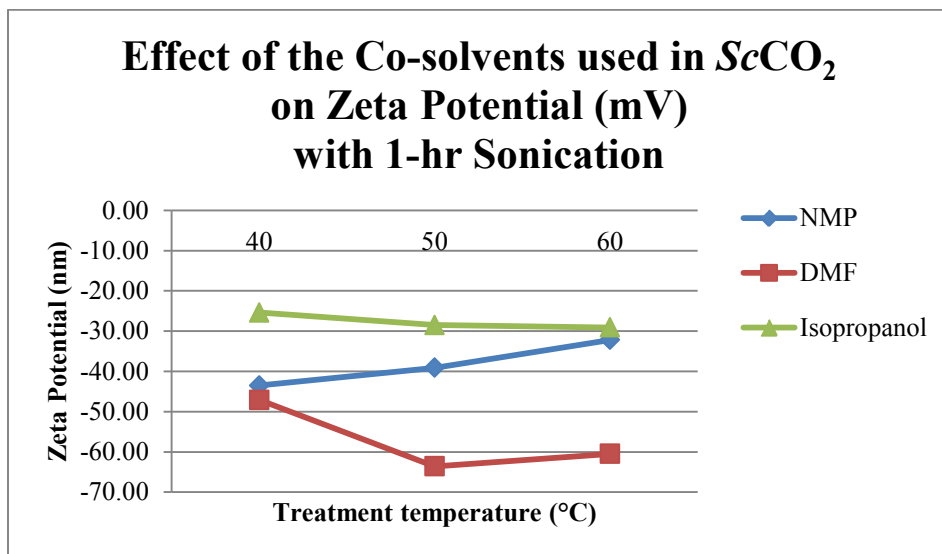


Figure 4.14 The zeta potential (mV) of graphitic flakes with different co-solvents used and treatment temperature (°C) at 3000 psi with additional one-hour sonication.

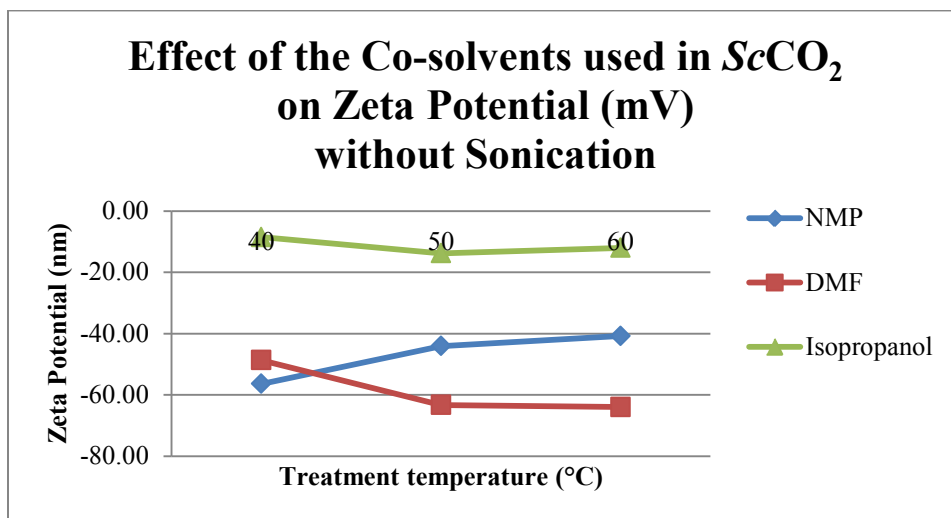


Figure 4.15 The zeta potential (mV) of graphitic flakes with different co-solvents used and treatment temperature (°C) at 3000 psi without sonication.

#### **4.1.3.4. Effects of sonication after supercritical carbon dioxide ( $\text{ScCO}_2$ ) treatment on sizes and zeta potentials of flakes obtained with different co-solvents**

Comparing the effects of the sonication on the diameters of the flakes of different co-solvents used in the supercritical treatment (Table 4.3 and Figure 4.16), all NMP- and DMF-flakes show the same trend. The diameters are relatively smaller after sonication. However, for the isopropanol treated flakes, the sonicated diameters are larger than the non-sonicated diameter at the same temperatures. This is due to the non-sonicated flakes of isopropanol not being as stable as shown by the zeta potentials data (Table 4.3 and Figure 4.15). These flakes more readily reaggregate with each other. After sonication, the flakes are broken down into smaller pieces which are less stable than before. Therefore, reaggregation occurs faster and easier than those before sonication. The diameters shown for the sonicated flakes treated in isopropanol are the diameters those which are already reaggreated, and are therefore larger than the non-sonicated diameters.

For the effects of sonication on the z-average sizes (Table 4.3 and Figure 4.17), the trends are the same as that of the diameters. However, since the z-average sizes are calculated from the mean of the size distribution, there is less difference in the z-average sizes than the diameters. From the data (Table 4.3 and Figure 4.12, and 4.13), at 40°C, the z-average size of the non-sonicated isopropanol-flakes (226.20 nm) is slightly larger than that of the sonicated flakes (202.20 nm), and at 50°C, the z-average size of non-sonicated DMF flakes (122.10 nm) is essentially the same as that of the sonicated flakes (123.10 nm). This might be due to the PDI of the non-sonicated flakes, which more variance in the results.

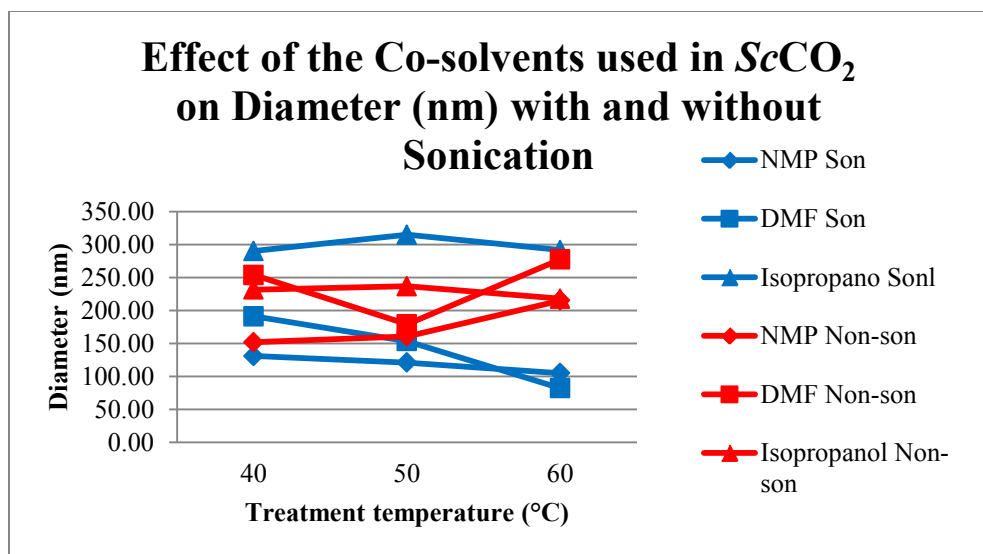


Figure 4.16 The diameters (nm) of sonicated and non-sonicated samples from different co-solvents used and treatment temperatures at 3000 psi.

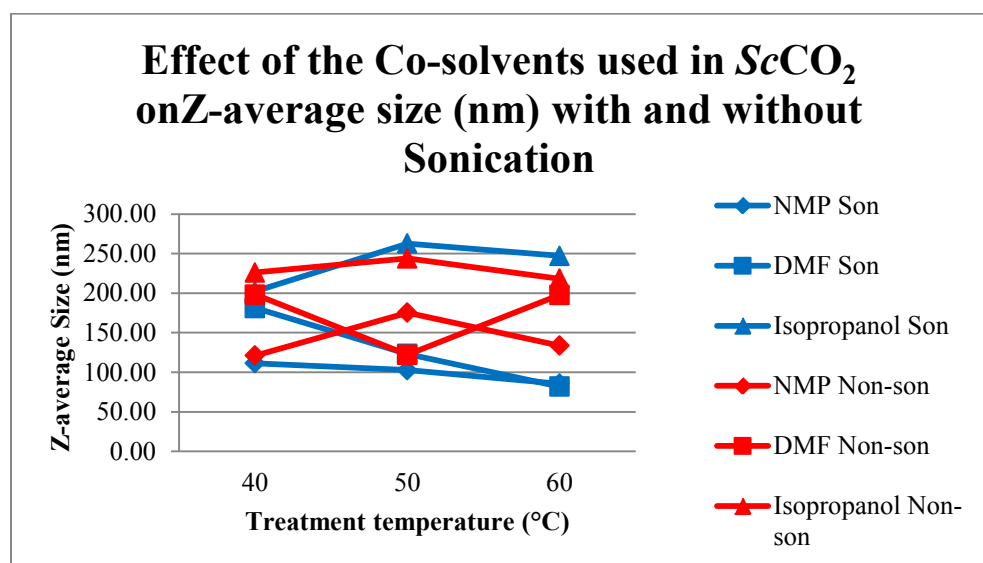


Figure 4.17 The diameters (nm) of sonicated and non-sonicated samples from different co-solvents used and treatment temperatures at 3000 psi.

For both sizes measurements, it is obvious that sonication brings about more homogeneity in the sizes of the flakes. The evidence can be observed in appendix A which shows the PCS analyzing software. For the sizing analysis, most of the non-

sonicated flakes show the message: “Refer to quality report” for the result quality, which means these obtained data are not punctually sharp. This might be due to the solution containing inhomogeneous sizes (high PDI) or reaggregations of flakes<sup>71</sup>. After sonication, the software shows “good” result quality for most samples, which mean the deviation of the suspended flakes is low (observed from low PDI, appendix A). This might be due to the sonicated samples being more homogeneous in size. The sonication makes the samples more homogeneous since the energy from vibration is transferred equally to the flakes, and the flakes are broken down to the same degree.

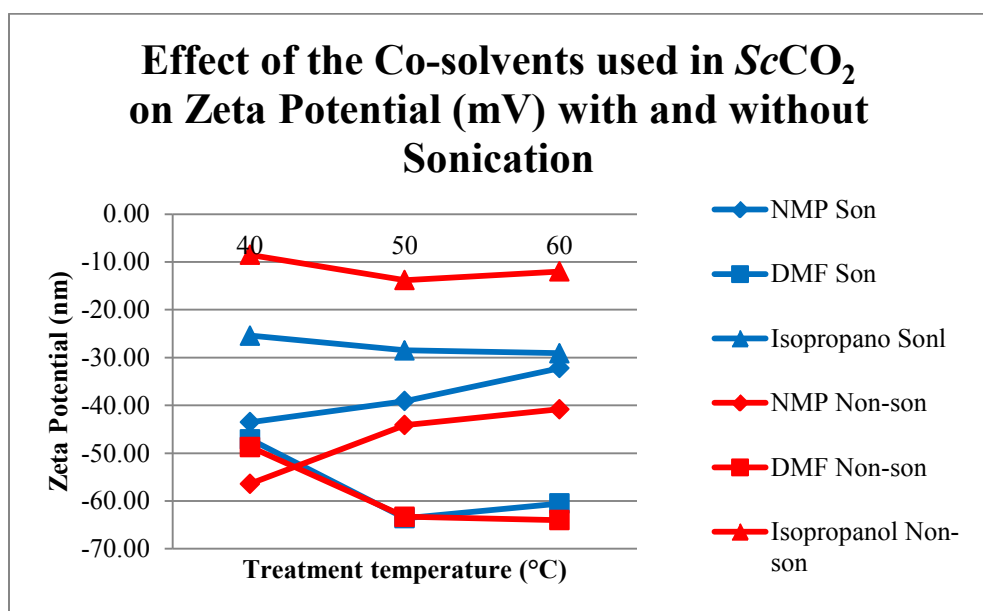


Figure 4.18 The zeta potential (mV) of sonicated and non-sonicated samples from different co-solvents used and treatment temperatures at 3000 psi.

In the case of the effects of sonication on the zeta potentials, the zeta potentials of the NMP- and DMF-sonicated samples tend to be smaller (lower) in terms of the negative charges than those of non-sonicated samples. This is because sonication breaks the graphitic flakes into small pieces. These broken pieces become less stable since they are smaller than those before sonication. Therefore, reaggregation could occur more easily than in large pieces. However, these are not important effects since the zeta potential of both the NMP- and DMF- samples before and after sonication are considered stable (the

zeta potentials less than -30 mV). Moreover, the zeta potentials of the samples before and after sonication are very similar. This trend is different from that in the isopropanol treated samples. In that case, the zeta potentials of the sonicated samples are approximately two times stronger than those of the non-sonicated samples in term of the negative charges. For isopropanol samples, both sonicated and non-sonicated samples may undergo reaggregation since their surface charges are less than -30 mV. In the sonicated samples, the flakes are broken up into smaller flakes and are more unstable than before. These broken flakes can be reaggregated more easily.

#### 4.1.4. Effects of treatment times on sizes and zeta potentials of graphitic flakes

To study the effects of the treatment times at one, two, and three hours on the sizes and the zeta potentials of the graphitic flakes, the supercritical carbon dioxide is set at 60°C and 3000 psi for one, two, and three hours. Additional one-hour sonication is applied after the supercritical treatment to compare with those of non-sonicated samples of each time. Table 4.4, Figure 4.19, 4.20, and 4.21 show the data of the diameters, z-average sizes, and zeta potentials of the flakes, respectively, for one-, two- and three-hour treatments with NMP with and without sonication.

**Table 4.4**

The sizes and zeta potentials (mV) of flakes obtained from the 1-hour, 2hour, and 3-hour treatment at 3000 psi and 60°C, with and without additional 1-hour sonication.

NMP was used as a co-solvent.

Condition	Time (hr)	Dimension (nm)	Z-ave.size (nm)	Zeta potential (mV)
3000psi/60 °C Sonication	1	105.10	85.58	-32.20
	2	137.70	168.30	-44.70
	3	161.70	235.10	-45.90
3000psi/60 °C No sonication	1	215.20	133.60	-40.80
	2	225.80	173.70	-47.10
	3	446.40*	1489.00*	-50.40

\* = the result is low quality due to a high PDI

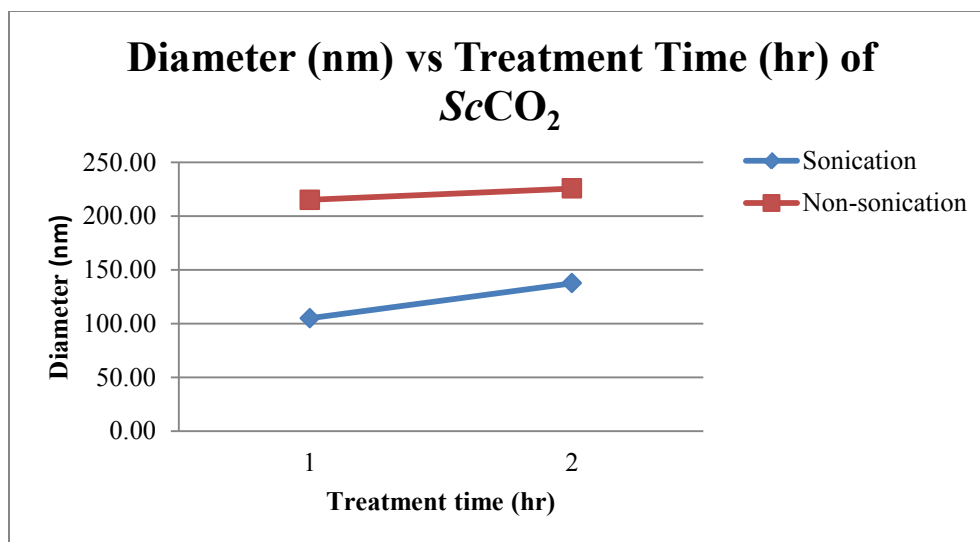


Figure 4.19 Effects of treatment time of supercritical  $\text{CO}_2$  treatment on diameter (nm) of graphitic flakes with and without additional sonication. NMP was used as a co-solvent.

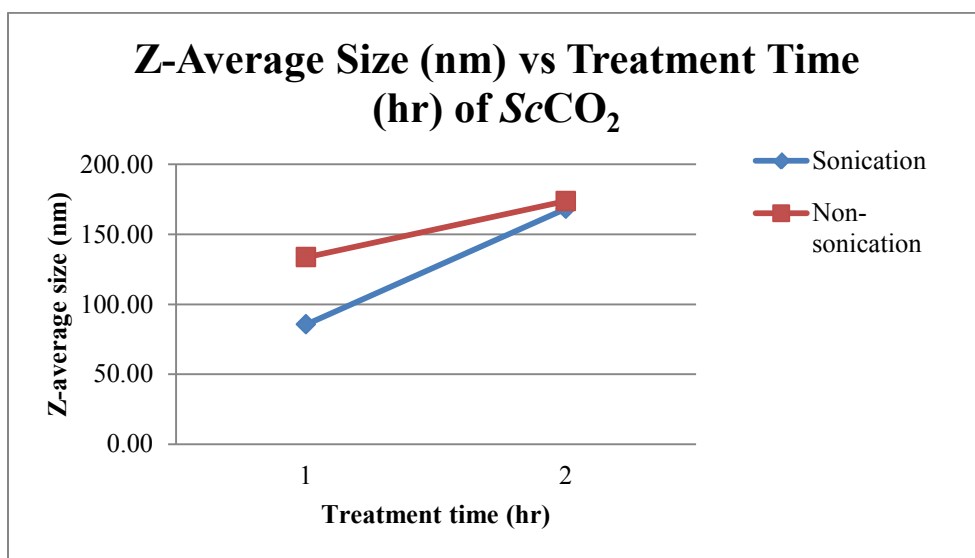


Figure 4.20 Effects of treatment time of supercritical  $\text{CO}_2$  treatment on z-average size (nm) of graphitic flakes with and without additional sonication. NMP was used as a co-solvent.

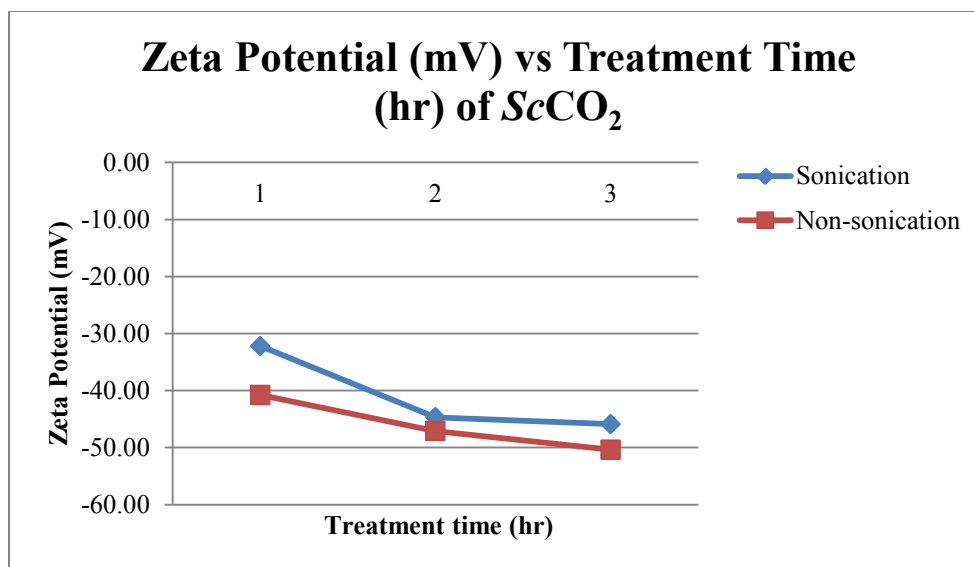


Figure 4.21 Effects of treatment time of supercritical  $\text{CO}_2$  treatment on zeta potential (mV) of graphitic flakes with and without additional sonication. NMP was used as a co-solvent.

In the case of the particle sizes, both diameters (Figure 4.19) and z-average sizes (Figure 4.20) have the same tendency to increase when treatment time increases. From Table 4.4, the diameters of sonicated flakes are 105.10 nm, 137.70 nm, and 161.70 nm for; and the z-average sizes are 85.58 nm, 168.30 nm, and 235.10 for 1, 2 and 3 hours treatment time, respectively. In the case of non-sonicated sample, the diameters of sonicated samples are 215.20 nm and 225.80 nm; and the z-average sizes are 133.60 nm and 173.70 nm for 1 and 2 hours treatment time, respectively. These are the same for both sonicated and non-sonicated samples. This may due to when the treatment time increases, the larger areas of graphite powder are exfoliated. As a result, we obtain larger flat graphenic materials. The non-sonicated sizes at 3 hours treatment time are not plotted in this case, since the PDI is extremely high (mean low accuracy of the data) (Figure A.19 (Appendix A)).

Examining zeta potentials with respect to treatment times (Figure 4.21), the zeta potentials tend to be more negative as the treatment times increase. However, the treatment time does not have a large effect on the zeta potential in sonicated sample (-32.20, -44.70, and -45.90 mV for 1, 2, and 3 hours treatment, respectively) and non-

sonicated sample (-40.80, -47.10, and -50.40 mV for 1,2, and 3 hours treatment, respectively). This may be because of the same reason that we obtain larger flat area sample since larger areas of graphite are exfoliated due to increasing of the treatment time. This large flat area sample has more stability due to the size is larger than that of shorter treatment. The zeta potentials of sonicated samples are less negative than non-sonicated samples at the same treatment time due to the flakes are broken down into smaller sizes from sonication. However, they are relatively close to each other and considered stable since the charges are more negative than -30 mV.

## **4.2. Brunauer, Emmett, and Teller (BET) analysis**

BET surface area analysis was done for both the N<sub>2</sub> and CO<sub>2</sub> adsorption. For the N<sub>2</sub> adsorption analysis, the analysis was done on untreated and treated graphite at different treatment conditions and co-solvents. The treated samples were selected from the highest (at 3000 psi, 40°C) to the lowest supercritical density treatment (at 2000 psi, 60°C) for easy comparison. For the comparison of the surface area of the sample obtained from different co-solvents treatment, the condition of 3000 psi and 40°C was fixed since, from the PCS data, the graphite layers were the most completely exfoliated and broken up. Therefore, the difference might be more easily noticed. In the case of the CO<sub>2</sub> adsorption, the purpose was to prove our hypothesis that CO<sub>2</sub> molecules could pass between the graphite layers better than N<sub>2</sub>, and compare the surface area between untreated and treated graphite. Since the adsorption process for CO<sub>2</sub> is very long due to its ability to intercalate between the layers, only untreated and graphite treated at 3000 psi and 40°C, the most highly exfoliated flakes, were analyzed. The experimental analysis and results of the BET for several samples are shown in Table 4.5 and 4.6, respectively. The BET surface area plots and the BET isotherm linear plots are shown in Figure 4.23-4.25 and 4.26-4.28, respectively.



**Table 4.5**

The BET experimental analysis. a = NMP, b = DMF, c = isopropanol,  
1 = analysis with N<sub>2</sub> adsorption, and 2 = analysis with CO<sub>2</sub> adsorption

Condition	Pressure (psi)	40°C	50°C	60°C
Sonication	2000			
	2500			
	3000			
No Sonication	2000			a(1)
	2500			a(1)
	3000	a(1,2),b(1),c(1)	a(1)	a(1)
Graphite		(1,2)		

**Table 4.6**

The BET surface areas of samples obtained from different supercritical carbon dioxide conditions.

Condition	Gas	Co-solvent	BET Surface Area (m <sup>2</sup> /g)
Graphite	N <sub>2</sub>	NMP	8.29
3000 psi, 40°C	N <sub>2</sub>	NMP	9.54
3000 psi, 50°C	N <sub>2</sub>	NMP	8.47
3000 psi, 60°C	N <sub>2</sub>	NMP	8.26
2500 psi, 60°C	N <sub>2</sub>	NMP	5.07
2000 psi, 60°C	N <sub>2</sub>	NMP	5.80
3000 psi, 40°C	N <sub>2</sub>	Isopropanol	7.53
3000 psi, 40°C	N <sub>2</sub>	DMF	10.00
Graphite	CO <sub>2</sub>	NMP	381.01
3000 psi, 40°C	CO <sub>2</sub>	NMP	-29.22

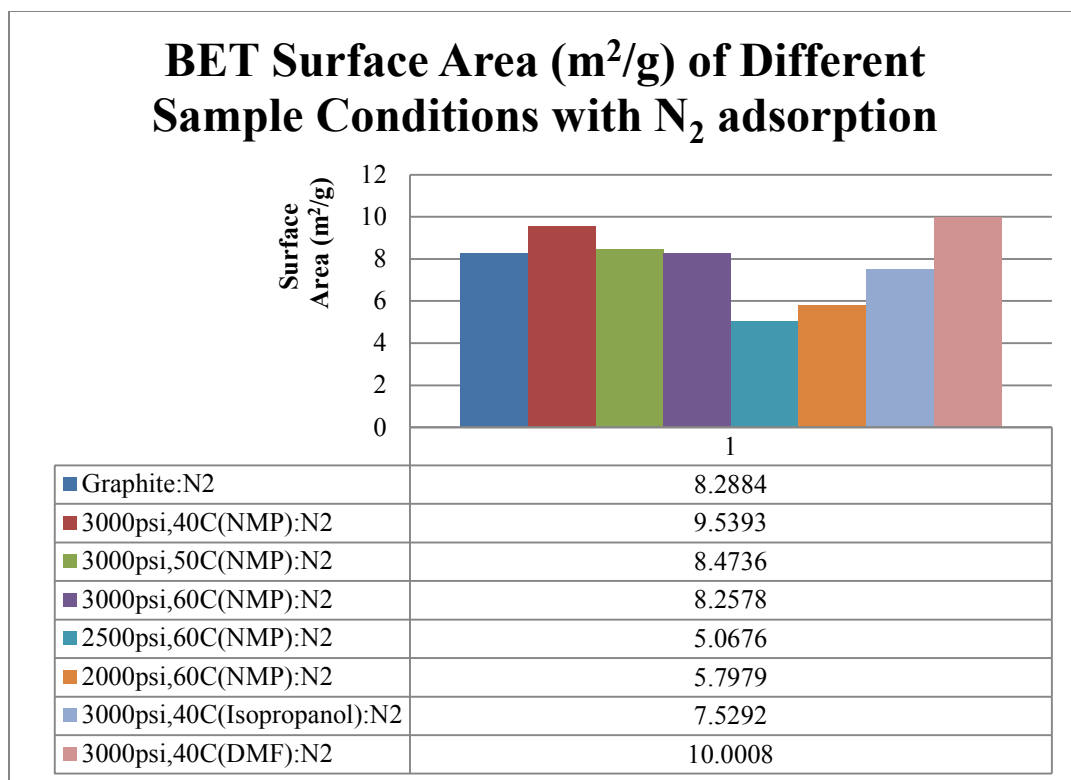


Figure 4.22 The differences in BET surface areas ( $\text{m}^2/\text{g}$ ) of various samples prepared by different supercritical conditions, co-solvents, with  $\text{N}_2$  adsorption.

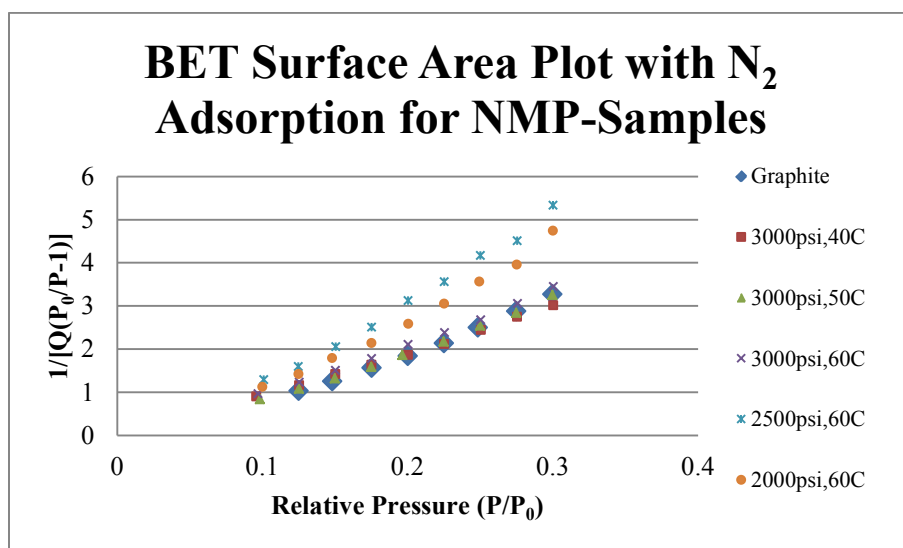


Figure 4.23 The BET surface area plot between relative pressure ( $P/P_0$ ) and value of  $1/[Q(P_0/P - 1)]$  with  $\text{N}_2$  adsorption of samples from different supercritical treatments.

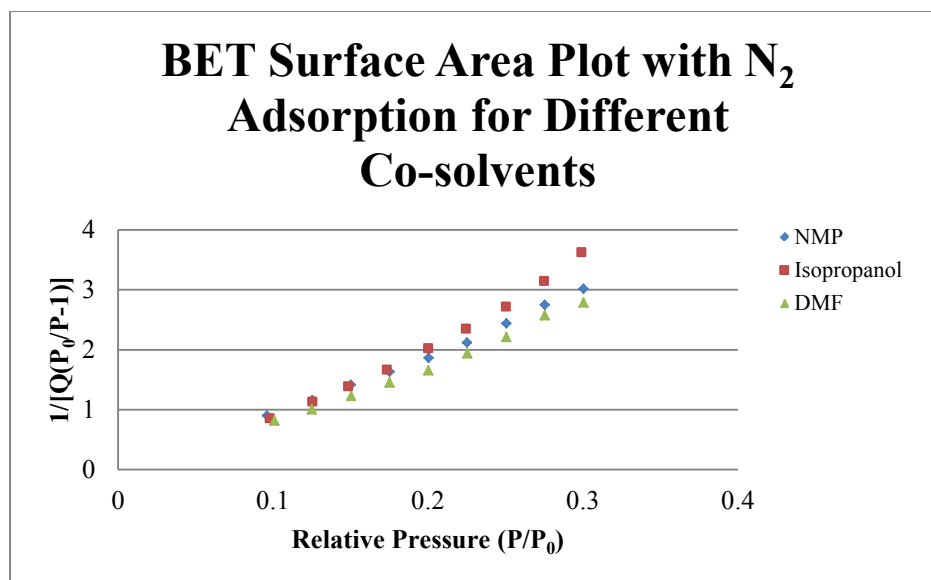


Figure 4.24 The BET surface area plot between relative pressure ( $P/P_0$ ) and value of  $1/[Q(P_0/P - 1)]$  with N<sub>2</sub> adsorption of samples from different co-solvents used in supercritical treatments at 3000 psi, 40°C.

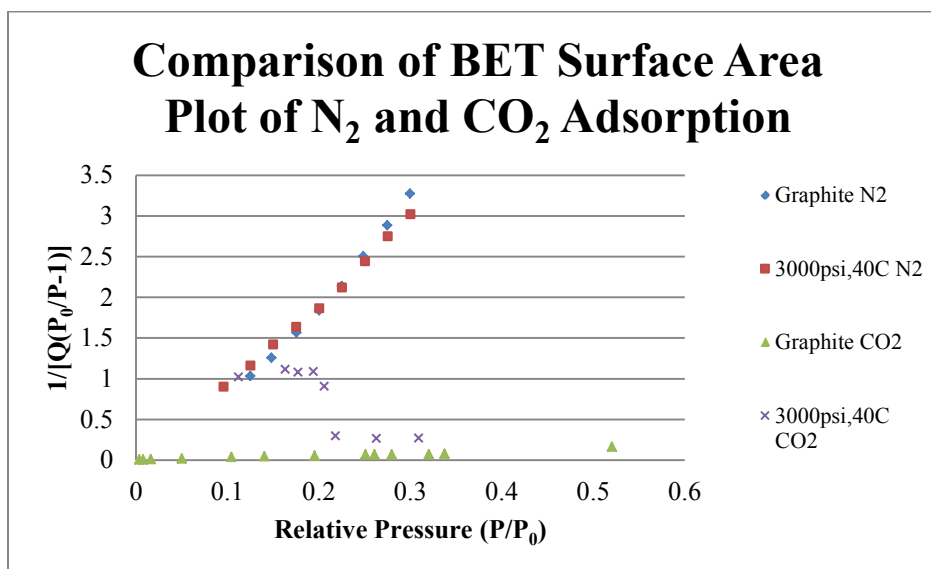


Figure 4.25 The BET surface area plot between relative pressure ( $P/P_0$ ) and value of  $1/[Q(P_0/P - 1)]$ , between N<sub>2</sub> and CO<sub>2</sub> adsorption of NMP-samples treated in supercritical treatments at 3000 psi, 40°C.

From Table 4.6 and Figure 4.22, the BET surface areas with N<sub>2</sub> adsorption of measured samples are slightly different from each other. This is because the low polarity of N<sub>2</sub> limits its ability to access the small volume between graphite layers<sup>76</sup>. Consequently, the absorption of N<sub>2</sub> can occur only on the outside of the graphite surface. This is completely different using CO<sub>2</sub> as the adsorption gas. In this case, although the molecule size of CO<sub>2</sub> is close to that of N<sub>2</sub>, CO<sub>2</sub> has higher polarity than that of N<sub>2</sub><sup>75,76</sup>. This allows carbon dioxide molecules to pass through and be adsorbed between the graphitic flakes. As a result, the BET surface area of untreated graphite with CO<sub>2</sub> adsorption is significantly higher than that of N<sub>2</sub>.

In the case of N<sub>2</sub> adsorption for NMP treated samples, the samples at 2500 psi and 60°C and at 2000 psi and 60°C had the smallest surface areas (5.07 and 5.80 m<sup>2</sup>/g, respectively), while at 3000 psi, 40°C had the largest surface area (9.54 m<sup>2</sup>/g), larger than untreated graphite powder (8.29 m<sup>2</sup>/g). This is because at 3000 psi and 40°C, the supercritical density of the supercritical carbon dioxide is the highest. Therefore, it can exfoliate and break down the graphite layer more completely than at a lower supercritical density. Consequently, the surface area measured by N<sub>2</sub> adsorption at this condition is the highest. In contrast, the supercritical carbon dioxide density at 2000 psi and 60°C is the lowest. At this condition, during the supercritical treatment, the graphite layers are not exfoliated as completely as at the highest critical density condition. Instead, the layers are expanded by the supercritical molecules of carbon dioxide which pass through and are adsorbed between the layers. This carbon dioxide adsorbed from the supercritical treatment may block the N<sub>2</sub> molecules during the BET surface measurement. As a result, the N<sub>2</sub> molecules are adsorbed less on the surface, and the measured surface area is less than the untreated graphite or high supercritical density treated graphite. Therefore, the sample at 2500 psi and 60°C should have more surface area than that of 2000 psi and 60°C. However, from Table 4.5 and Figure 4.22, the surface area of the 2500 psi and 60°C sample (5.07 m<sup>2</sup>/g) is slightly smaller than that of the 2000 psi and 60°C sample (5.80 m<sup>2</sup>/g). This is not significant and may be due to error in manually sample weighting. Figure 4.23 shows the plot between relative pressure (P/P<sub>0</sub>) and the value of

$1/[Q(P_0/P - 1)]$  of each sample. Using the BET equation<sup>79</sup>, the BET surface area can be calculated from the binomial equation of those lines.

To determining the effects of different co-solvents on the surface area with N<sub>2</sub> adsorption, the samples were run at supercritical condition of 3000 psi and 40°C with NMP, DMF and isopropanol. The surface areas are similar; however, the surface area of DMF-sample is the largest (10.00 m<sup>2</sup>/g), followed by those of NMP treated sample (9.54 m<sup>2</sup>/g) and isopropanol treated sample (7.53 m<sup>2</sup>/g), respectively (Table 4.5 and Figure 4.22). The low surface area of the isopropanol-sample may be due to reaggregation. Figure 4.24 shows the plot between relative pressure ( $P/P_0$ ) and the value of  $1/[Q(P_0/P - 1)]$  of each co-solvent used in the supercritical treatment at 3000 psi, 40°C.

In the case of CO<sub>2</sub> adsorption, the untreated graphite and treated sample at 3000 psi and 40°C were tested and compared with those of the N<sub>2</sub> adsorption. For the untreated graphite, the CO<sub>2</sub> adsorptive can provide much more surface area (381.01 m<sup>2</sup>/g) than that of the N<sub>2</sub> adsorption (8.29 m<sup>2</sup>/g) due to high polarity of CO<sub>2</sub><sup>70</sup>. However, for the treated sample, the surface area is negative (-29.22 m<sup>2</sup>/g). This might be due to the adsorbed carbon dioxide molecules from the supercritical treatment. When the CO<sub>2</sub> from the BET try to pass thought between the sample layers, they cannot be adsorbed since they are already occupied by the molecules from the supercritical treatment. Instead of adsorbing the BET CO<sub>2</sub>, the treated sample releases CO<sub>2</sub> stored between the layers during handling in the experiment. Consequently, the release CO<sub>2</sub> molecules are greater than that adsorbed. That is why the surface area calculated is negative for the treated sample. This does not occur with N<sub>2</sub>. N<sub>2</sub> molecules are adsorbed only on the outer surface of the sample. Figure 4.25 shows the plot between relative pressure ( $P/P_0$ ) and the value of  $1/[Q(P_0/P - 1)]$  of N<sub>2</sub> and CO<sub>2</sub> adsorption of untreated graphite and treated graphite at 3000 psi, 40°C with NMP as a co-solvent.

Ghosh A et al. measured the surface areas of graphene using BET with H<sub>2</sub> and CO<sub>2</sub> adsorption<sup>66</sup>. The graphenic samples were synthesized from the method using graphene oxide<sup>55,68</sup> and nanodiamond transformation<sup>71</sup>. As a result, BET surface areas of graphene

synthesized from graphene oxide were 639-1550 m<sup>2</sup>/g; and from nanodiamond conversion are 280-1013 m<sup>2</sup>/g, while completely single layer graphene is expected to have a surface area of 2600 m<sup>2</sup>/g<sup>66</sup>. These show that the surface areas of graphene do not only depend on types of the adsorption gas, but also synthesis methods. The surface areas measured are less than what is expected in the single layer graphene.

For isotherm linear plot which show the relationship between the quantity absorbed (mmol/g) and relative pressure ( $P/P_0$ ), the plots are shown in figure 4.26, 4.27, and 4.28. Figure 4.26 shows the relationship of the samples with N<sub>2</sub> adsorptive gas. The relationship shows that when the relative pressure increases, the quantity adsorbed tends to decrease at the beginning. However, when the relative pressure approaches one, the quantity adsorbed increased dramatically. This shows that when the equilibrium pressure of the sample ( $P$ ) is equal to the saturated pressure of the sample ( $P_0$ ),  $P/P_0 = 1$ , the ability to absorb gas reaches its highest point. Moreover, the order of the conditions for quantity absorbed at the same relative pressure points of the samples is (from highest to lowest) 3000 psi and 40°C; 3000 psi, and 50°C; 3000 psi and 60°C; untreated graphite; 2000 psi and 60°C; and 2500 psi and 60°C; respectively. The surface area is determined by the quantity of the adsorbed gas on the sample; therefore, the surface areas have the same order.

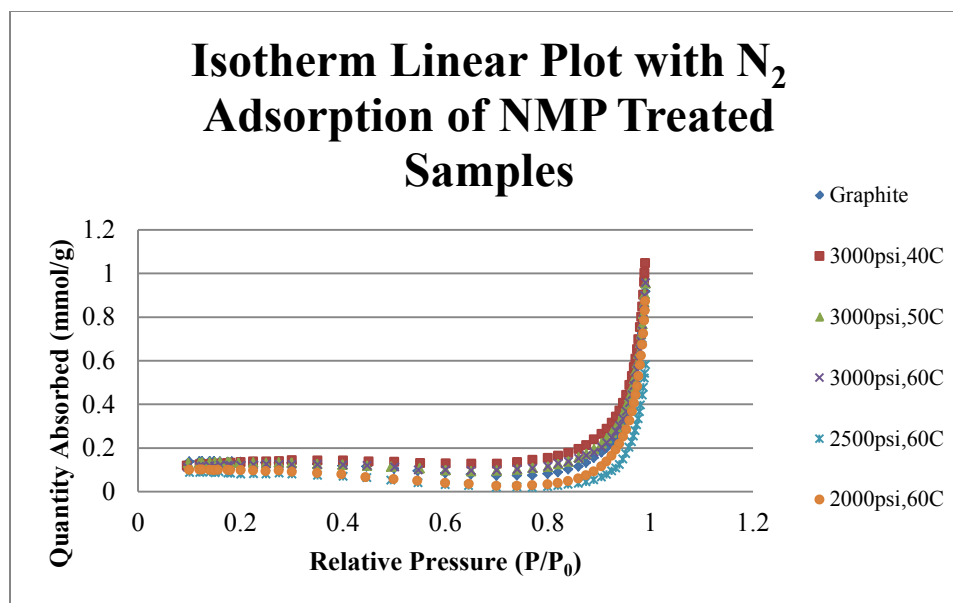


Figure 4.26 The isotherm linear plot between relative pressure ( $P/P_0$ ) and quantity absorbed (mmol/g) of N<sub>2</sub> adsorption for the original graphite and NMP treated graphites from different conditions of supercritical treatment.

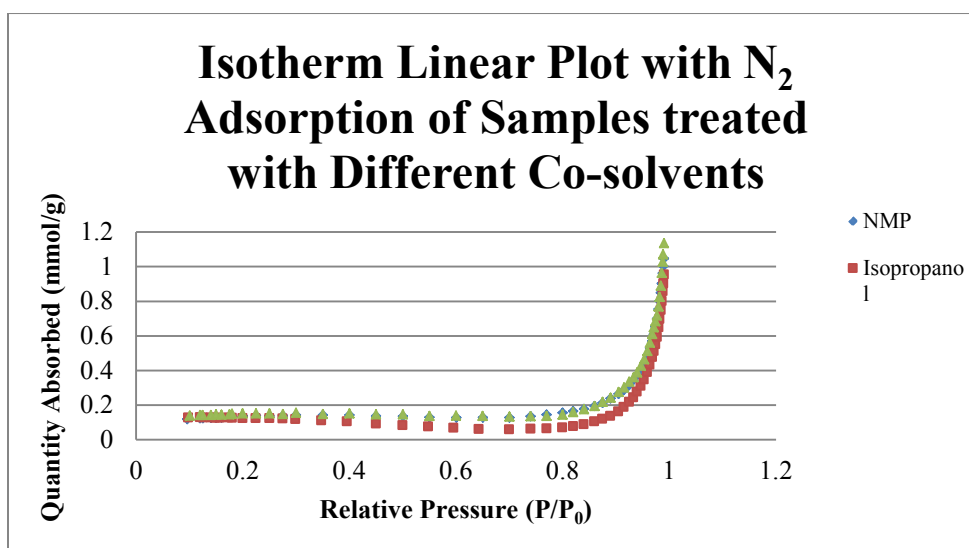


Figure 4.27 The isotherm linear plot between relative pressure ( $P/P_0$ ) and quantity absorbed (mmol/g) of N<sub>2</sub> adsorption for the treated graphites with different co-solvents used in supercritical treatment at 3000 psi and 40°C.

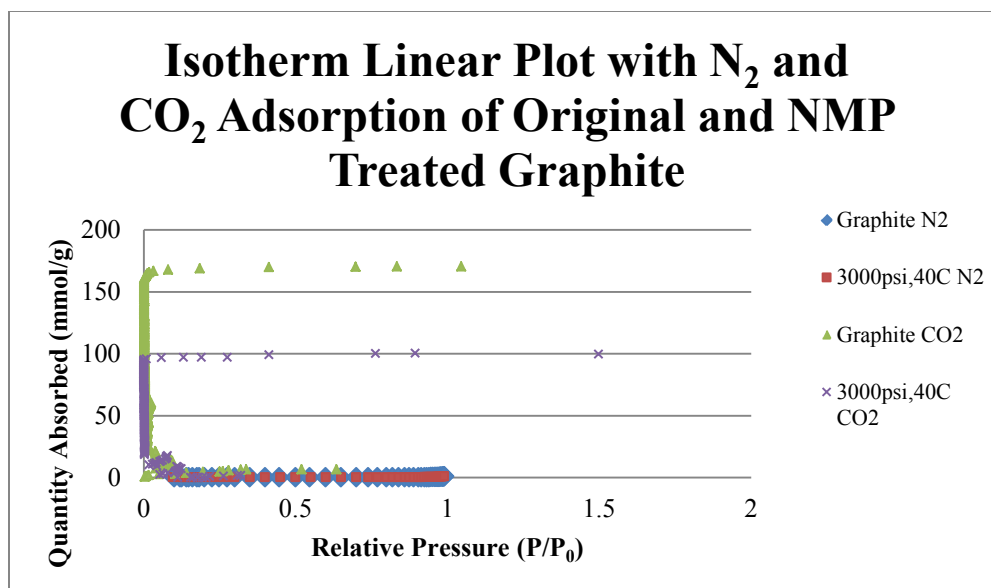


Figure 4.28 The isotherm linear plot between relative pressure ( $P/P_0$ ) and aquantity absorbed(mmol/g) of  $N_2$  and  $CO_2$  for the original and treated graphites. The supercritical treatment was operated at 3000 psi, 40°C with NMP as a co-solvent.

For the relationship between the quantity absorbed (mmol/g) and relative pressure ( $P/P_0$ ) of the samples with different co-solvents used, a plot is shown in Figure 4.27. The samples were treated at supercritical condition of 3000 psi and 40°C with NMP, DMF, and isopropanol as co-solvents. The trend of the relationship is similar to that in Figure 4.26 and can be explained in the same way. The quantity of  $N_2$  absorbed of the NMP- and DMF- samples are equal at the same relative pressures. However, that of isopropanol-sample is noticeably lower than those of the NMP- and DMF- samples. This may be due to reaggregation of the flakes. Since isopropanol has the lowest dielectric constant compared to those of NMP and DMF, reaggregation occurs significantly in the isopropanol sample before the degasification process. This reaggregation reduces the adsorbing surfaces of the flakes. As a result, the  $N_2$  molecules are somewhat less adsorbed and the surface area is the lowest for isopropanol-sample.

For the effects of different adsorptive gases on the quantity adsorbed, the  $N_2$  and  $CO_2$  gases were used as adsorptive materials. The untreated graphite and treated graphite at 3000 psi and 40°C, with NMP co-solvent, were used in the comparison. The relationship



between the quantity absorbed (mmol/g) and relative pressure ( $P/P_0$ ) of  $N_2$  and  $CO_2$  adsorptive gases is shown in Figure 4.28. For  $CO_2$ , the absorption increases dramatically even at very low relative pressure. This means when  $CO_2$  gas is injected into the sample, it is absorbed immediately due to its ability to pass readily between the graphitic layers. When it reaches a maximum point, the quantity adsorbed becomes stable. The relative pressure increases at this point since  $CO_2$  molecules are no longer adsorbed. The untreated graphite adsorbed more  $CO_2$  molecules than the treated graphite due to more unoccupied spaces. When compared with the quantity absorbed of  $N_2$  molecules, the quantity adsorbed of  $CO_2$  is much more significant at the same conditions.

### 4.3. FE-SEM images

The purpose of FE-SEM analysis is to observe the shape and morphology of the flakes obtained. Therefore, there is no need to do the analysis for flakes obtained at all treatment conditions. The samples obtained from the highest temperature treatment ( $60^\circ C$ ) were analyzed because the PCS data shows that the flakes at  $60^\circ C$  and 2000 psi without sonication were the largest. However, the sample obtained from  $40^\circ C$  and 3000 psi was also observed in 9.94 mg/mL SDBS solution for more comparison. The 0.5 mg/mL SDBS solution left some undesirable residue. This residue ultimately conceals the appearance of the flakes in the FE-SEM image. To avoid the effect of the remaining surfactant, the samples were prepared in two ways. The first method was to deposit the NMP sample containing flakes directly onto the sample holder. NMP will evaporate completely without any residues. Only the flakes will remain on the sample holder. The second method is to drop the NMP sample into a 9.94 mg/mL SDBS solution (1% w/w of SDBS in water). At this concentration, the residue will cover all of the sample holder surface, including the deposited flakes. The deposited flakes were also observed under this condition. In this analysis, the Hitachi S-4700 FE-SEM is used to observe the graphitic flakes. The samples prepared at  $60^\circ C$  with the pressures of 2000, 2500, and 3000 psi are observed. The samples do not need to be coated by metal before doing FE-SEM since they are conductive. Moreover, coating interferes with the flakes appearance on the FE-SEM images. The beam energy, working distance and scan speed were

adjusted to yield the highest quality of the images. The experimental analysis are shown in Table 4.7.

**Table 4.7**

The experimental analysis for FE-SEM.

Condition	Pressure (psi)	40°C	50°C	60°C
NMP No sonication	2000			Y
	2500			Y
	3000			Y
9.94 mg/mL SDBS Sonication	2000			Y
	2500			Y
	3000	Y		Y

#### **4.3.1. FE-SEM images for the samples in N-methyl pyrrolidinone (NMP) without additional sonication**

Figure 4.29 shows the FE-SEM image of sampled NMP after 60°C and 3000 psi treatment with 3k× magnification. The deposited flakes, small pale pieces, are scattered randomly on the sample holder. Most of the flakes are less than 0.5 micron. These sizes are comparable to the diameter (215.20 nm) and z-average size (133.60 nm) of the NMP treated flakes with no sonication at 60°C and 3000 psi of the PCS data (table 4.2). However, several large pieces with diameters larger than one micron, occur. This may be due to reaggregation since the sample holder was coated three times. The roughness of the sample holder is shown as unordered pattern on the background.

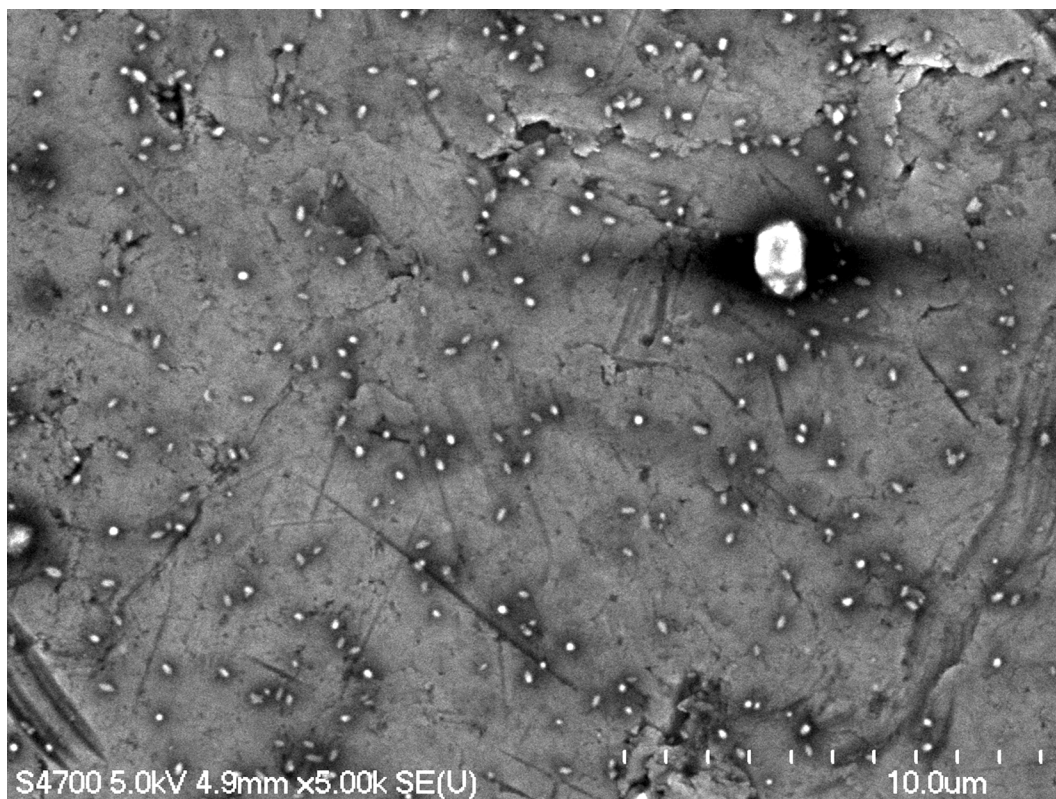


*Figure 4.29 FE-SEM image of NMP treated sample from 60°C and 3000 psi treatment. The Hitachi S-4700 FE-SEM was used at 5.0 kV beam energy, 4.9 mm working distance, and 5k $\times$  magnification, with slow scan speed. The sample holder was dosed three times.*

From Figure 4.30, which show the FE-SEM images of sampled NMP after 60°C and 2500 psi treatment with 6k $\times$  magnification, the deposit flakes, small pale pieces, are scattered randomly on the sample holder. Their sizes are approximately 0.5 micron in diameter. These sizes are comparable to the diameter (207.10 nm) and z-average size (167.80 nm) of non-sonicated samples observed by the PCS analysis of the treated flakes at 60°C and 2500 psi (Table 4.2). Reaggregation cannot be observed clearly since the sample holder was dosed once. The roughness of the sample holder is shown as unordered pattern on the background.



*Figure 4.30 FE-SEM of NMP treated sample from 60°C and 2500 psi treatment. The Hitachi S-4700 FE-SEM was used at 5.0 kV beam energy, 5.0 mm working distance, and 6k $\times$  magnification, with fast scan speed. The sample holder was dosed once.*

Figure 4.31 shows the FE-SEM images of sampled NMP after 60°C and 2000 psi treatment with 10k $\times$  magnification, respectively. The supercritical density of CO<sub>2</sub> is lowest at this condition. From the PCS data, the non-sonicated flakes are the largest, compared to other conditions. From the images, the deposit flakes show some unique patterns with approximately sizes one micron. This might be because at 60°C and 2000 psi, where the supercritical density is the lowest, the flakes were not exfoliated and broken down as much as at higher supercritical density. Therefore, the sizes are larger than those of at higher supercritical density. However, the flakes in Figure 4.36-4.38 are relatively larger than the diameter (175.50nm) and z-average size (167.80) of non-sonicated samples shown at this condition in the PCS data (table 4.2). This may be because the FE-SEM specifically observes the samples in a small area, and does not calculate the distribution data as completely as the PCS do.

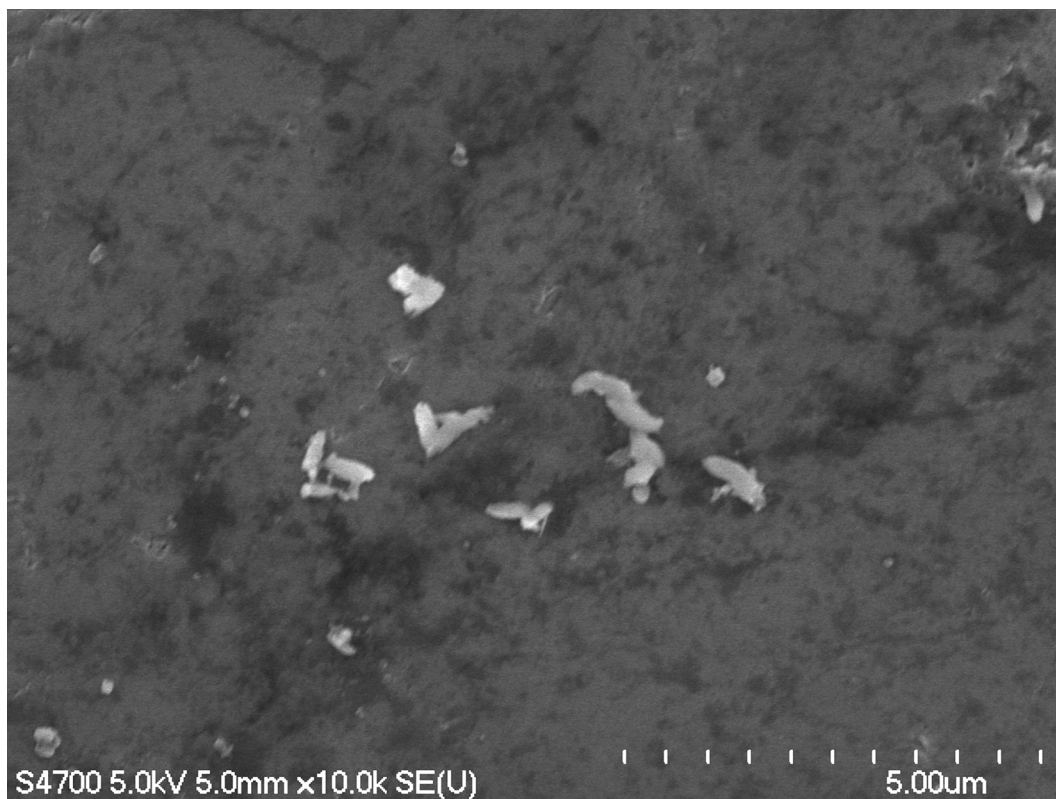


*Figure 4.31 FE-SEM of NMP treated sample from 60°C and 2000 psi treatment. The Hitachi S-4700 FE-SEM was used at 5.0 kV beam energy, 5.0 mm working distance, and 10k $\times$  magnification, with fast scan speed. The sample holder was dosed once.*

In conclusion, for samples collected in NMP without additional sonication (Figures 4.29-4.31), the flakes appear to be in a very small size range. The largest sizes are approximately one micron, while the smallest sizes are smaller than 0.5 microns. Large chunks (two microns) could be due to reaggregation. Reaggregation of the flakes is clearly noticeable for the treatment at 60°C and 3000 psi (Figures 4.29). This is due to the preparation procedure of the FE-SEM sample that used three dosages of the samples onto the sample holder, while other NMP treated samples are only one dosage. The relationship between the sizes and the pressures is not clear from these images. The flakes appear in many shapes and sizes.

#### **4.3.2. FE-SEM images for the samples in a one percent by weight solution of sodium dodecylbenzene sulfonate (SDBS) with additional one-hour sonication**

The FE-SEM images of samples in 9.94 mg/mL SDBS surfactant are shown in Figure 4.32-4.35. Figure 4.32 shows the FE-SEM image of the sonicated flakes at 60°C and 3000 psi treatment in 9.94 mg/mL SDBS surfactant at 3k $\times$  magnification, respectively. The images show different features than the flakes prepared in NMP (Figure 4.29-4.31). In this case, the flakes are larger with approximate sizes more than three microns. The sizes are relatively larger than the diameter (105.10 nm) and z-average size (85.58 nm) shown in the PCS data of the sonicated flakes at 60°C and 3000 psi (Table 4.2). This might be because the small flakes reaggregate due to the low stability of the water-based surfactant (SDBS). Some reaggregation can be seen in Figure 4.32. Moreover, several layers can be clearly seen in many flakes. This shows that most of the flakes are not a single layer material. The roughness of the sample holder cannot be observed since the surface is covered by the SDBS surfactant residue.

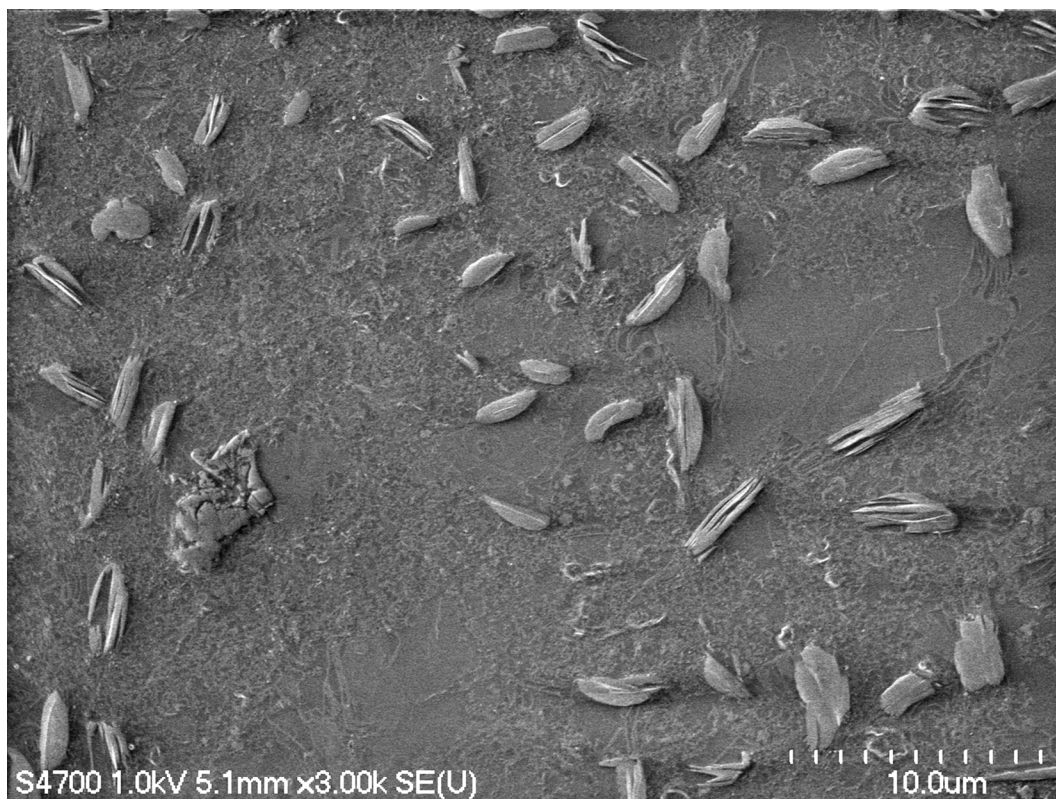


*Figure 4.32 FE-SEM image of the sample from 60°C and 3000 psi treatment in a 1% w/w solution of SDBS. The Hitachi S-4700 FE-SEM was used at 1.0 kV beam energy, 5.1 mm working distance, and 3k $\times$  magnification, with fast scan speed. The sample holder was dosed three times.*

Figure 4.33 show the FE-SEM image of the sonicated flakes with 60°C and 2500 psi treatment in 9.94 mg/mL SDBS surfactant at 3k $\times$  magnification, respectively. The sizes of the flakes are various (Figure 4.33). If compared with those of at 60°C and 3000, the layers of the flakes at 60°C and 2500 psi cannot be seen as clearly as at 60°C and 3000. This might be due to the effect of sonication since at 60°C and 2500 psi, the layers were not exfoliated or broken up as completely as at 60°C and 3000 psi. Therefore, when sonication was applied, the sonicated flakes of 60°C and 2500 psi became more exfoliated and broken down than the sonicated flakes treated at 60°C and 3000 psi. As a result, the layers of the flakes of 60°C and 2500 psi are less visible than those of 60°C and 3000 psi after sonication. This result is in agreement with the PCS data. However, the sizes are larger than the diameter (85.28 nm) and z-average (96.86 nm) of the PCS

analysis for the sonicated sample at 60°C and 2500 psi due to low stability of the water-based surfactant (SDBS).



*Figure 4.33 FE-SEM image of the sample from 60°C and 2500 psi treatment in a 1% w/w solution of SDBS. The Hitachi S-4700 FE-SEM was used at 1.0 kV beam energy, 5.2 mm working distance, and 3k $\times$  magnification, with fast scan speed. The sample holder was dosed three times.*

Figure 4.34 shows the FE-SEM image of the sonicated flaked of 60°C and 2000 psi treatment in 9.94 mg/mL SDBS surfactant at 3k $\times$  magnification, respectively. The images show that these flakes are obviously smaller than those of 60°C and 3000 psi (Figure 4.32) and 60°C and 2500 psi (Figure 4.33). Moreover, the layers of the flakes are difficult to see. This could be explained using the PCS data (Table 4.2). At 60°C and 2000 psi, the treated flakes are the largest if compare with other conditions due to low supercritical density, which leads to low degree of exfoliation. However, when sonication was applied, these incompletely exfoliated flakes are broken up and exfoliated more than those treated at high supercritical density where the flakes are more completely exfoliated. As a result,



the sonicated flakes at 60°C and 2000 psi are smaller and contain fewer layers. Also, the sizes are relatively larger than the diameter (78.66 nm) and z-average (82.15 nm) obtained from the PCS analysis for the sonicated sample at 60°C and 2500 psi due to low stability of the water-based surfactant (SDBS).

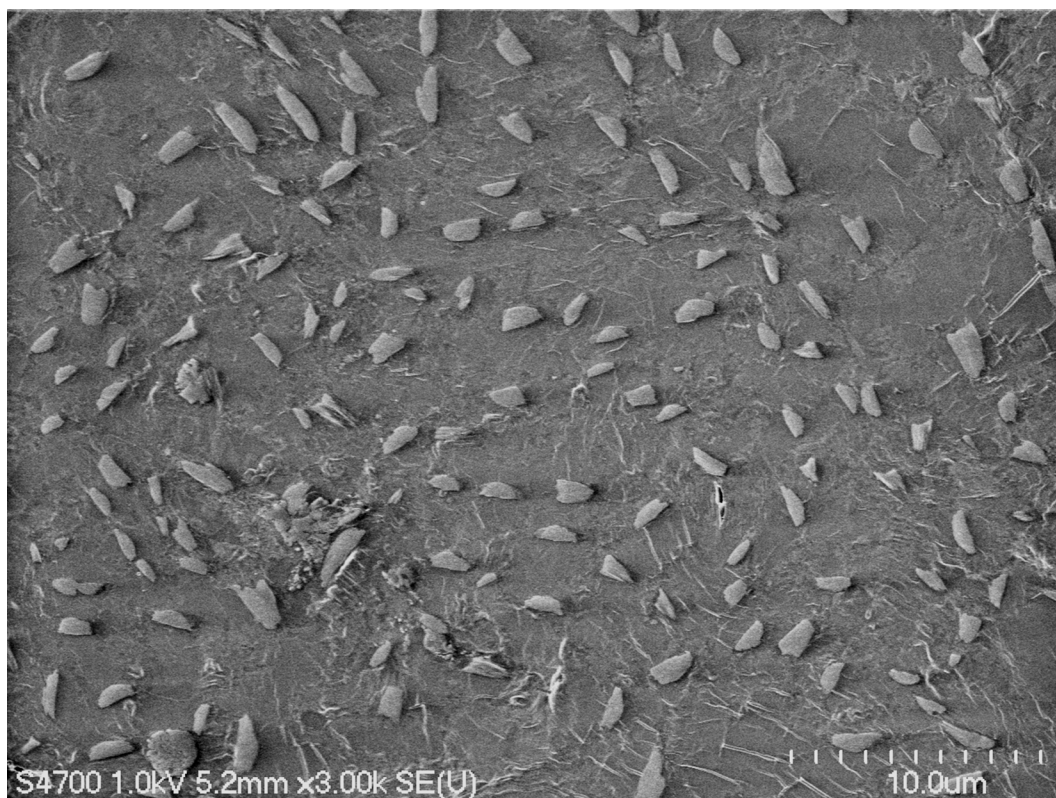


*Figure 4.34 FE-SEM image of the sample from 60°C and 2000 psi treatment in a 1% w/w solution of SDBS. The Hitachi S-4700 FE-SEM was used at 1.0 kV beam energy, 5.2 mm working distance, and 3k $\times$  magnification, with fast scan speed. The sample holder was dosed three times.*

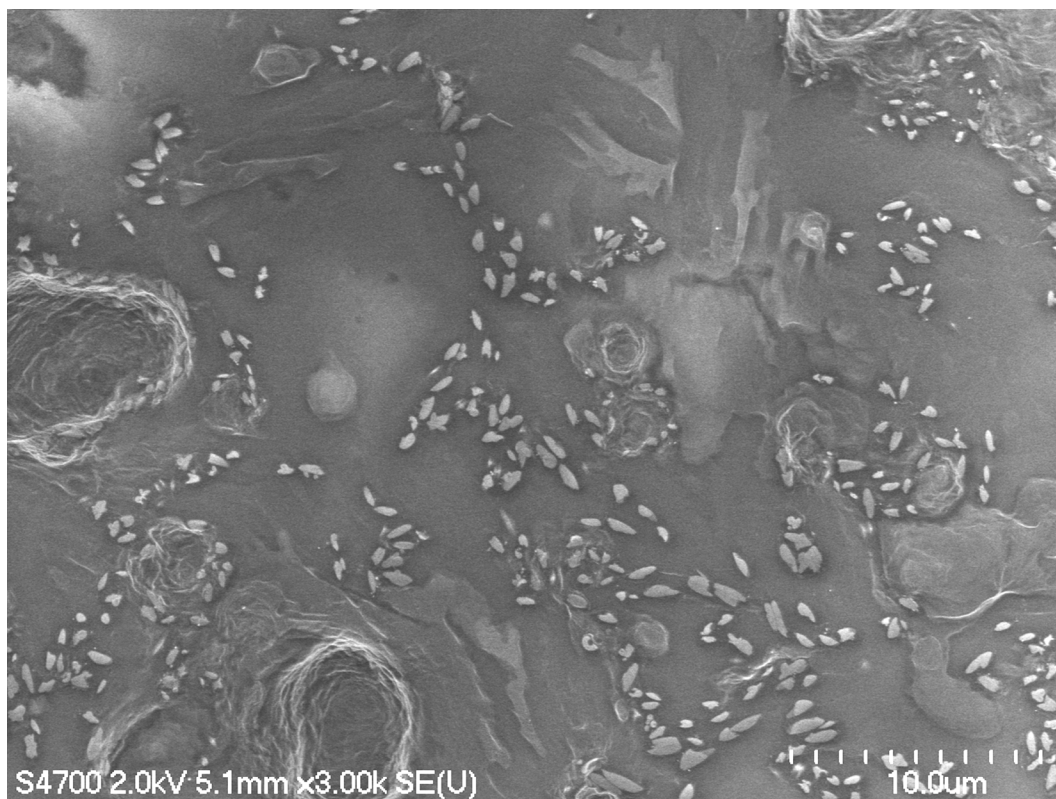


*Figure 4.35 FE-SEM image of the sample from 40°C and 3000 psi treatment in a 1% w/w solution of SDBS. The Hitachi S-4700 FE-SEM was used at 2.0 kV beam energy, 5.1 mm working distance, and 3k $\times$  magnification, with fast scan speed. The sample holder was dosed three times.*

Figure 4.35 shows the FE-SEM image of the sonicated flaked of 40°C and 3000 psi treatment in 9.94 mg/mL SDBS surfactant at 3k $\times$  magnification. At 40°C and 3000 psi, the supercritical density is the highest compared to other conditions. The sizes of the flakes are smallest compared to the other FE-SEM images. Moreover, the layers of the flakes cannot be seen. This might be because these flakes contain only a very few layers. This high degree of exfoliation is due to the high supercritical density treatment. Moreover, when sonication was applied after the treatment, those flakes were exfoliated more completely. The FE-SEM flakes at 40°C and 3000 psi (Figure 4.35) are slightly larger than the diameter (130.90 nm) and z-average size (111.40 nm) of the sonicated flakes at this condition as shown in the PCS data (Table 4.2). Moreover, the PCS data show that the sonicated flakes of 60°C and 2000 psi should have smaller size than those of 40°C and 3000 psi. However, if we consider the zeta potentials, the flakes of 60°C and

2000 psi are less stable than those of 40°C and 3000 psi (Table 5). Therefore, the reason that the lateral sizes of the flakes of 60°C and 2000 psi become larger than those of 40°C and 3000 psi might be due to reaggregation. Reaggregation might be severe from the water-based surfactant and the FE-SEM preparation that needs to leave the sample for long time to let the surfactant evaporate. However, the layers of the both flakes of 60°C and 2000 psi and 40°C and 3000 psi are not clearly seen. This shows that both the high critical density treatment condition together with additional sonication can produce few graphene layers materials from synthetic graphite.

However, the FE-SEM does not allow us distinguish the quantitative differences between the flakes obtained at different treatment conditions. It can give us an overview of what the graphitic flakes look like, but cannot quantity the differences between flakes. With these limitations, the transmission electron microscopy (TEM) needs to be used in future studies to examine these smaller details.

#### **4.4. AFM analysis**

For AFM analysis, samples were prepared by depositing the exit NMP sample directly on a silicon substrate, which has a low surface roughness<sup>3,21</sup>. The substrate was cleaned by thirty minutes sonication in a water bath then washed by DI water and ethanol. Like FE-SEM, AFM can observe flakes only in specific areas. It cannot determine the average size of the flakes or reveal clearly the effect of the treatment condition of the flakes. The main objective of AFM is to determine the vertical thickness of the flakes to approximately determine its numbers of layer as well as its shape via the tip-surface interaction. To construct a sharp image, the flakes obtained from 60°C treatment were considered since it can produce larger flakes than at lower temperature. The experimental analysis and the results are shown in Table 4.8 and Table 4.9, respectively. In this analysis some AFM images and size analysis are shown in Figure 4.36-4.39.

**Table 4.8**

The experimental analysis for AFM.

Condition	Pressure (psi)	40°C	50°C	60°C
NMP Non-sonication	2000			Y
	2500			Y
	3000			Y

**Table 4.9**

The horizontal and vertical sizes of the flakes at some supercritical conditions.

Condition	Flake Number	Horizontal distance (nm)	Vertical distance (nm)
60°C, 3000 psi	1.1	1006.000	182.910
	1.2	1367.000	145.550
	1.3	556.640	49.997
60°C, 2500 psi	2.1	1465.000	59.153
	2.2	488.280	48.630
	2.3	1074.000	51.750
	2.4	205.080	6.670
	2.5	537.110	52.064
	2.6	224.610	12.488
	2.7	390.630	35.382
	2.8	156.250	21.793
	2.9	332.030	10.157
	2.10	97.656	1.897
	2.11	87.891	1.864
	2.12	93.750	3.703
	2.13	74.219	1.816
	2.14	64.453	2.135
60°C, 2000 psi	3.1		10.129
	3.2		204.130
	3.3	195.310	48.536
	3.4	468.750	78.791
	3.5	419.920	160.650
	3.6	537.110	83.522
	3.7	332.030	35.846
	3.8	175.780	62.432
	3.9	292.970	37.390
	3.10	195.310	20.081
	3.11	107.420	58.594
	3.12	62.500	3.707
	3.13	68.359	4.507

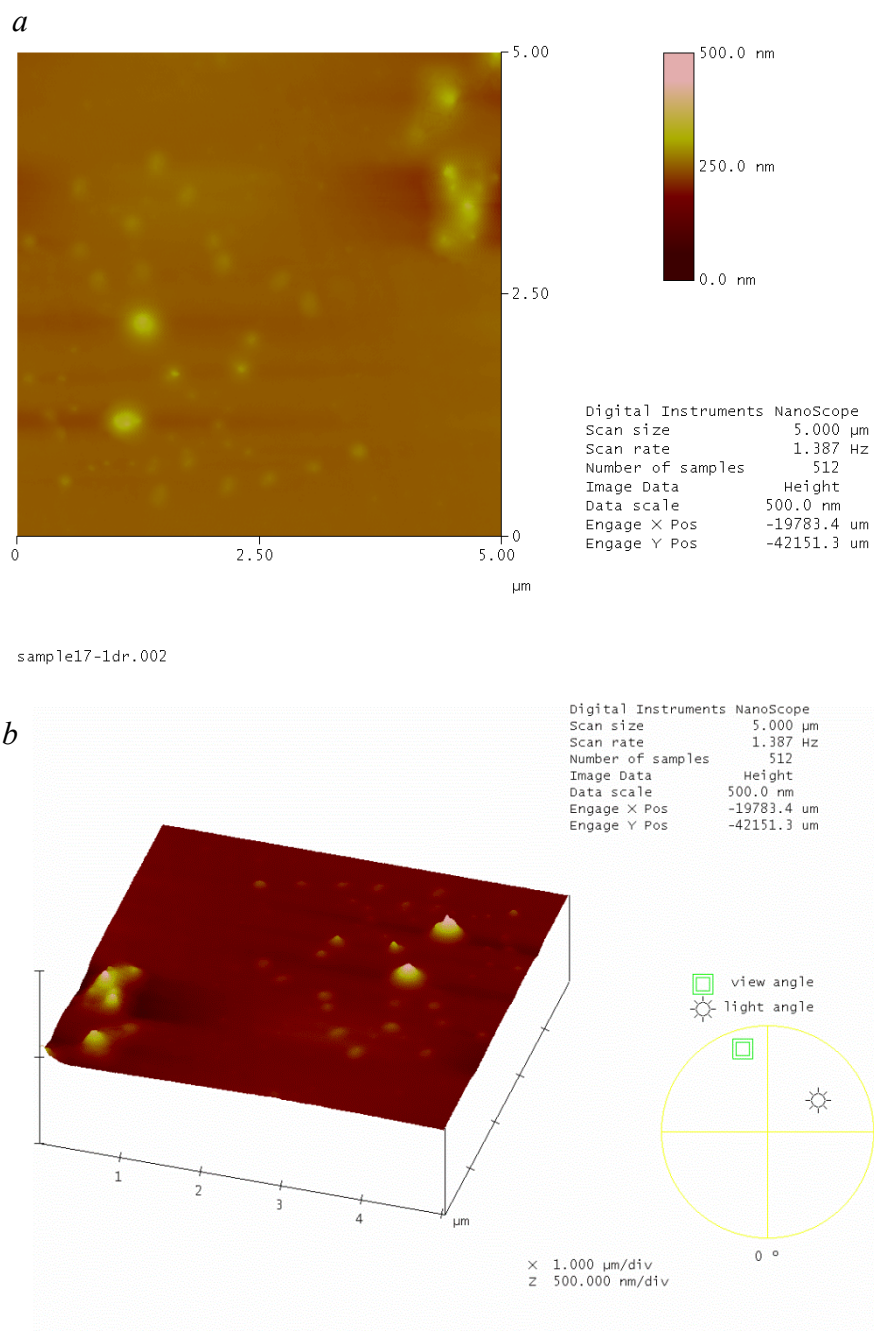


*Figure 4.36 AFM two- (a) and three-dimensional image (b) of the graphitic flakes obtained from 60°C and 2000 psi treatment, on the silicon substrate. The image was constructed at a 5.00 μm scan size, a 1.387 Hz scan rate, 512 numbers per line, and a 500.0 nm data scale.*

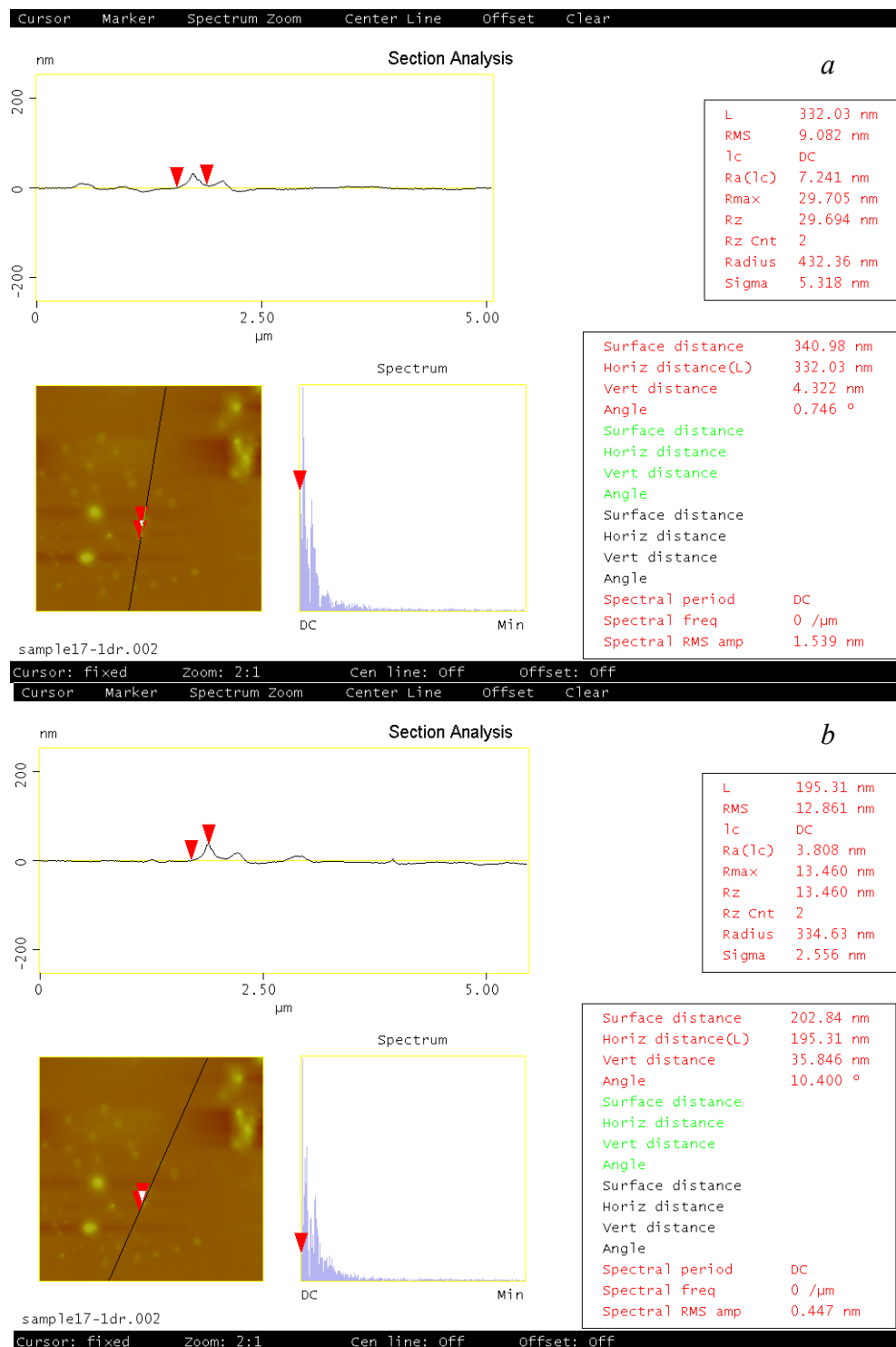
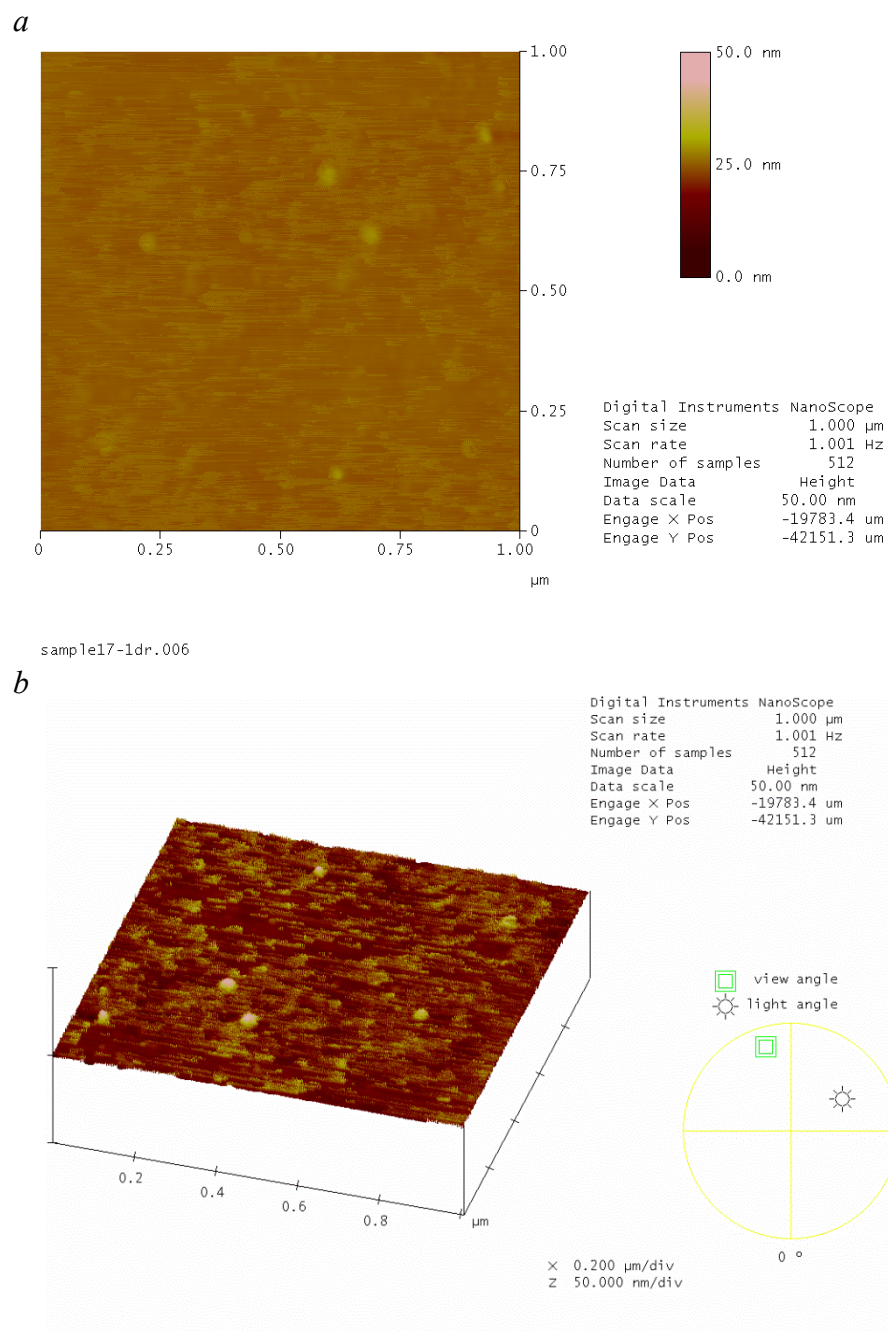


Figure 4.37 Horizontal (a) and vertical section analysis (b) of the flake 3.7 of Figure 4.53 (60°C, 2000 psi). The image was constructed at a 5.00 μm scan size, a 1.387 Hz scan rate, 512 numbers per line, and a 500.0 nm data scale.



*Figure 4.38 AFM two- (a) and three-dimensional image (b) of the graphitic flakes obtained from 60°C and 2000 psi treatment, on the silicon substrate. The image was constructed at a 1.00 μm scan size, a 1.001 Hz scan rate, 512 numbers per line, and a 50.00 nm data scale.*



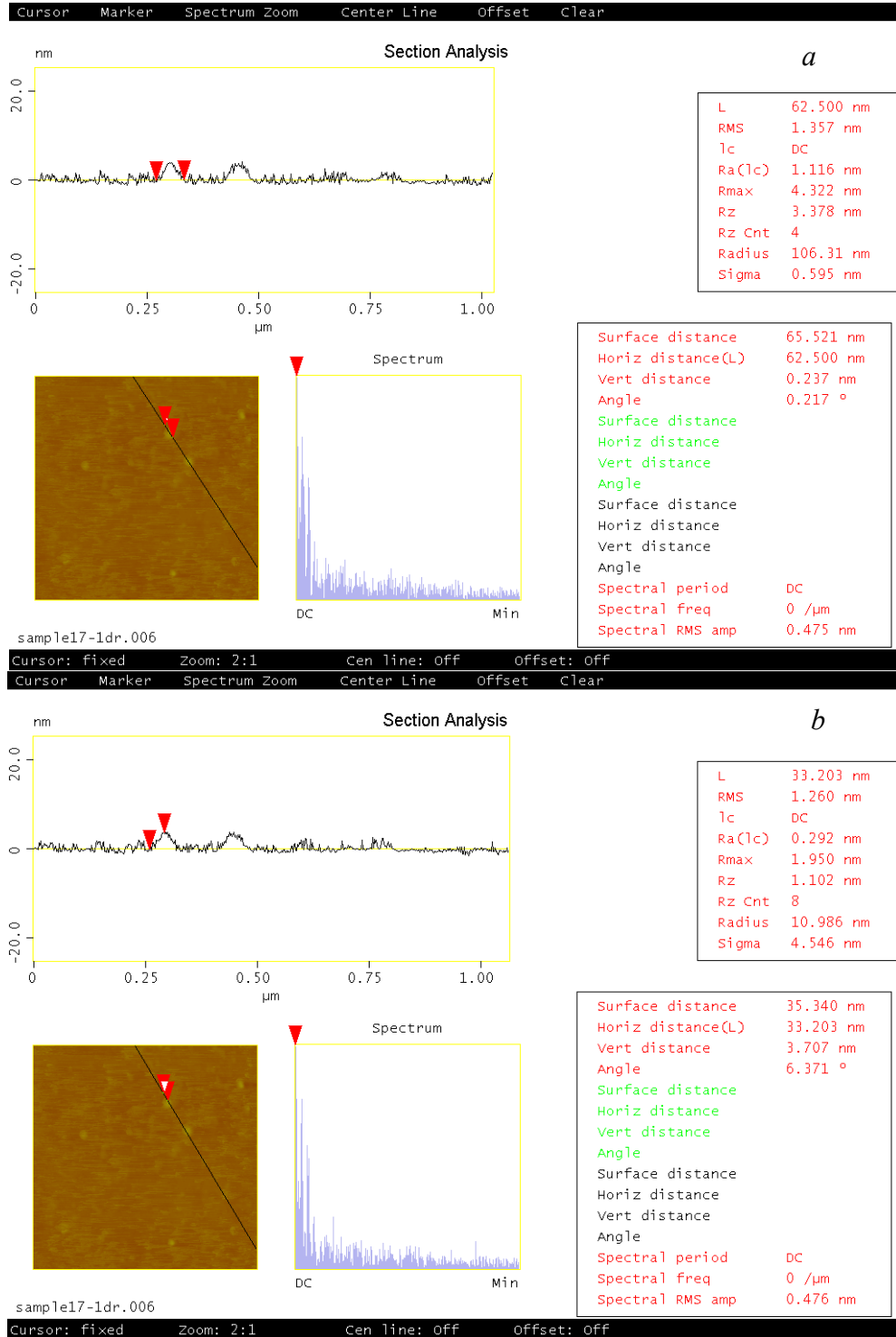


Figure 4.39 Horizontal (a) and vertical section analysis (b) of the flake 3.12 of Figure 4.55 (60°C, 2000 psi). The image was constructed at a 1.00 μm scan size, a 1.001 Hz scan rate, 512 numbers line, and a 50.0 nm data scale.

The AFM samples were prepared by dropping the NMP carrier solution, which contains the graphitic flakes from the supercritical carbon dioxide treatment, directly onto the silicon substrate<sup>3,21</sup>. The water-based surfactant (SDBS) was not used for the AFM samples since it affects the topography of the image due to residual surfactant when it dries out. The samples were put in a chemical hood to let the NMP co-solvent evaporate, until only the treated flakes on the substrates remained. The exiting NMP was collected from the release valve of the supercritical carbon dioxide extractor. The supercritical conditions were set at 60°C and 3000, 2500, and 2000 psi. From the zeta analysis data, the flakes sizes of these samples are the largest, with low stability. Therefore, they might be easier to observe by AFM than the small flakes of the treatments at 40° and 50°C. At these treatment temperatures, the critical densities are higher than that of at 60°C at the same pressure, so some features might be distorted or lost due to the more complete exfoliation. The samples were not sonicated since sonication could destroy the original features of the flakes obtained.

From the section analysis shown in Table 4.8, the horizontal and vertical sizes of the flakes are quite varied. At 60°C and 3000 psi, the largest horizontal distance flake observed was 1367 nm (flake 1.2) and the largest vertical distance was 182.91 nm (flake 1.1). The smallest flake observed was 556.64 nm horizontal distance, and 49.997 nm vertical distance (flake 1.3). At 60°C and 2500 psi, the largest flakes observed was 1465 nm horizontal distance and 59.153 nm vertical distance (flake 2.1). The smallest flake was 87.891 nm and 1.864 nm for horizontal and vertical distances (flake 2.11), respectively. This flake is around six graphene layers thick. For the treatment at 60°C and 2000 psi, the largest flake in term of the horizontal distance observed was 468.75 (flake 3.4) nm. In terms of the vertical distance, the largest was 204.13 nm (flake 3.2). The smallest flake was 62.5 nm horizontal and 3.707 nm vertical distances (flake 3.12). This flake contains approximately twelve layers of graphene. Some examples of section analysis of flakes 3.7 and 3.12 are shown in Figure 4.37 and 4.39, respectively. From these figures, the horizontal and vertical distances of the flakes can be examined by using the AFM software drawing straight line across each flakes and moving the arrows to

reach its width and height. More sections analysis of these flakes are shown in appendix C.

Figure 4.36-4.39 shows the various shapes and horizontal and vertical sizes of the flakes. The bright yellow shows the flakes with higher vertical heights. However, the brightness of the flakes depends on the data scale set in the examination. More accurate distances (horizontal and vertical) analysis of the flakes are shown in section analysis in Appendix C. As a result, the flakes show a wide range of sizes. They can be as big as a thousand nanometers or less than ten nanometers, with the layers are less than ten layers. Therefore, we can say that at these conditions of the supercritical treatment, few graphene layers materials less than ten layers (less than two nanometers) were produced. These were not shown in the PCS data, which indicated that the smallest treated flakes were approximately eighty nanometers in sizes (Table 4.2). This might be since the PCS measures the sizes from correlation of laser light that is scattered from the dispersed flakes and detected by the detector. Although, few-layer materials were produced, the absolute amounts were not large compared to the larger flakes.

The limitations of AFM in this experiment are that it can only examine the flakes in small areas. It cannot estimate the overall sizes of the flakes obtained or even the average sizes as the PCS analysis can do. Therefore, we did not do AFM for all of the samples since they indicate the same trends in terms of the shapes of the flakes. Another disadvantage of AFM in this case is the tip is easy to be convoluted by the small flakes due to tip-sample interaction. Moreover, some images blur due to instability of the sample.

## 5. Conclusion

The supercritical carbon dioxide treatment can exfoliate the graphite layers into ten to several-hundred nanometer thick flakes. The supercritical density, which depends on the temperature and pressure of the supercritical conditions, is a major factor that affects the sizes and stabilities of the flakes obtained. From the experiment, the sizes of the treated flakes at low supercritical density (high temperature and low pressure) are larger with lower stability, while the sizes at the high supercritical density (low temperature and high pressure) are smaller with higher stability. Inversely, if sonication is applied, the sonicated samples of low critical density treatments have smaller sizes than at high supercritical density treatments due to incomplete exfoliation of the layers. Instead, the layers are expanded due to carbon dioxide molecules that pass and be adsorbed between the layers of those flakes. After sonication, the flakes obtained from low supercritical density treatment, therefore, are smaller than those of from high supercritical density treatment. The zeta potentials are more negative on average, which means they are more stable after applying sonication. Moreover, the temperature has more significant effects on the exfoliation than pressure.

NMP can maintain the stability of the flakes as well as DMF due to the highly negative charges of their flakes in zeta potential analysis. This is because NMP and DMF have high polarity (high dielectric constant). However, the zeta potentials of the samples treated with isopropanol are significantly lower indicating (low stability). Although sonication is applied, the zeta potential of the isopropanol treated samples are still out of acceptance range (-30 mV to +30 mV)<sup>77</sup> for the stable dispersions. This is because isopropanol has a lower dielectric constant than NMP or DMF. Therefore, isopropanol does not have the ability to maintain stability and prevent reaggregation of the dispersed flakes.

For the effects of treatment time on the sizes and zeta potential of the flakes, when the treatment time increases, the sizes of the flake sheets increased. The zeta potentials are

more negative (more stable) when the treatment time increases due to larger flake sheets produced from longer treatment time.

The evidence that proves that CO<sub>2</sub> molecules can pass between the graphite layers is the BET surface area results. With the CO<sub>2</sub> adsorption, the BET surface area of untreated graphite is much larger than that with N<sub>2</sub> adsorptive. Moreover, the BET surface area with CO<sub>2</sub> adsorption of treated graphite is negative due to the CO<sub>2</sub> molecules are adsorbed or intercalated between the graphite layers from the supercritical treatment.

The FE-SEM and AFM images show the various sizes and shapes of the graphitic flakes. The horizontal and vertical sizes also varied from several nanometers to more than a hundred nanometers. The effect of the water-based surfactant (sodium dodecylbenzene sulfonate, SDBS) can be observed clearly in the FE-SEM images in terms of larger appeared flakes from reaggregation due to low stability of the SDBS surfactant.

## 6. Future work

This research gives an initial explanation of how graphite is exfoliated by supercritical carbon dioxide. The parameter that plays a major role on the sizes and stability of the obtained graphenic flakes is the supercritical density of the exfoliant. Supercritical density relies mainly on temperature. From this work, we can conclude that carbon dioxide at low supercritical density with NMP as a co-solvent, and one hour sonication, can produce graphenic flakes smaller than 100 nm. However, due to agglomeration, large flakes are present, and there is high deviation in flake sizes obtained. In order to apply this method in a commercial production, further process to separate the graphenic flakes, which are less than ten layers thick, from the large flakes, is necessary.

Further examinations and experiments are required to improve the graphene synthesis method outlined in this thesis. These include:

- 1) Examine the treated flakes using transmission electron microscopy (TEM) to study the crystallography of the graphenic flakes. TEM can also clearly indicate whether the obtained flakes are actually graphene, since graphene is transparent<sup>46</sup>.
- 2) Determine the number of layers in the graphenic flakes produced using Raman spectroscopy<sup>61</sup>. Certain peaks in the Raman spectra will change in size, position, and shape with the number of graphene layers and defects/impurities.
- 3) Study more in-depth the reaggregation of the obtained flakes that inevitably occurs in this experiment. Investigations of the time effects of reaggregation are necessary to predict the active life of the obtained flakes before reaggregating.
- 4) More study on effects of treatment time on intercalation of the supercritical carbon dioxide and graphite layers, since treatment time has a significant effect on the size and stability of the treated flakes. The treatment time should be extended to times longer than three hours, which was the maximum used during these experiments.

## References

1. Geim AK, Novoselov KS. The rise of graphene. *Nature Materials*. 2007;6:183-191.
2. Delhaes P. Graphite and Precursors. Amsterdam(the Netherlands): OPA (Overseas Publishers Association) N.V. Published by license under the Gordon and Breach Science Publishers imprint; 2001.p. 141-178.
3. Soldano C, Mahmood A, Dujardin E. Production, properties and potential of graphene. *ScienceDirect*. 2010;48:2127-2150.
4. The graphite project 2006 [Internet]. Toronto(Canada): Worldwide Graphite Producers Ltd.; 2011 [cited 2011 July 28]. Available from: [http://www.worldwidegraphite.com/Images/WWG\\_BP\\_111306.pdf](http://www.worldwidegraphite.com/Images/WWG_BP_111306.pdf)
5. The reference in natural & synthetic graphite powders and highly conductive carbon black [Internet]. Bodio(Switzerland): Timcal Limited. Hight-purity graphite powders for high performnance; 2011 [cited 2011 Jul 10]. Available from: [http://www.timcal.com/scopi/group/timcal/timcal.nsf/pagesref/MCOA-7S6H6L/\\$File/High\\_purity\\_graphite\\_powders\\_for\\_high\\_performance.pdf](http://www.timcal.com/scopi/group/timcal/timcal.nsf/pagesref/MCOA-7S6H6L/$File/High_purity_graphite_powders_for_high_performance.pdf)
6. Carbon Materials [Internet]. USA: SubTech (Substances and Technologies). Graphite manufacturing process; 2011 [cited 2011 Jul 10]. Available from: [http://www.substech.com/dokuwiki/doku.php?id=graphite\\_manufacturing\\_process&DokuWiki=308bce2cd72f41493e1b6bb315cec9e6#powder\\_preparation](http://www.substech.com/dokuwiki/doku.php?id=graphite_manufacturing_process&DokuWiki=308bce2cd72f41493e1b6bb315cec9e6#powder_preparation)
7. Minerals infromation [Internet]. Reston(VA): US Geological Survey (USGS). Graphite; 2011 [cite 2011 Jul 10]. Available from: <http://minerals.usgs.gov/minerals/pubs/commodity/graphite/graphmyb04.pdf>
8. Material Safety Data Sheet [Internet]. Saint Louis (MO): Sigma-Aldrich Corporation. Synthetic Graphite (282863); 2011 [updated 1989 Aug 11, cited 2011 Jul 10]. Available from: <http://www.sigmaaldrich.com/catalog/DisplayMSDSContent.do>

9. Graphite 2H properties - Jaszczak JA – Physics - Michigan Technological University. Houghton (MI). Graphite 2H properties; 2011 [cited 2011 July 28]. Available from: <http://www.phy.mtu.edu/~jaszczak/graphprop.html>
10. Billings BH, Frederikse HPR, Bleil DF, Lindsay RB, Cook RK, Marion JB, Crosswhite HM, Zemansky M, Gray DE. American Institute of Physics Handbook. 3<sup>rd</sup> ed. New York(USA): McGraw-Hill; 1972. p. 4-142 to 4-160, 4-119 to 4-142.
11. Peckett A. The Color of Opaque Minerals. New York(USA): John Wiley & Sons Inc; 1992. p. 204-207.
12. Kelly BT. Physics of Graphite. London(UK): Applied Science Publishers; 1981. 477 p.
13. Ruoff RS, Ruoff AL. The bulk modulus of C60 molecules and crystals: A molecule mechanics approach. Applied Physics Letters. 2009;59(13):1553-1555.
14. Boey SY, Bacon DJ. Deformation of Polycrystalline graphite under pressure. Carbon. 1986;24(5):557-564.
15. Simon MD, Geim AK. Diamagnetic levitation: flying frogs and floating magnets (invited). Journal of Applied Physics. 2000;87:6200-6204.
16. Kim KS, Zhao Y, Jang H, Lee SY, Kim JM, Kim KS, Ahn JH, Kim P, Choi JY, Hong BH. Large-scale pattern growth of graphene films for stretchable transparent electrodes. Nature. 2009;457: 7230-706 to 7230-710.
17. Jiang Z, Henriksen EA, Tung LC, Wang YJ, Schwarts ME, Han MY, Kim P, Stormer HL. Infrared spectroscopy of Landau level of graphene. Physical Review Letters. 2007;98(19):197403-1 to 197403-4.
18. Geim AK, MacDonald AH. Graphene: Exploring carbon flatland. American Institute of Physics. 2007;6:35-41.
19. Fraundorf P, Wackenhut M. The core structure of presolar graphite onions. The Astrophysical Journal. 2002;578:L153-L156.
20. Wang C, Li D, Too CO, Wallace. Electrochemical properties of graphene paper electrodes used in lithium batteries. Chemistry of Materials. 2009;21(13):2604-2606.



21. Pu NW, Wang CA, Sung Y, Liu YM, Ger MD. Production of few-layer graphene by supercritical CO<sub>2</sub> exfoliation of graphite. *Materials Letters*. 2009;63:1987-1989.
22. Li Q, Zhang Z, Zhong C, Liu Y, Zhou Q. Solubility of solid solutes in supercritical carbon dioxide with and without cosolvents. Elsevier Science. 2003;207:183-192.
23. Supercritical Fluid Extraction [Internet]. New York(USA): Supercritical Fluid Extraction. Density consideration; 2011 [cited 2011 July 28]. Available from: <http://eng.ege.edu.tr/~otles/SupercriticalFluidsScienceAndTechnology/Wc488d76f2c655.htm>
24. Green DW, Perry RH. Perry's Chemical Engineers's Handbook. 8<sup>th</sup> ed. New York(USA): McGraw-Hill; 2007. p. 2-138 to 2-142.
25. Material Safety Data Sheet [Internet]. Saint Louis(MO): Sigma-Aldrich Corporation. 1-Methyl-2-pyrrolidione (M79603); 2011 [updated 2011 Mar 3, cited 2011 Jul 1]. Available from: <http://www.sigmaaldrich.com/catalog/DisplayMSDSContent.do>
26. Material Safety Data Sheet [Internet]. Houston (TX). Sciencelab.com, Incorporation. N-Methyl-2-pyrrolidione (M79603); 2010 [updated 2010 Nov 1, cited 2011 Jul 1]. Available from: <http://www.sciencelab.com/msds.php?msdsId=9926094>
27. NIST Chemistry Webbook [Internet]. Gaithersburg(MD): National Institute of Standards and Technology (NIST). 1-Methyl-2-Pyrrolidinone; 2011 [cited 2011 Jul 10]. Available from: <http://webbook.nist.gov/cgi/cbook.cgi?ID=C872504&Units=CAL&Mask=6F>
28. Material Safety Data Sheet [Internet]. Fair Lawn (NJ): Fisher Scientific Incorporation. N, N Dimethylformamide (ACC#07860); 2008 [updated 2008 AUG 30, cited 2011 Jul 1]. Available from: <http://fscimage.fishersci.com/msds/07860.htm>
29. NIST Chemistry Webbook [Internet]. Gaithersburg(MD): National Institute of Standards and Technology (NIST). N-Methyl-Formamide; 2011 [cited 2011 Jul

- 10]. Available from:  
<http://webbook.nist.gov/cgi/cbook.cgi?ID=C68122&Units=SI&Mask=6F>
30. Material Safety Data Sheet [Internet]. Brookfield (CT): Pharmco-Aaper. Isopropyl Alcohol 99%; 2011 [cited 2011 Jul 1]. Available from:  
[http://www.pharmcoaaper.com/pages/MSDS/MSDS\\_I/isopropanol\\_99\\_percent.pdf](http://www.pharmcoaaper.com/pages/MSDS/MSDS_I/isopropanol_99_percent.pdf)
31. IPA [Internet]. Silver Spring(MD): CAMEO Chemicals. Isopropyl Alcohol; 1999 [created 1999 Jun, cited 2011 Jul 1]. Available from:  
<http://cameochemicals.noaa.gov/chris/IPA.pdf>
32. NIST Chemistry Webbook [internet]. Gaithersburg(MD): National Institute of Standards and Technology (NIST). Isopropyl alcohol; 2011 [cited 2011 Jul 10]. Available from:  
<http://webbook.nist.gov/cgi/cbook.cgi?Name=isopropanol&Units=SI&cTG=on&cTC=on&cTP=on&cTR=on&cIE=on&cIC=on>
33. Supercritical Fluid Extraction [Internet]. New York(USA): Supercritical Fluid Extraction. Introduction; 2011 [cited 2011 July 28]. Available from  
<http://eng.ege.edu.tr/~otles/SupercriticalFluidsScienceAndTechnology/Wc97b52abd63c8.htm>
34. Atomic structures of graphene, benzene and methane with bond lengths as sums of the single, double and resonance bond radii of carbon [Internet]. Czech Republic: Institute of Biophysics, Academy of Sciences of the Czech Republic; 2011 [cited 2011 JUL 7]. Available from:  
<http://arxiv.org/ftp/arxiv/papers/0804/0804.4086.pdf>
35. Geim AK, MacDonald AH. Graphene: Exploring carbon flatland. American Institute of Physics. 2007;6:35-41.
36. Lee C, Wei X, Kysar JW, Hone J. Measurement of the elastic properties and intrinsic strength of monolayer graphene. Science. 2008;321:385-388.
37. Saito K, Nakamura J, Natori A. Ballistic thermal conductance of a graphene sheet. Physical Review. 2007;76: 115409-1 to 115409-4.

38. Novoselov KS, Geim AK, Morozov SV, Jiang D, Zhang Y, Dubonos SV, Grigorieva IV, Firsov AA. Electric field effect in atomically thin carbon films. *Science*. 2004; 306: 5696-666 to 5696-669.
39. Lemme MC, Echtermeyer TJ, Baus M, Kurz H. A graphene field effect device. *IEEE Electron Device Letters*. 2007;28(4):282-284.
40. Wang X, Zhi L, Müllen K. Transparent, conductive graphene electrodes for dye-sensitized solar cells. *Nano Letters*. 2008;8(1):323-327.
41. Stoller MD, Park S, Zhu Y, An J, Ruoff RS. Graphene-based ultracapacitors. *Nano Letters*. 2008;8(10):3498-3502.
42. Mohanty N, Berry V. Graphene-based single-bacterium resolution biodevice and DNA transistor: interfacing graphene derivatives with nanoscale and microscale biocomponents. *Nano Letters*. 2008;8(12):4469-4476.
43. Xu M, Fujita D, Hanagata N. Perspectives and challenges of emerging single-molecule DNA sequencing technologies. *Wiley InterScience*. 2009;5(23):2638-2649.
44. Peierls RE. Quelques propriétés typiques des corps solides. *Annales de l'Institut Henri Poincaré*. 1935;5:177-222.
45. Landau LD. Zur Theorie der Phasenumwandlungen II. *Phys. Z. Sowjetunion*. 1937;11: 26-35.
46. Novoselov KS, Jiang D, Booth TJ, Khotkevich VV, Morozov SV, Geim AK. Two dimensional atomic crystals. *Proceeding of the National Academy of Sciences (PNAS)*. 2005;102(30):10451-10453.
47. Zhang YB, Small JP, Pontius WV, Kim P. Fabrication and electric-field-dependent transport measurements of mesoscopic graphite devices. *Applied Physics Letters*. 2005;86: 073104-1 to 073104-3.
48. Malesevic A, Vitchev R, Schouteden K, Volodin A, Zhang L, Tendeloo GV, Vanhulsel A, Haesendonck CV. Synthesis of few-layer graphene via microwave plasma-enhanced chemical vapour deposition. *Nanotechnology*. 2008;19: 305604-1 to 305604-6

49. Lee Y, Bae S, Jang H, Jang S, Zhu SE, Sim SH, Song YI, Hong BH, Ahn JH. Wafer-scale synthesis and transfer of graphene films. *Nano Letters*. 2010; 10:490-493.
50. Shi Y, Kim KK, Reina A, Hofmann M, Li LJ, Kong J. Work function engineering of graphene electrode via chemical doping. Article. *Americal Chemical Society Nano*. 2010;4(5):2689-2694.
51. Reina A, Jia X, Ho J, Nezich D, Son H, Bulovic V, Dresselhaus MS, Kong J. Large area, few layer graphene film on arbitrary substrates by chemical vapor deposition. *Nano Letters*. 2009;9(1):30-35.
52. Li XS, Cai W, An J, Kim S, Nah J, Yang D, Piner R, Velamakanni A, Jung I, Tutuc E, Banerjee SK, Colombo L, Ruoff RS. Large-area synthesis of high-quality and uniform graphene films on copper foils. *Science*. 2009;324: 5932-1312 to 5932-1314.
53. Shen J, Hu Y, Shi M, Lu X, Qin C, Li C, Ye M. Preparation of graphene oxide and reduced graphene oxide nanoplatelets. *Chemistray of Materials Article*. 2009;21:3514-3520.
54. Wu ZS, Ren W, Gao L, Liu B, Jiang C, Cheng HM. Synthesis of high-quality graphene with a pre-determined number of layers. *ScienceDirect*. 2009;47:493-499.
55. Schniepp HC, Li JL, McAllister MJ, Sai H, Alonso MH, Adamson DH, Prud'homme RK, Car R, Saville DA, Aksay A. Functionalized single graphene sheets derived from splitting graphite oxide. *The Journal of Physical Chemistry B*. 2006;110(17):8535-8539.
56. Boehm HP. Dunnste Kohlenstoff-Folin. *Zeitschrift Fur Naturforschung Part B-Chemie Biochemie Biophysik Biologie Und Verwandten Gebiete*. 1962;B17(3):150.
57. Eda G, Fanchini G, Chhowalla M. Large-area ultrathin films of reduced graphene oxide as a transparent and flexible electronic material. *Nature Nanotechnology*. 2008;3(5):270-274.
58. Gilje S, Han S, Wang M, Wang KL, Kaner RB. A chemical route to graphene for device applications. *Nano Letters*. 2007;7(11):3394-3398.

59. Navarro CG, Weitz RT, Bittner AM, Scolari M, Mews Alf, Burghard M, Kern K. Electronic transport properties of individual chemically reduced graphene oxide sheets. *Nano Letters* 2007;7(11):3499-3503.
60. Lotya M, Hernandez Y, King PJ, Smith RJ, Nicolosi V, Karlsson LS, Blighe FM, De S, Wang Z, McGovern IT et al. Liquid phase production of graphene by exfoliation of graphite in surfactant/water solutions. *Journal of the American Chemical Society (JACS)*. 2009;131(10),3611-3620.
61. Ferrari AC, Meyer JC, Scardaci V, Casiraghi C, Lazzeri M, Mauri F, Piscanec S, Jiang D, Novoselov KS, Roth S et al. Raman spectrum of graphene and graphene layers. *Physical Review Letters*. 2006;97: 187401-1 to 187401-4.
62. Rangappa D, Sone K, Wang M, Gautam UK, Golberg D, Itoh H, Ichihara M, Honma I. Rapid and direct conversion of graphite crystals into high-yielding, good-quality graphene by supercritical fluid exfoliation. *Chemistry-A European Journal*. 2010;16(22):6488-6494.
63. Woods HM, Silva M, Nouvel C, Shakesheff KM, Howdle SM. Materials processing in supercritical carbon dioxide: surfactants, polymers and biomaterials. *Journal of Materials Chemistry*. 2004;14:1663-1678.
64. Kaschak DM, Reynolds RA, Krassowski DW, Ford BM. Graphite intercalation and exfoliation process. United States Patent. Patent no.: US 7,105,108 B2; date of patent: Sep. 12, 2006. p.1-14.
65. Green AA, Hersam MC. Solution phase production of graphene with controlled thickness via density differentiation. *Nano Letters*. 2009;9(12):4031-4036.
66. Ghosh A, Subrahmanyam KS, Krishna KS, Datta S, Govindaraj A, Pati SK, Rao C. Uptake of H<sub>2</sub> and CO<sub>2</sub> by graphene. *The Journal of Physic Chemistry C*. 2008;112(40):15704-15707.
67. Behabtu N, Lomeda JR, Green MJ, Higginbotham AL, Sinitskii A, Kosynkin DV, Tsentalovich D, Vasquez NG, Schmidt J, Kesselman E et al. Spontaneous high-concentration dispersions and liquid crystals of graphene. *Nature Nanotechnology*. 2010;5:406-411.

68. Subrahmanyam KS, Vivekchand S, Govindaraj A, Rao C. A study of graphene prepared by different methods: characterization, properties and solubilization. *Journal of Materials Chemistry*. 2008;18:1517-1523.
69. Kozhemyakina NV, Englert JM, Uang G, Spiecker E, Schmidt CD, Hauke F, Hirsch A. Non-covalent chemistry of graphene: electronic communication with dendronized perylene bisimides. *Advanced Materials*. 2010;22:5483-5487.
70. Li Q, Zhang Z, Zhong C, Liu Y, Zhou Q. Solubility of solid solutes in supercritical carbon dioxide with and without cosolvents. *Fluid Phase Equilibria*. 2003;207:183-192.
71. Material Safety Data Sheet [Internet]. Saint Louis(MO): Sigma-Aldrich Corporation. 1-Methyl-2-pyrrolidione (M79603); 2011 [updated 2011 Mar 3, cited 2011 Jul 1]. Available from: <http://www.sigmaaldrich.com/catalog/DisplayMSDSContent.do>
72. DDB Explorer Edition [Internet]. Oldenburg (Germany). Dortmund Data Bank Software & Separation Technology (DDBST). DEC (dielectric constant) data for N-methyl-2-pyrrolidinone; 2009 [updated 2009 Jul 9, cited 2011 Jul 1]. Available from: [http://ddbonline.ddbst.de/EE/284%20DEC%20\(Dielectric%20Constant\).shtml](http://ddbonline.ddbst.de/EE/284%20DEC%20(Dielectric%20Constant).shtml)
73. IPCS international programme on chemical safety, health and safety guide no. 43 [Internet]. Hamilton(Canada): International Programme on Chemical Safety (IPCS). Dimethylformamide (DMF) health and safety guide; 2011 [cited 2011 Jul 1]. Available from: <http://www.inchem.org/documents/hsg/hsg/hsg043.htm>
74. DDB Explorer Edition [Internet]. Oldenburg (Germany). Dortmund Data Bank Software & Separation Technology (DDBST). DEC (dielectric constant) data for 2-propanol; 2009 [updated 2009 Jul 9, cited 2011 Jul 1]. Available from: [http://ddbonline.ddbst.de/EE/95%20DEC%20\(Dielectric%20Constant\).shtml](http://ddbonline.ddbst.de/EE/95%20DEC%20(Dielectric%20Constant).shtml)
75. Scholes CA, Kentish SE, Stevens GW. Carbon dioxide separation through polymeric membrane systems for flue gas applications. *Recent Patents on Chemical Engineering*. 2008;1:52-66.

76. Omi H, Ueda T, Mityakubo K, Eguchi T. Dynamics of CO<sub>2</sub> molecules confined in the micropores of solids as studied by <sup>13</sup>C NMR. *Applied Surface Science*. 2005;252(3):660-667.
77. Malvern Instruments. Zetasizer Nano Series - user manual. Worcestershire (UK). Malvern Instruments Limited; 2008. p. 1-1 to 16-12.
78. Micromeritics. ASAP 2020: Accelerated Surface Area and Porosimetry System - Operator's Manual. Norcross(GA): Micromeritics Instrument Corporation; p. 1-1 to 9-19.
79. Brunauer S, Emmett PH, Teller E. Adsorption of gases in multimolecular layers. *The American Journal Society*. 1938;60:309-319.

## **Appendix A. PCS analysis**



## A.1. Overall PCS data

**Table A.1**

Overall PCS data of flakes obtained from different treatment temperature and pressure.

The supercritical treatment was processed for one hour with NMP as a co-solvent.

Parameter	Pressure (psi)	Sonication			No sonication		
		40°C	50°C	60°C	40°C	50°C	60°C
Diameter (nm)	2000	131.50	112.70	73.29	111.50	114.20	155.80
		153.80	117.50	78.66	157.30	143.20	175.70
		182.30	120.30	89.31	210.10	185.30	183.90
	2500	136.80	112.90	74.72	116.50	107.90	175.00
		144.60	122.22	85.28	155.90	122.30	207.10
		142.70	135.00	91.81	178.60	153.90	277.90
	3000	126.70	123.40	97.81	131.90	131.20	118.30
		130.90	121.10	105.10	151.90	160.90	215.20
		132.30	129.10	102.90	170.60	194.80	276.40
Z-average size (nm)	2000	110.00	138.30	91.26	106.40	118.10	209.50
		142.90	100.90	82.15	148.30	158.40	167.10
		144.10	121.60	104.90	212.10	241.50	169.20
	2500	134.50	115.30	71.48	210.80	183.70	191.80
		136.80	107.40	96.86	163.80	161.80	167.80
		138.90	116.00	96.86	93.89	111.60	236.50
	3000	111.80	103.80	102.00	183.30	184.60	556.00
		111.40	102.70	85.58	121.10	175.40	133.60
		113.90	104.50	85.52	136.00	119.40	242.60
Zeta potential (mV)	2000	-33.90	-36.10	-23.60	-30.10	-28.90	-28.50
		-56.90	-41.20	-27.80	-33.30	-29.10	-32.20
		-66.10	-46.00	-34.20	-45.90	-28.50	-37.80
	2500	-54.30	-36.20	-26.40	-26.90	-29.00	-12.30
		-57.80	-42.40	-28.50	-32.10	-29.20	-20.20
		-64.70	-45.40	-32.10	-36.90	-52.70	-19.60
	3000	-46.20	-33.60	-30.90	-51.70	-32.50	-44.50
		-43.50	-39.10	-32.20	-56.40	-44.10	-40.80
		-48.70	-54.40	-29.10	-69.90	-37.80	-35.20

**Table A.2**

Overall PCS data of flakes obtained from different co-solvents treated. The supercritical treatment was processed for one hour.

Parameter	Co-solvent	Sonication			No Son.		
		40°C	50°C	60°C	40°C	50°C	60°C
Diameter (nm)	NMP	126.70	123.40	97.81	131.90	131.20	118.30
		130.90	121.10	105.10	151.90	160.90	215.20
		132.30	129.10	102.90	170.60	194.80	276.40
	DMF	228.60	156.50	61.74	340.10	161.30	226.30
		191.20	153.60	82.27	253.70	178.90	277.50
		222.30	177.90	78.22	443.10	169.90	350.60
	Iso.	257.50	349.00	195.50	209.80	230.60	209.50
		290.10	314.9	291.50	231.60	236.80	217.80
		323.60	338.80	196.80	234.80	278.90	280.80
Z-average size (nm)	NMP	111.80	103.80	88.02	183.30	184.60	556.00
		111.40	102.70	85.58	121.10	175.40	133.60
		113.90	104.50	85.52	136.00	119.40	242.60
	DMF	187.50	125.20	118.50	255.00	110.50	154.10
		181.20	123.10	81.87	198.20	122.10	197.90
		194.50	140.30	79.29	182.10	123.50	167.40
	Iso.	202.50	271.30	186.60	182.50	224.20	269.00
		202.20	262.70	247.10	226.20	243.90	218.20
		246.90	268.70	181.00	225.10	224.00	275.90
Zeta potential (mV)	NMP	-46.20	-33.60	-30.90	-51.70	-32.50	-44.50
		-43.50	-39.10	-32.2	-56.40	-44.10	-40.80
		-48.70	-54.40	-29.10	-69.90	-37.80	-35.50
	DMF	-50.60	-62.70	-48.20	-31.30	-54.60	-58.00
		-47.10	-63.60	-60.50	-48.70	-63.30	-64.00
		-54.80	-67.70	-48.40	-41.60	-59.30	-69.40
	Iso.	-33.50	-24.30	-22.20	-10.70	-20.10	-12.20
		-25.40	-28.50	-29.10	-8.52	-13.80	-12.00
		-22.30	-29.10	-30.10	-13.80	-22.80	-19.50

**Table A.3**

Overall PCS data of flakes obtained from different treatment time.

NMP was used as a co-solvent.

Condition	Time (hr)	Dimension (nm)	Z-ave.size (nm)	Zeta potential (mV)
3000 psi/ 60 °C Sonication	1	97.80	85.52	-30.90
		105.10	85.58	-32.20
		102.90	88.02	-29.10
	2	147.50	183.30	-43.30
		137.70	168.30	-44.70
		184.50	292.50	-45.10
	3	144.20	174.10	-53.10
		161.70	235.10	-45.90
		164.40	327.30	-52.80
3000 psi/ 60 °C No sonication	1	118.30	556.00	-35.20
		215.20	133.60	-40.80
		276.40	242.00	-44.50
	2	204.50	189.00	-42.40
		225.80	173.70	-47.10
		250.70	159.20	-47.70
	3	461.20	1772.00	-49.90
		446.40	1489.00	-50.40
		604.60	1626.00	-51.20

## A.2. Sonicated NMP-samples

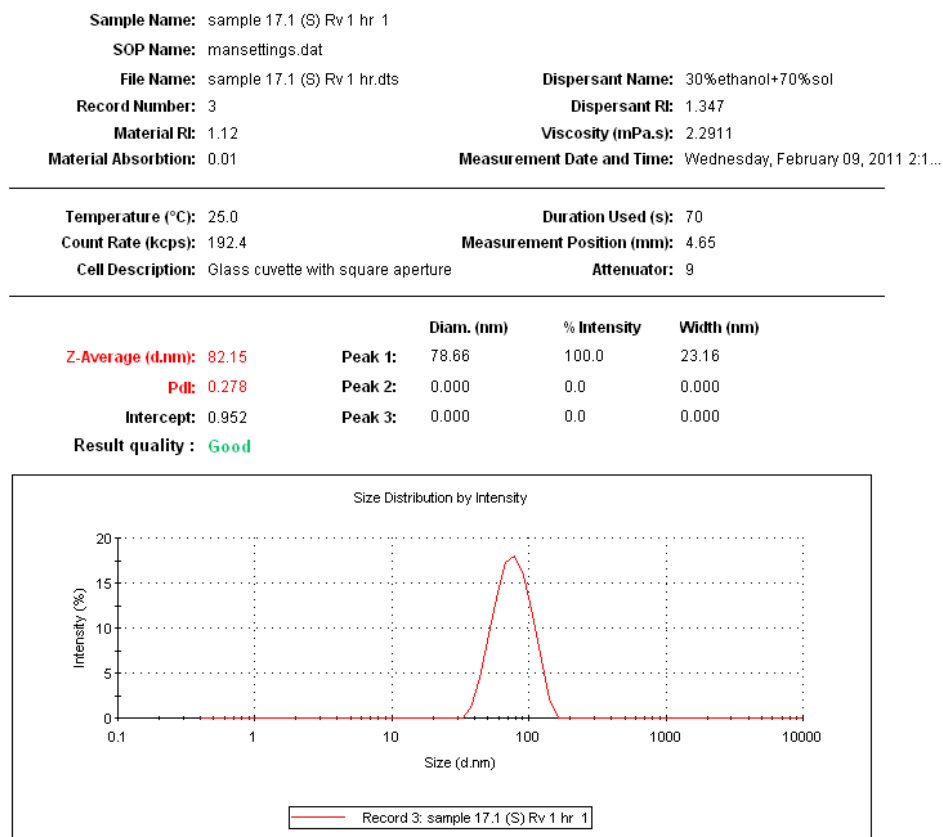


*Figure A.1 PCS software for sizing analysis of the NMP-treated sample obtained from the 2000 psi and 60°C treatment with additional 1-hour sonication.*

<b>Sample Name:</b> sample 17.1 (S) Rv 1 hr 1			
<b>SOP Name:</b> mansettings.dat			
<b>File Name:</b> sample 17.1 (S) Rv 1 hr.dts		<b>Dispersant Name:</b> 30%ethanol+70%sol	
<b>Record Number:</b> 14		<b>Dispersant Rf:</b> 1.347	
<b>Date and Time:</b> Wednesday, February 09, 2011 4:59:28 ...		<b>Viscosity (cP):</b> 2.2917	
		<b>Dispersant Dielectric Constant:</b> 78.5	
<hr/>			
<b>Temperature (°C):</b> 25.1		<b>Zeta Runs:</b> 14	
<b>Count Rate (kcps):</b> 8.4		<b>Measurement Position (mm):</b> 4.50	
<b>Cell Description:</b> Zeta dip cell		<b>Attenuator:</b> 8	
<hr/>			
	<b>Mean (mV)</b>	<b>Area (%)</b>	<b>Width (mV)</b>
<b>Zeta Potential (mV):</b> -27.8	<b>Peak 1:</b> -27.8	100.0	10.5
<b>Zeta Deviation (mV):</b> 10.5	<b>Peak 2:</b> 0.00	0.0	0.00
<b>Conductivity (mS/cm):</b> 0.00746	<b>Peak 3:</b> 0.00	0.0	0.00
<b>Result quality :</b> Good			

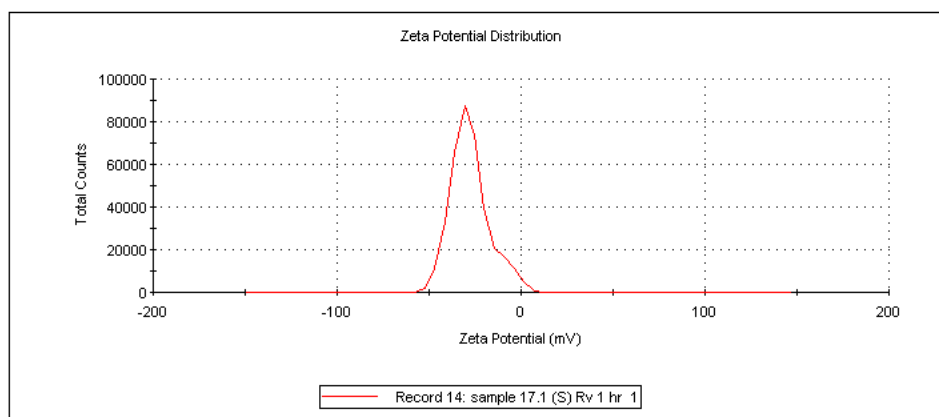


*Figure A.2 PCS software for zeta potential analysis of the NMP-treated sample obtained from the 2000 psi 60°C treatment with additional 1-hour sonication.*

<b>Sample Name:</b> sample 13.4 RV(son) 1			
<b>SOP Name:</b> mansettings.dat			
<b>File Name:</b> sample 13.4 Rv(son).dts		<b>Dispersant Name:</b> 30%ethanol+70%sol	
<b>Record Number:</b> 2		<b>Dispersant RI:</b> 1.347	
<b>Material RI:</b> 1.12		<b>Viscosity (mPa.s):</b> 2.2926	
<b>Material Absorbion:</b> 0.01		<b>Measurement Date and Time:</b> Friday, January 21, 2011 4:24:18 PM	
<b>Temperature (°C):</b> 25.1		<b>Duration Used (s):</b> 70	
<b>Count Rate (kcps):</b> 201.0		<b>Measurement Position (mm):</b> 4.65	
<b>Cell Description:</b> Glass cuvette with square aperture		<b>Attenuator:</b> 7	
		<b>Diam. (nm)</b>	<b>% Intensity</b>
<b>Z-Average (d.nm):</b> 111.4	<b>Peak 1:</b>	130.9	100.0
<b>Pdl:</b> 0.142	<b>Peak 2:</b>	0.000	0.0
<b>Intercept:</b> 0.958	<b>Peak 3:</b>	0.000	0.0
<b>Result quality :</b> <span>Good</span>		<b>Width (nm)</b>	

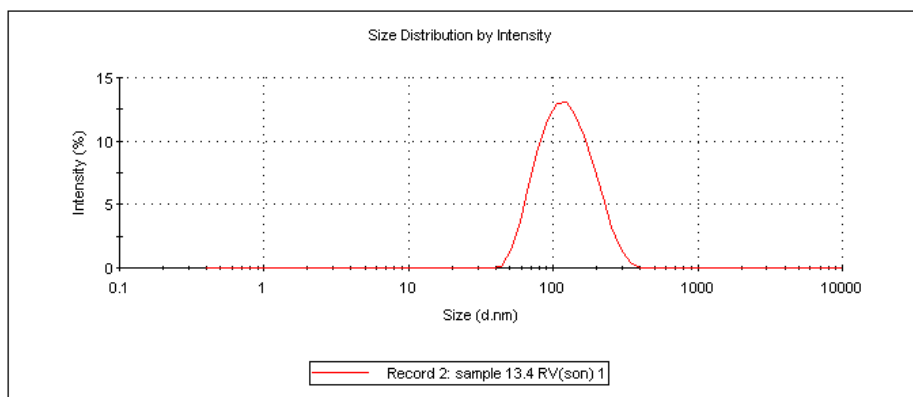
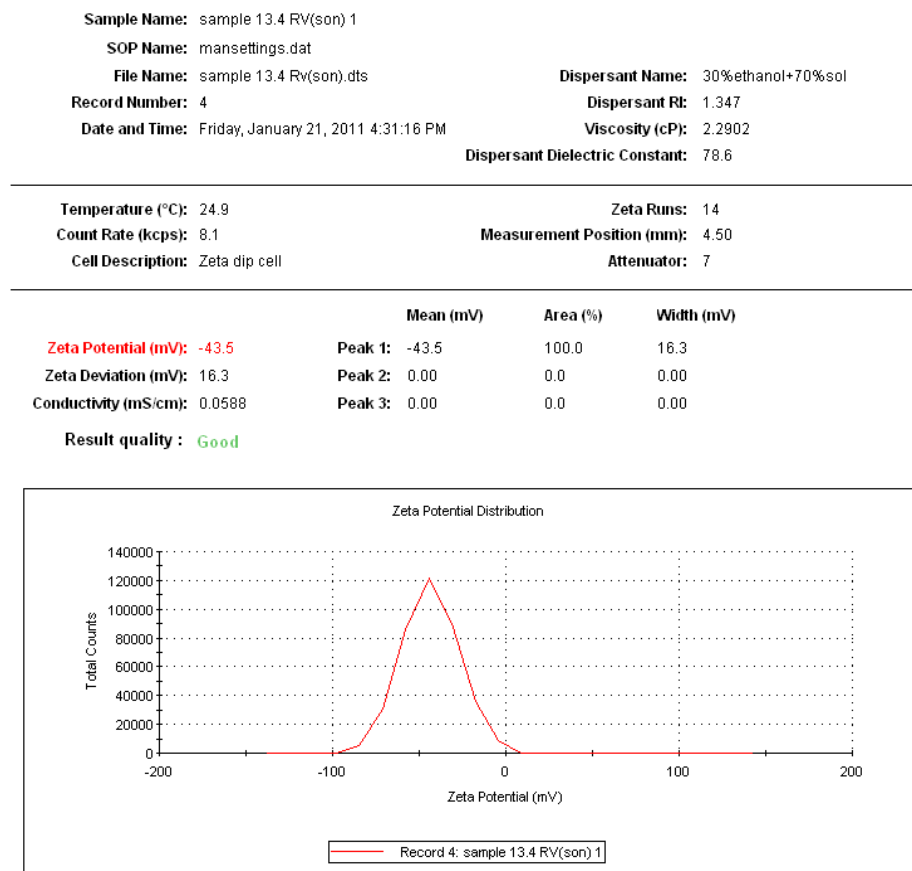
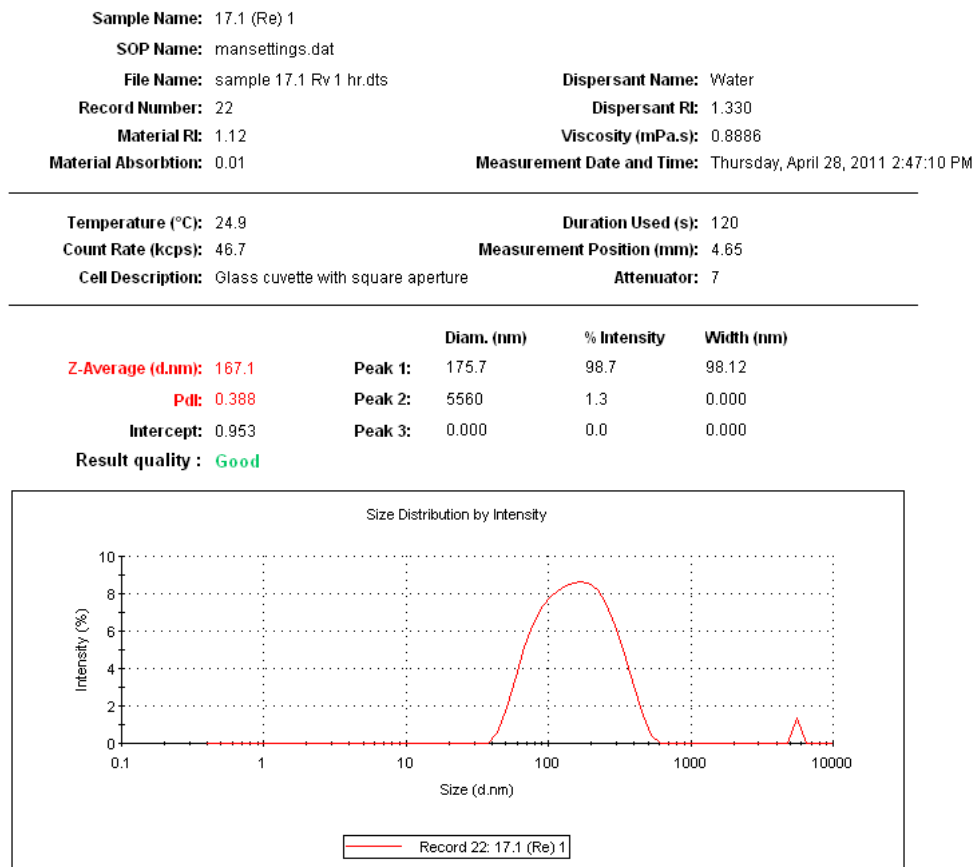


Figure A.3 PCS software for sizing analysis of the NMP-treated sample obtained from the 3000 psi 40°C treatment additional 1-hour sonication.



*Figure A.4 PCS software for zeta potential analysis of the NMP-treated sample obtained from the 3000 psi 40°C treatment with additional 1-hour sonication.*

### A.3. Non-sonicated NMP-samples



*Figure A.5 PCS software for sizing analysis of the NMP-treated sample obtained from the 2000 psi 60°C treatment without additional sonication.*



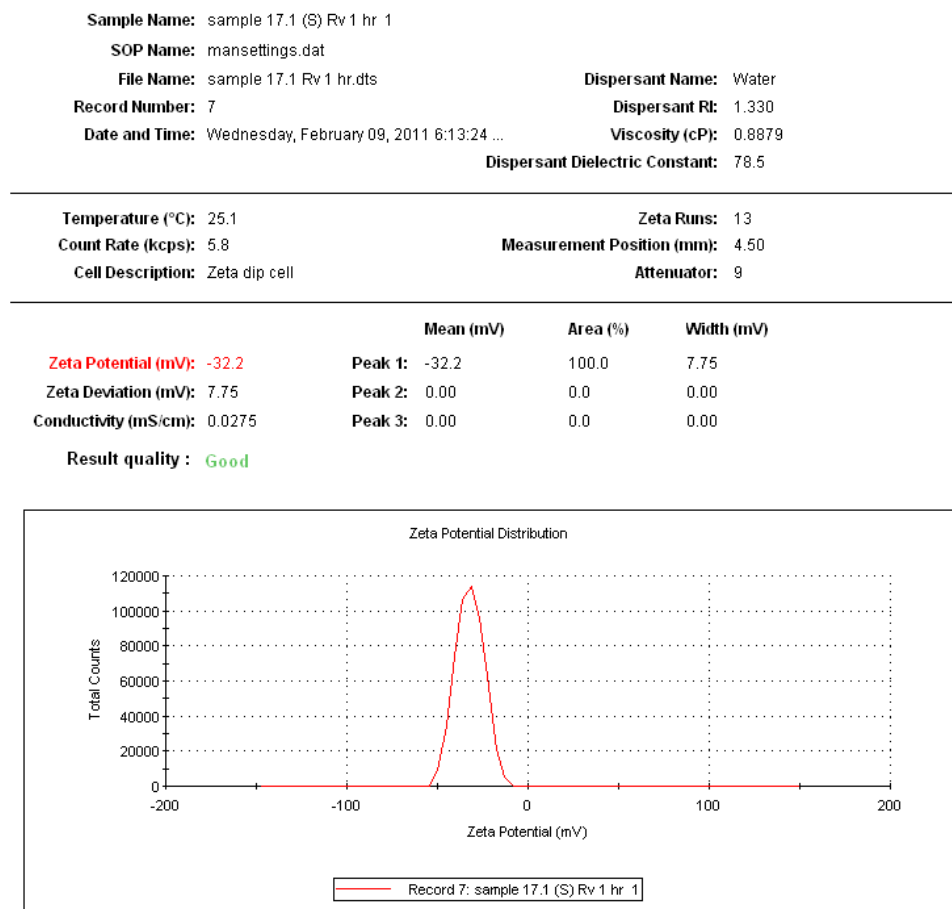


*Figure A.6 PCS software for zeta potential analysis of the NMP-treated sample obtained from the 2000 psi 60°C treatment without additional sonication.*

<b>Sample Name:</b> sample 13.3 RV 1			
<b>SOP Name:</b> mansettings.dat			
<b>File Name:</b> sample 13.3 Rv.dts		<b>Dispersant Name:</b> Water	
<b>Record Number:</b> 2		<b>Dispersant RI:</b> 1.330	
<b>Material RI:</b> 1.12		<b>Viscosity (mPa.s):</b> 0.8885	
<b>Material Absorption:</b> 0.01		<b>Measurement Date and Time:</b> Friday, January 21, 2011 3:12:11 PM	
<b>Temperature (°C):</b> 25.0		<b>Duration Used (s):</b> 70	
<b>Count Rate (kcps):</b> 145.6		<b>Measurement Position (mm):</b> 4.65	
<b>Cell Description:</b> Glass cuvette with square aperture		<b>Attenuator:</b> 10	

	Diam. (nm)	% Intensity	Width (nm)
<b>Z-Average (d.nm):</b> 121.1	<b>Peak 1:</b> 151.9	96.8	74.86
<b>Pdl:</b> 0.346	<b>Peak 2:</b> 4999	3.2	609.3
<b>Intercept:</b> 0.909	<b>Peak 3:</b> 0.000	0.0	0.000
<b>Result quality :</b> Good			

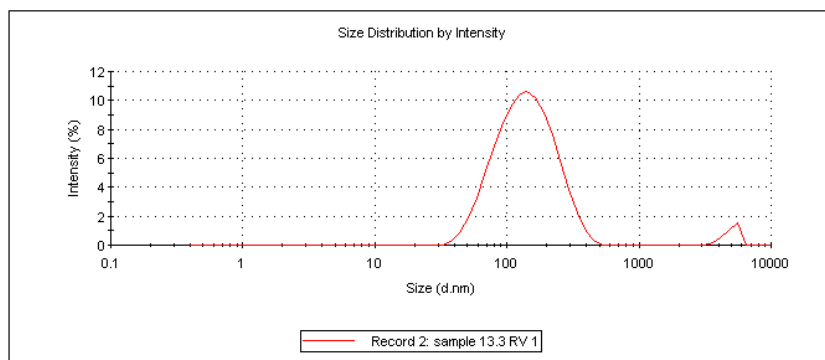
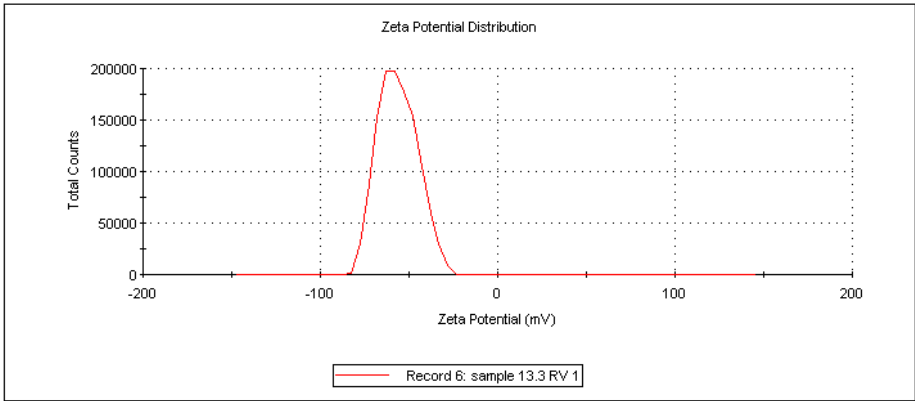


Figure A.7 PCS software for sizing analysis of the NMP-treated sample obtained from the 3000 psi 40°C treatment without additional sonication.

<b>Sample Name:</b> sample 13.3 RV 1			
<b>SOP Name:</b> mansettings.dat			
<b>File Name:</b> sample 13.3 Rv.dts		<b>Dispersant Name:</b> Water	
<b>Record Number:</b> 6		<b>Dispersant RI:</b> 1.330	
<b>Date and Time:</b> Friday, January 21, 2011 3:31:22 PM		<b>Viscosity (cP):</b> 0.8862	
		<b>Dispersant Dielectric Constant:</b> 78.6	
<b>Temperature (°C):</b> 25.0		<b>Zeta Runs:</b> 18	
<b>Count Rate (kcps):</b> 48.9		<b>Measurement Position (mm):</b> 4.50	
<b>Cell Description:</b> Zeta dip cell		<b>Attenuator:</b> 9	
	<b>Mean (mV)</b>	<b>Area (%)</b>	<b>Width (mV)</b>
<b>Zeta Potential (mV):</b> -56.4	<b>Peak 1:</b> -56.4	100.0	10.9
<b>Zeta Deviation (mV):</b> 10.9	<b>Peak 2:</b> 0.00	0.0	0.00
<b>Conductivity (mS/cm):</b> 0.131	<b>Peak 3:</b> 0.00	0.0	0.00
<b>Result quality :</b> <span>Good</span>			



*Figure A.8 PCS software for zeta potential analysis of the NMP-treated sample obtained from the 3000 psi 40°C treatment without additional sonication.*

## A.4. DMF- and isopropanol-samples

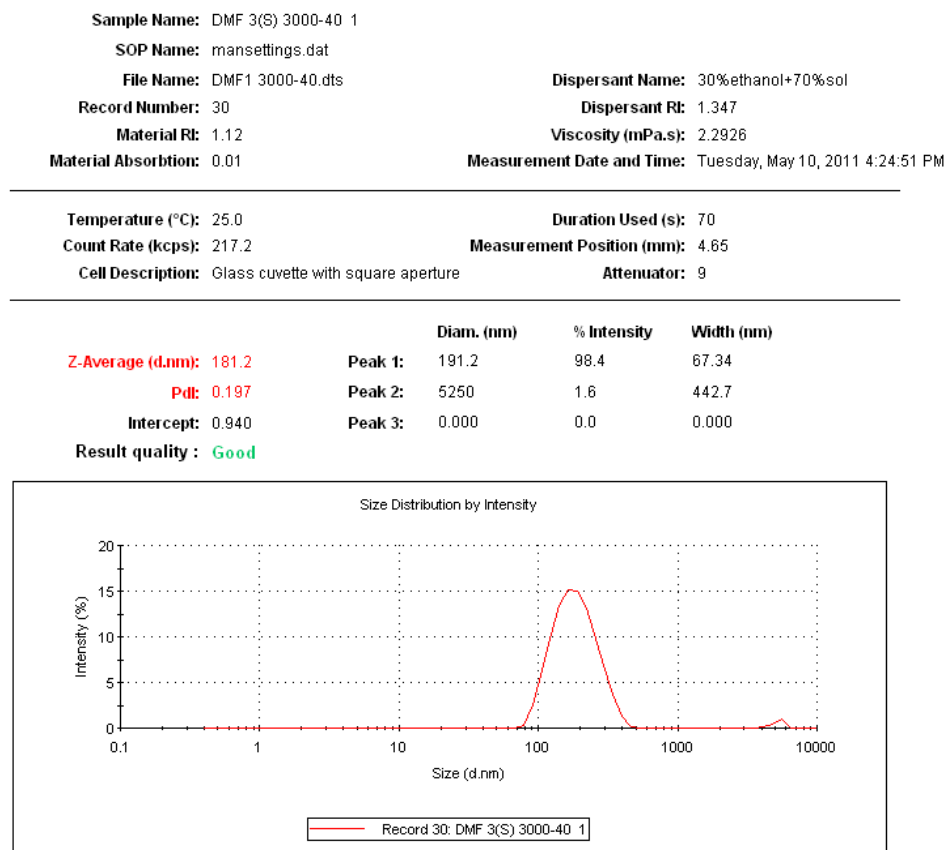
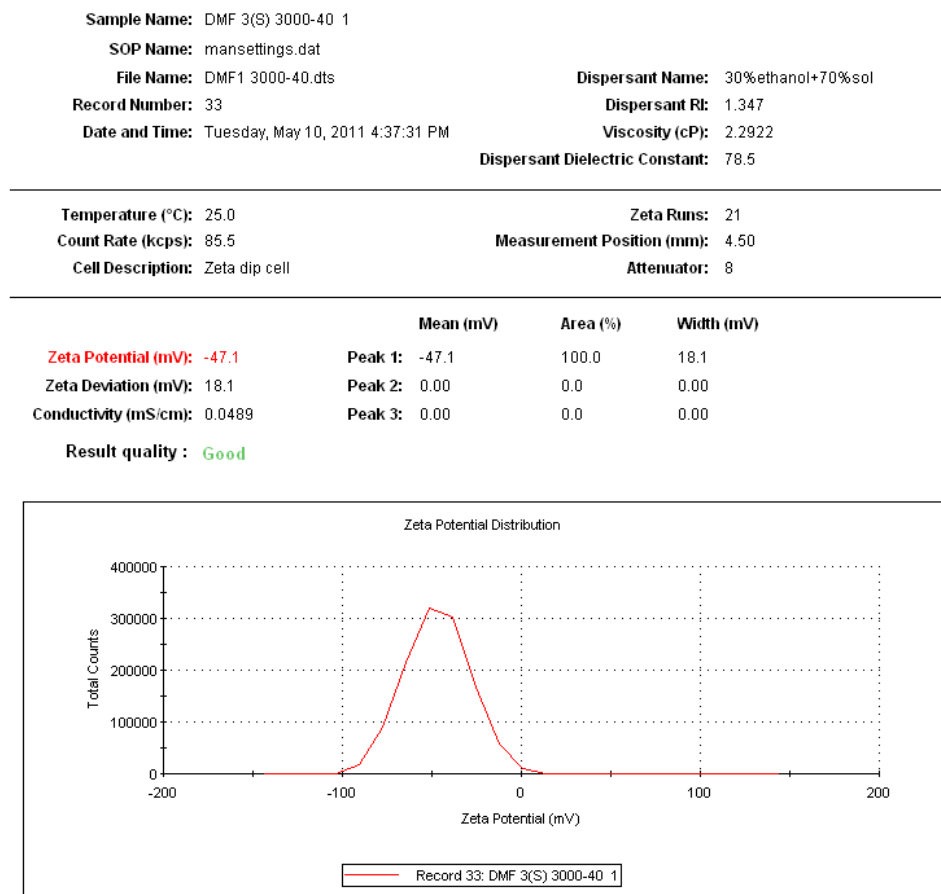
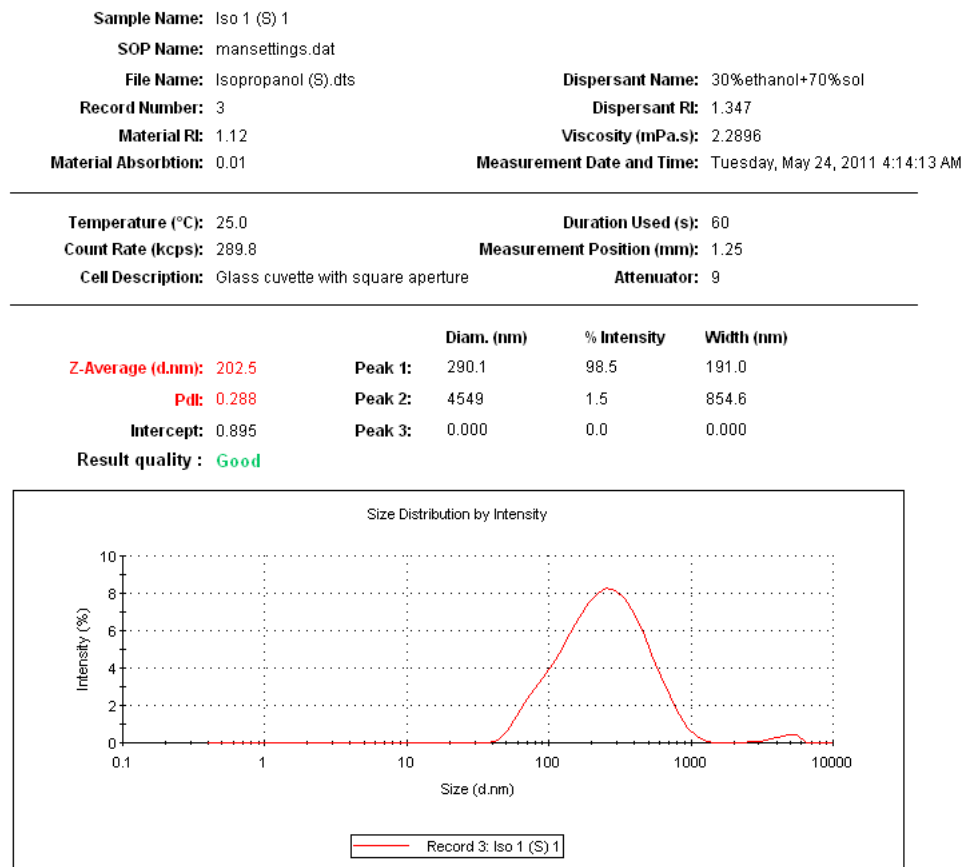


Figure A.9 PCS software for sizing analysis of the DMF-treated sample obtained from the 3000 psi 40°C treatment with additional 1-hour sonication.



*Figure A.10 PCS software for zeta potential analysis of the DMF-treated sample obtained from the 3000 psi 40°C treatment with additional 1-hour sonication.*



*Figure A.11 PCS software for sizing analysis of the isopropanol-treated sample obtained from the 3000 psi 40°C treatment with additional 1-hour sonication.*

Sample Name: Iso 1 (S) 1

SOP Name: mansettings.dat

File Name: Isopropanol (S).dts

Record Number: 5

Date and Time: Tuesday, May 24, 2011 4:42:26 AM

Dispersant Name: 30%ethanol+70%sol

Dispersant Rf: 1.347

Viscosity (cP): 2.2916

Dispersant Dielectric Constant: 78.5

Temperature (°C): 25.1

Count Rate (kcps): 36.0

Cell Description: Zeta dip cell

Zeta Runs: 12

Measurement Position (mm): 4.50

Attenuator: 8

	Mean (mV)	Area (%)	Width (mV)
<b>Zeta Potential (mV): -25.4</b>	<b>Peak 1: -25.4</b>	100.0	13.7
<b>Zeta Deviation (mV): 13.7</b>	<b>Peak 2: 0.00</b>	0.0	0.00
<b>Conductivity (mS/cm): 0.0361</b>	<b>Peak 3: 0.00</b>	0.0	0.00

Result quality : **Good**

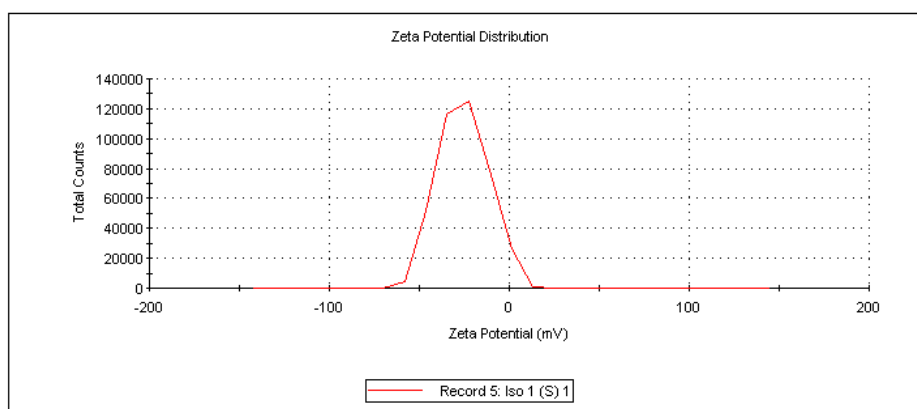


Figure A.12 PCS software for zeta potential analysis of the isopropanol-treated sample obtained from the 3000 psi 40°C treatment with additional 1-hour sonication.

## A.5. Effect of treatment time on the obtained flakes

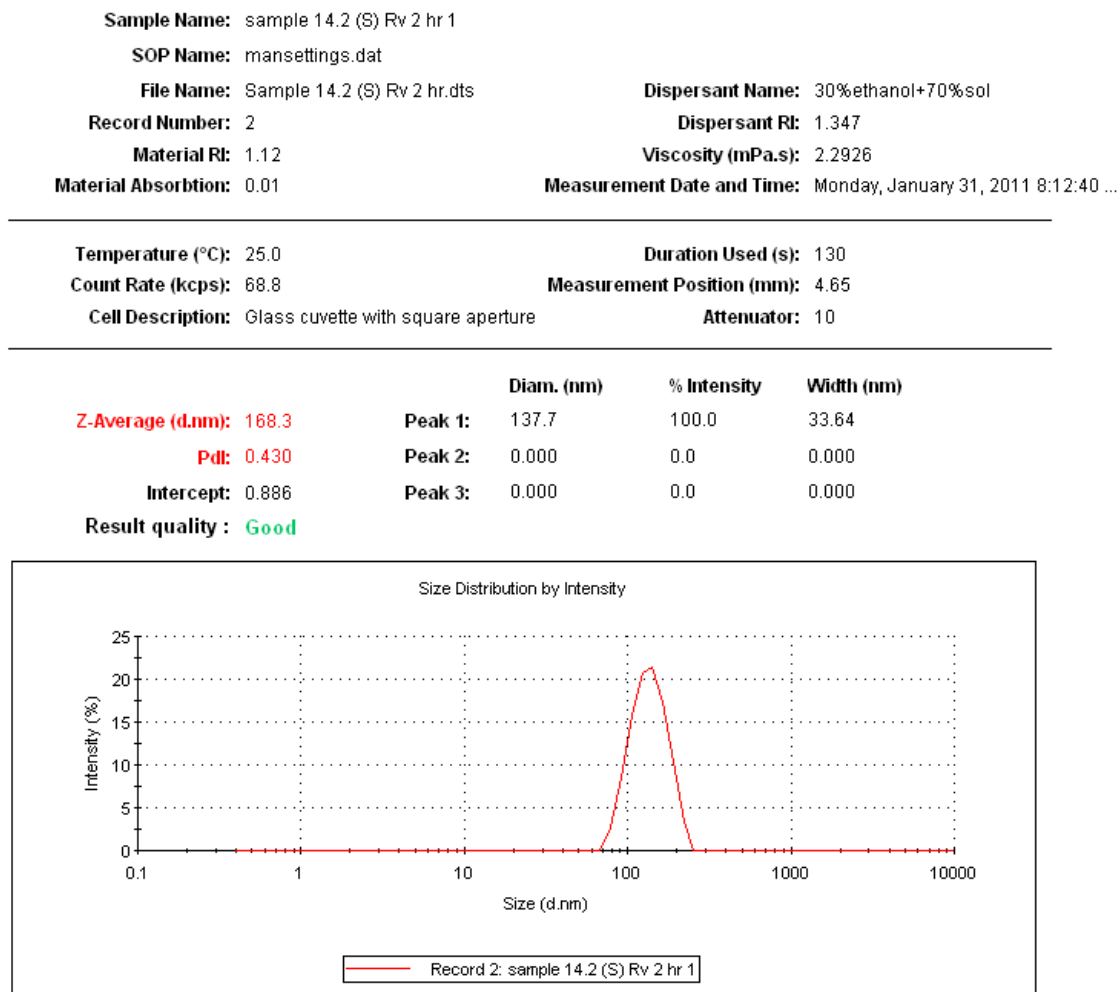
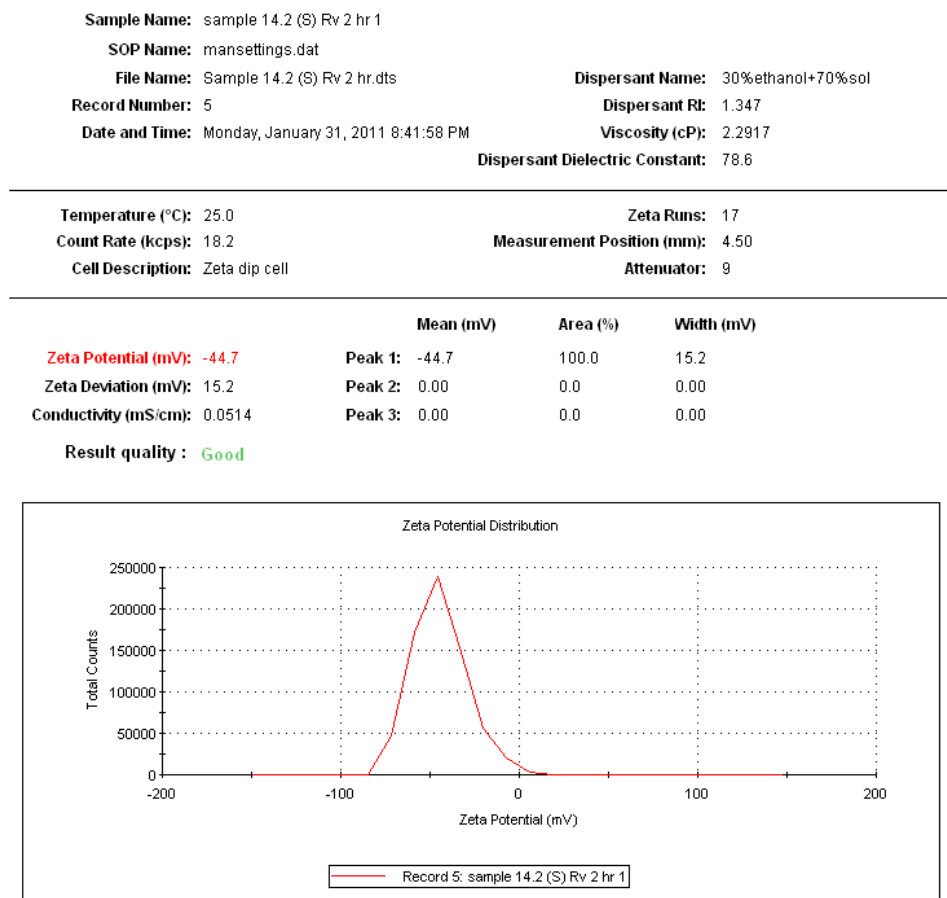
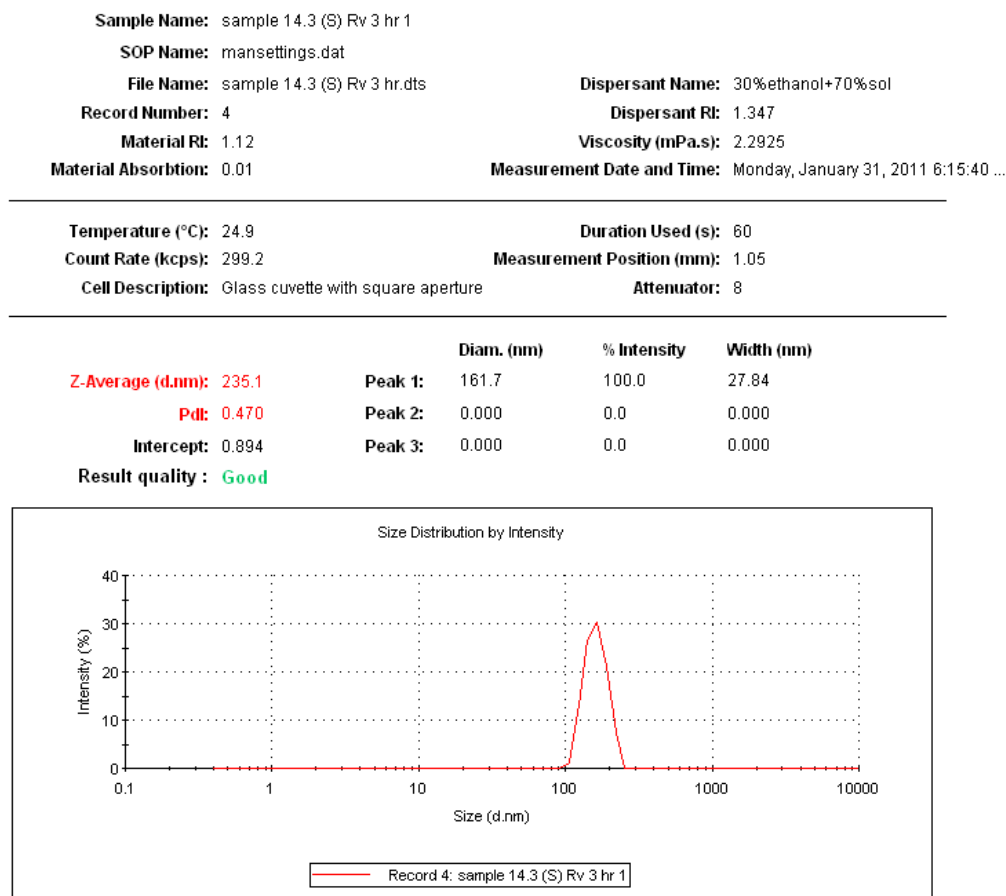


Figure A.13 PCS software for sizing analysis of the 2-hour treated sample obtained from the 3000 psi and 60°C treatment with additional 1-hour sonication. NMP was used as a co-solvent.





*Figure A.14 PCS software for zeta potential analysis of the 2-hour treated sample obtained from the 3000 psi and 60°C treatment with additional 1-hour sonication. NMP was used as a co-solvent.*



*Figure A.15 PCS software for sizing analysis of the 3-hour treated sample obtained from the 3000 psi and 60°C with additional 1-hour sonication. NMP was used as a co-solvent.*

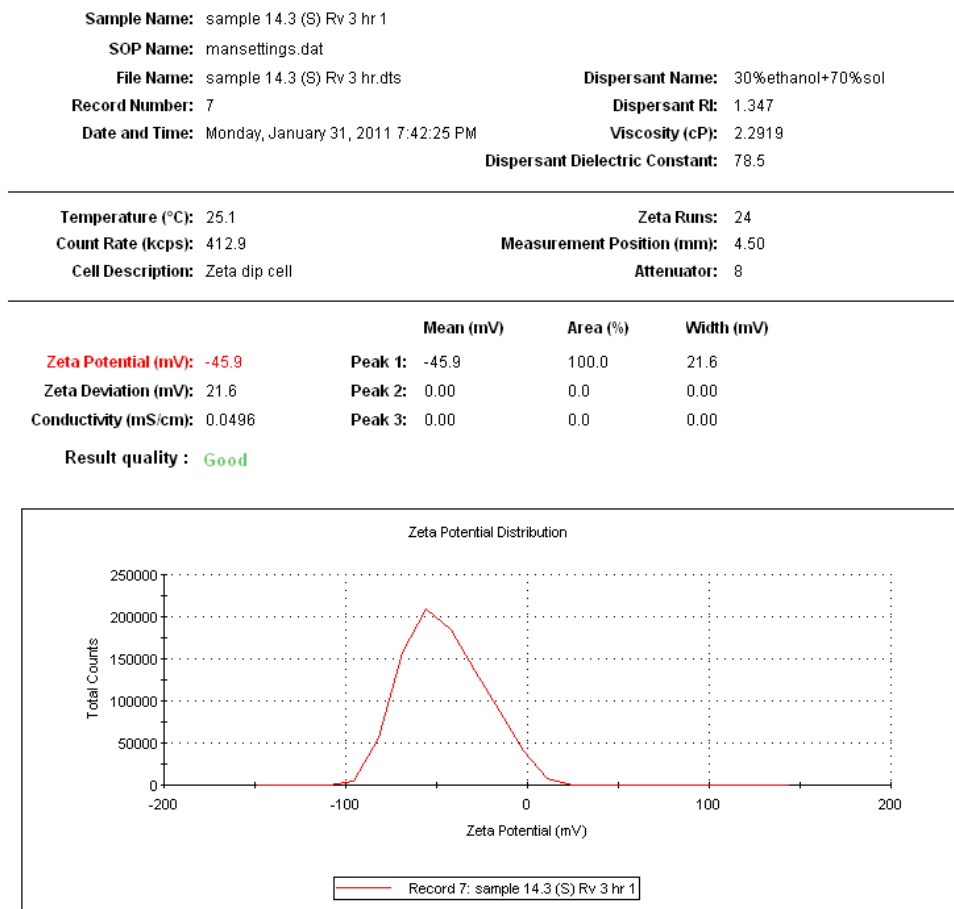


*Figure A.16 PCS software for zeta potential analysis of the 3-hour treated sample obtained from the 3000 psi and 60°C treatment with additional 1-hour sonication. NMP was used as a co-solvent.*

<b>Sample Name:</b> sample 14.2 Rv 2 hr 1			
<b>SOP Name:</b> mansettings.dat			
<b>File Name:</b> sample 14.2 Rv 2 hr.dts		<b>Dispersant Name:</b> Water	
<b>Record Number:</b> 2		<b>Dispersant RI:</b> 1.330	
<b>Material RI:</b> 1.12		<b>Viscosity (mPa.s):</b> 0.8871	
<b>Material Absorption:</b> 0.01		<b>Measurement Date and Time:</b> Sunday, January 30, 2011 11:28:16...	
<b>Temperature (°C):</b> 25.0		<b>Duration Used (s):</b> 120	
<b>Count Rate (kcps):</b> 71.3		<b>Measurement Position (mm):</b> 4.65	
<b>Cell Description:</b> Glass cuvette with square aperture		<b>Attenuator:</b> 10	
		<b>Diam. (nm)</b>	<b>% Intensity</b>
<b>Z-Average (d.nm):</b> 173.7	<b>Peak 1:</b>	225.8	87.3
<b>Pdl:</b> 0.382	<b>Peak 2:</b>	34.73	9.7
<b>Intercept:</b> 0.791	<b>Peak 3:</b>	13.83	3.0
<b>Result quality :</b> Refer to quality report		<b>Width (nm)</b>	
			86.15
			9.971
			2.723

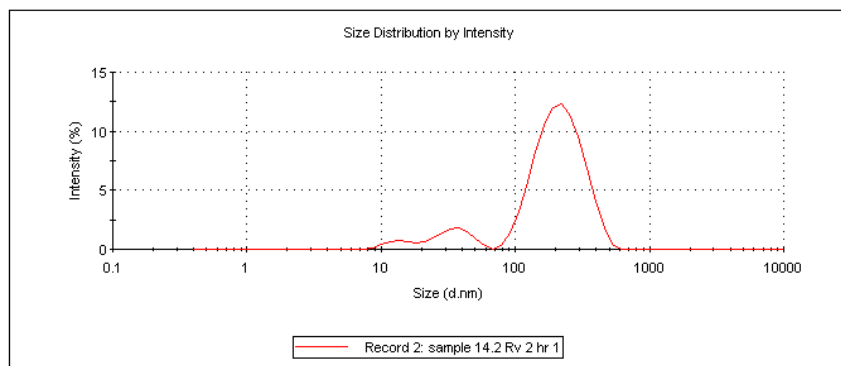


Figure A.17 PCS software for sizing analysis of the 2-hour treated sample obtained from the 3000 psi and 60°C without additional sonication. NMP was used as a co-solvent.

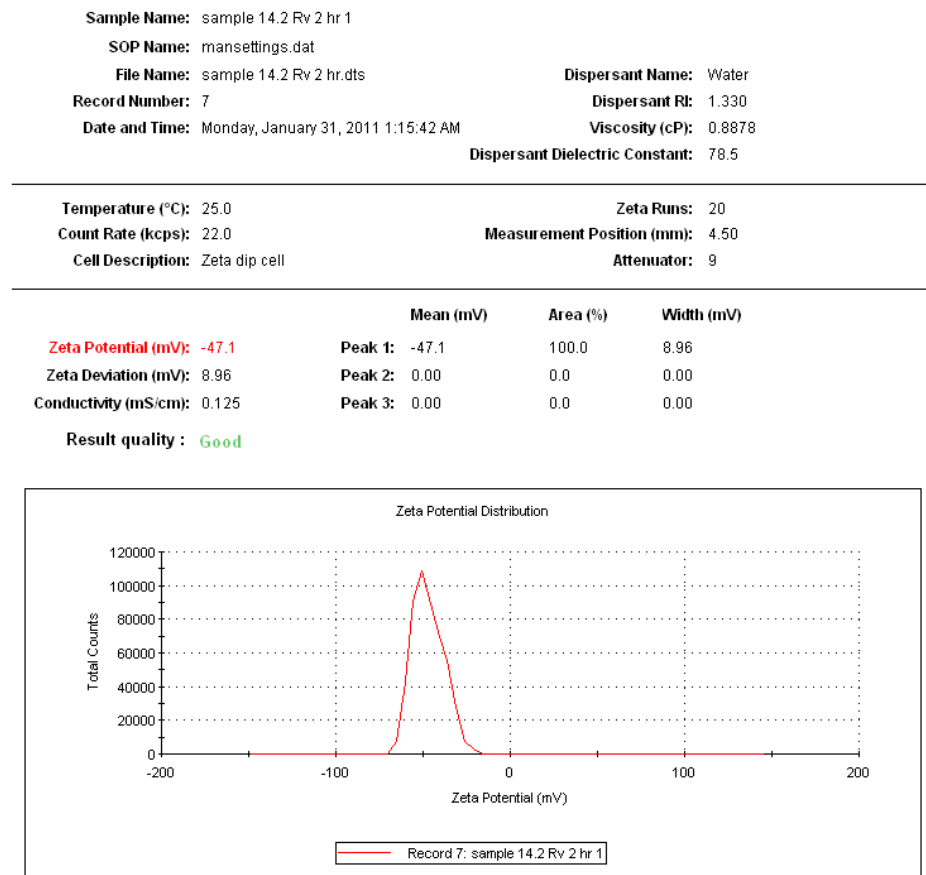
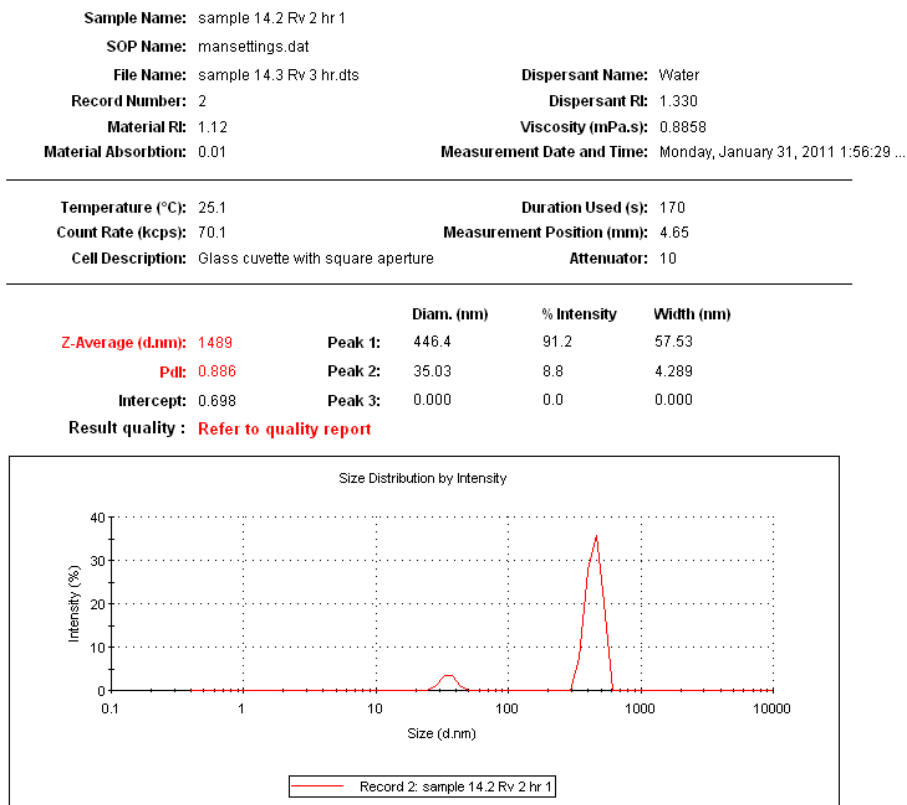


Figure A.18 PCS software for zeta potential analysis of the 2-hour treated sample obtained from the 3000 psi and 60°C without additional sonication. NMP was used as a co-solvent.



*Figure A.19 PCS software for sizing analysis of the 3-hour treated sample obtained from the 3000 psi and 60°C without additional sonication. NMP was used as a co-solvent.*

<b>Sample Name:</b> sample 14.3 Rv 3 hr 1			
<b>SOP Name:</b> mansettings.dat			
<b>File Name:</b> sample 14.3 Rv 3 hr.dts		<b>Dispersant Name:</b> Water	
<b>Record Number:</b> 6		<b>Dispersant RI:</b> 1.330	
<b>Date and Time:</b> Monday, January 31, 2011 2:19:57 AM		<b>Viscosity (cP):</b> 0.8877	
		<b>Dispersant Dielectric Constant:</b> 78.6	
<b>Temperature (°C):</b> 25.0		<b>Zeta Runs:</b> 16	
<b>Count Rate (kcps):</b> 10.8		<b>Measurement Position (mm):</b> 4.50	
<b>Cell Description:</b> Zeta dip cell		<b>Attenuator:</b> 8	
		<b>Mean (mV)</b>	<b>Area (%)</b>
<b>Zeta Potential (mV):</b> -50.4	<b>Peak 1:</b> -50.4	100.0	11.0
<b>Zeta Deviation (mV):</b> 11.0	<b>Peak 2:</b> 0.00	0.0	0.00
<b>Conductivity (mS/cm):</b> 0.116	<b>Peak 3:</b> 0.00	0.0	0.00
<b>Result quality :</b> <span>Good</span>			

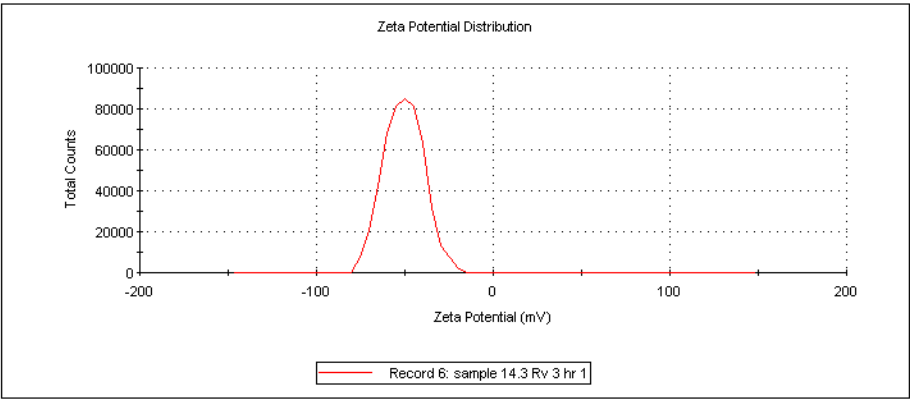


Figure A.20 PCS software for zeta potential analysis of the 3-hour treated sample obtained from the 3000 psi and 60°C without additional sonication. NMP was used as a co-solvent.

## **Appendix B. BET analysis data**



**Table B.1**

The data of relative pressure ( $P/P_0$ ) and the value of  $1/[Q(P_0/P - 1)]$  of each sample from different supercritical treatment condition.

Graphite: N <sub>2</sub>		3000 psi, 40°C (NMP): N <sub>2</sub>	
Relative Pressure ( $P/P_0$ )	$1/[Q(P_0/P - 1)]$	Relative Pressure ( $P/P_0$ )	$1/[Q(P_0/P - 1)]$
0.125096107	1.033468036	0.096123732	0.898335313
0.148229356	1.256862387	0.1255397	1.156014305
0.175293887	1.56631249	0.150378841	1.415329524
0.200264787	1.837758491	0.175345382	1.633968549
0.225157132	2.135584397	0.200504514	1.860856672
0.248609243	2.500609484	0.225354107	2.118343386
0.27491877	2.881901823	0.250633884	2.438327557
0.299794099	3.270809835	0.275514798	2.746981366
		0.300445911	3.015273895

**Table B.1 (cont.)**

3000 psi, 50°C (NMP): N <sub>2</sub>		3000 psi, 60°C (NMP): N <sub>2</sub>	
Relative Pressure ( $P/P_0$ )	$1/[Q(P_0/P - 1)]$	Relative Pressure ( $P/P_0$ )	$1/[Q(P_0/P - 1)]$
0.098386948	0.83837791	0.097128279	0.9664418
0.125363032	1.083720801	0.125632618	1.235436222
0.150092563	1.320194083	0.150435434	1.510195993
0.175084799	1.590033367	0.17546813	1.779735814
0.196423046	1.860341934	0.200540808	2.10795877
0.225044668	2.176729891	0.225581943	2.383518743
0.249999922	2.548962372	0.25049426	2.678660236
0.274875815	2.841820748	0.275768598	3.056374996
0.299907229	3.254269051	0.300578049	3.453187854

**Table B.1 (cont.)**

2500 psi, 60°C (NMP): N <sub>2</sub>		2000 psi, 60°C (NMP): N <sub>2</sub>	
Relative Pressure (P/P <sub>0</sub> )	1/[Q(Po/P - 1)]	Relative Pressure (P/P <sub>0</sub> )	1/[Q(Po/P - 1)]
0.101062629	1.289261191	0.100288838	1.123893348
0.125013483	1.593151921	0.125026915	1.421660507
0.150639986	2.052620814	0.14832988	1.788771539
0.175461908	2.508251634	0.175370248	2.139947923
0.200516992	3.123081944	0.20062975	2.581094415
0.225487265	3.560943089	0.225368281	3.051550412
0.250288461	4.171508728	0.249517938	3.562295716
0.27555234	4.509963031	0.275326215	3.957429755
0.300352606	5.333303559	0.300361052	4.7430308

**Table B.1 (cont.)**

3000 psi, 40°C (Iso): N <sub>2</sub>		3000 psi, 40°C (DMF): N <sub>2</sub>	
Relative Pressure (P/P <sub>0</sub> )	1/[Q(Po/P - 1)]	Relative Pressure (P/P <sub>0</sub> )	1/[Q(Po/P - 1)]
0.098121356	0.855218414	0.100964378	0.816157814
0.125635762	1.12799448	0.125111932	1.003925115
0.14872568	1.385771758	0.150569265	1.225850351
0.173676803	1.665914699	0.175292053	1.451784722
0.200332208	2.024995639	0.200366215	1.652838089
0.224624126	2.350218705	0.225463648	1.936725052
0.250470892	2.715800315	0.250589983	2.208916974
0.274942434	3.141178232	0.275516199	2.569846283
0.299288193	3.623342748	0.300397881	2.786770545

**Table B.1 (cont.)**

3000 psi, 40°C (NMP): CO <sub>2</sub>		Graphite : CO <sub>2</sub>	
Relative Pressure (P/P <sub>0</sub> )	1/[Q(Po/P - 1)]	Relative Pressure (P/P <sub>0</sub> )	1/[Q(Po/P - 1)]
0.112048745	1.020787263	0.003795029	0.006126219
0.163116177	1.112511478	0.007860901	0.006061596
0.177274705	1.07931605	0.016228289	0.008136095
0.193860233	1.085516034	0.050195556	0.019018857
0.205737502	0.904094263	0.104267201	0.038428859
0.218091047	0.296523768	0.140304726	0.043682405
0.263018988	0.265470532	0.195292702	0.054440146
0.308983156	0.267407208	0.250930203	0.069508322
		0.260680497	0.069933993
		0.279599253	0.067113619
		0.320368387	0.072870294
		0.337433528	0.077765633
		0.52047158	0.163374492

**Table B.2**

The isotherm relationship between relative pressure ( $P/P_0$ ) and quantity absorbed (mmol/g) of absorbtive gases ( $N_2$  and  $CO_2$ ) for various samples.

Graphite : $N_2$		Graphite $N_2$	
Relative Pressure ( $P/P_0$ )	Quantity Absorbed (mmol/g)	Relative Pressure ( $P/P_0$ )	Quantity Absorbed (mmol/g)
0.100421784	0.137246515	0.839474278	0.102289381
0.120170404	0.138821998	0.859581654	0.115310724
0.125096107	0.138352304	0.874293097	0.132533884
0.140309738	0.138208534	0.88944084	0.155039065
0.148229356	0.138459839	0.904522377	0.179717562
0.160316339	0.136704327	0.914417989	0.200435153
0.175293887	0.135702905	0.924433643	0.22420217
0.183362612	0.137418215	0.932336655	0.250479109
0.200264787	0.136260487	0.939434401	0.277017634
0.225157132	0.136067789	0.946206355	0.313484924
0.248609243	0.132313924	0.952383446	0.343289069
0.27491877	0.131564448	0.958162806	0.383111459
0.299794099	0.130900715	0.963235689	0.423628436
0.349667271	0.127218115	0.967205652	0.460136197
0.399585178	0.117709135	0.970208819	0.491169784
0.446176852	0.114394904	0.973080416	0.528122275
0.499933093	0.104887971	0.976120225	0.576526153
0.546130197	0.095077449	0.979026095	0.632252584
0.599742971	0.083911354	0.982340347	0.685646994
0.649977039	0.077773378	0.98389047	0.727527861
0.699912026	0.072091359	0.986412802	0.781420521
0.739760869	0.073851252	0.987869896	0.831232712
0.769761899	0.073982394	0.989273204	0.873854359
0.799606697	0.081157776	0.989902955	0.917706307
0.819674965	0.088520985		

**Table B.2 (cont.)**

3000 psi, 40°C (NMP): N <sub>2</sub>		3000 psi, 40°C (NMP): N <sub>2</sub>	
Relative Pressure (P/P <sub>0</sub> )	Quantity Absorbed (mmol/g)	Relative Pressure (P/P <sub>0</sub> )	Quantity Absorbed (mmol/g)
0.096123732	0.118381317	0.840156521	0.176286667
0.12055014	0.123790159	0.860119256	0.193816124
0.1255397	0.12418747	0.875290316	0.212412868
0.140418196	0.125546044	0.890197212	0.238114238
0.150378841	0.125055802	0.905335653	0.264035933
0.16032517	0.126569041	0.915225836	0.286767007
0.175345382	0.130130334	0.925251602	0.314496392
0.180626209	0.130574275	0.933150141	0.342705808
0.200504514	0.134770616	0.940229419	0.371007744
0.225354107	0.13733015	0.947161831	0.405031597
0.250633884	0.137168278	0.95311543	0.442246257
0.275514798	0.138439397	0.959202304	0.487638742
0.300445911	0.142435495	0.964263827	0.52963829
0.350560598	0.141036185	0.968149094	0.569638191
0.40055127	0.141475736	0.971156206	0.607483107
0.45054533	0.13718023	0.974217436	0.651637137
0.500583984	0.13510526	0.977115489	0.697860175
0.550814844	0.129805158	0.980219304	0.75396082
0.600811803	0.12785885	0.982226434	0.799871463
0.650707487	0.126673787	0.984235047	0.847601014
0.700689609	0.127180943	0.986199426	0.901137671
0.74014952	0.134316304	0.988118996	0.960498579
0.770150788	0.144222281	0.989080593	1.001786894
0.800210046	0.15394018	0.990215416	1.046461942
0.820079949	0.164243582		

**Table B.2 (cont.)**

3000 psi, 50°C (NMP): N <sub>2</sub>		3000 psi, 50°C (NMP): N <sub>2</sub>	
Relative Pressure (P/P <sub>0</sub> )	Quantity Absorbed (mmol/g)	Relative Pressure (P/P <sub>0</sub> )	Quantity Absorbed (mmol/g)
0.098386948	0.130159979	0.840272936	0.136873226
0.120197307	0.131016941	0.860139238	0.155518813
0.125363032	0.1322587	0.875313524	0.172737303
0.140425154	0.132291569	0.890192998	0.193699919
0.150092563	0.133767239	0.905079495	0.22051366
0.160110617	0.13426158	0.915288104	0.244505522
0.175084799	0.133485133	0.925268049	0.271275322
0.180327507	0.132155569	0.933181446	0.295228679
0.196423046	0.131392989	0.940243724	0.32091312
0.225044668	0.133409734	0.947084689	0.359129652
0.249999922	0.130772113	0.953208221	0.394710442
0.274875815	0.133391286	0.959211215	0.435626035
0.299907229	0.131636972	0.964134263	0.477073724
0.349773678	0.125476192	0.968194513	0.517517476
0.399590997	0.123173327	0.971169346	0.554898807
0.447162952	0.117853345	0.974219557	0.589321944
0.494386306	0.114027594	0.97705564	0.630909363
0.549762978	0.106920052	0.980239292	0.681490918
0.600375727	0.097441568	0.982093509	0.720661815
0.650362795	0.093255243	0.984159404	0.766123
0.700122752	0.095745422	0.986112845	0.81457061
0.740203496	0.100023523	0.988168205	0.866241308
0.77007947	0.107762822	0.988974817	0.905836119
0.800325633	0.113196316	0.990449371	0.954511929
0.820034892	0.125148447		

**Table B.2 (cont.)**

3000 psi, 60°C (NMP): N <sub>2</sub>		3000 psi, 60°C (NMP): N <sub>2</sub>	
Relative Pressure (P/P <sub>0</sub> )	Quantity Absorbed (mmol/g)	Relative Pressure (P/P <sub>0</sub> )	Quantity Absorbed (mmol/g)
0.097128279	0.111312501	0.840224217	0.136525773
0.120336377	0.114671829	0.860120643	0.151910509
0.125632618	0.116302254	0.875280807	0.164502889
0.140413484	0.118381815	0.890150536	0.179535604
0.150435434	0.117252049	0.905151299	0.202494597
0.160452305	0.121059179	0.915238916	0.22335636
0.17546813	0.119573588	0.925194345	0.248729712
0.180572116	0.120168363	0.93316728	0.276647736
0.200540808	0.118999284	0.940240957	0.302711669
0.225581943	0.122210998	0.947025106	0.333867341
0.25049426	0.124768566	0.953138583	0.3675154
0.275768598	0.124583585	0.959161269	0.406622322
0.300578049	0.12445083	0.964110616	0.44348085
0.350802697	0.123229687	0.96814784	0.484673399
0.400759039	0.122320858	0.971301472	0.519238764
0.447222616	0.11988266	0.97419914	0.557267443
0.501024057	0.112022054	0.977159809	0.600999323
0.547288905	0.099603436	0.980144723	0.649695721
0.600307175	0.098289364	0.98205135	0.689126025
0.650268623	0.095601402	0.984233733	0.736276891
0.700222568	0.097053855	0.98599506	0.789154241
0.74020723	0.102367314	0.988279368	0.86160605
0.770198942	0.106068716	0.988864608	0.898728432
0.800118582	0.115515759	0.990662879	0.957569186
0.820142908	0.127752621		

**Table B.2 (cont.)**

2500 psi, 60°C (NMP): N <sub>2</sub>		2500 psi, 60°C (NMP): N <sub>2</sub>	
Relative Pressure (P/P <sub>0</sub> )	Quantity Absorbed (mmol/g)	Relative Pressure (P/P <sub>0</sub> )	Quantity Absorbed (mmol/g)
0.101062629	0.087200755	0.839501183	0.032230798
0.120480562	0.087605165	0.859511849	0.037551928
0.125013483	0.089680558	0.874474472	0.044780373
0.140583608	0.08832576	0.889503245	0.053506813
0.150639986	0.086405169	0.904375232	0.066080014
0.158499936	0.090343894	0.914224746	0.078960839
0.175461908	0.08484007	0.924360796	0.094406507
0.180528692	0.084275882	0.932347247	0.108493962
0.200516992	0.080307954	0.939236756	0.123912233
0.225487265	0.081757654	0.946103953	0.148170376
0.250288461	0.080030121	0.952147363	0.173970241
0.27555234	0.084338157	0.958227057	0.202611196
0.300352606	0.080492586	0.963142199	0.227828865
0.350313159	0.073335456	0.96697751	0.254372233
0.400359615	0.069589266	0.970113972	0.279871647
0.446864485	0.063061593	0.973094966	0.305876465
0.493456792	0.052643286	0.975990774	0.333924901
0.546894737	0.039744387	0.978854865	0.366410158
0.600044603	0.031656179	0.98091598	0.396251251
0.64557833	0.02677175	0.984265631	0.442365546
0.699817158	0.019671891	0.986147813	0.477775849
0.739802664	0.021505937	0.988220062	0.519533034
0.769797713	0.017824497	0.988789602	0.541903799
0.799548705	0.023321038	0.990484606	0.581068689
0.819631224	0.026939201		



**Table B.2 (cont.)**

2000 psi, 60°C (NMP): N <sub>2</sub>		2000 psi, 60°C (NMP): N <sub>2</sub>	
Relative Pressure (P/P <sub>0</sub> )	Quantity Absorbed (mmol/g)	Relative Pressure (P/P <sub>0</sub> )	Quantity Absorbed (mmol/g)
0.100288838	0.099180066	0.839531055	0.047605379
0.120257256	0.10087546	0.859639522	0.059916149
0.125026915	0.100510844	0.874491904	0.073982678
0.140433355	0.098359527	0.889519838	0.091177766
0.14832988	0.097364886	0.904395592	0.114777844
0.156386148	0.098325137	0.914484136	0.136455214
0.175370248	0.099378792	0.924426674	0.163475229
0.180188727	0.098044574	0.932437047	0.190951533
0.20062975	0.097239666	0.939402346	0.217247581
0.225368281	0.095340399	0.947139884	0.251174234
0.249517938	0.093332197	0.953131044	0.283941498
0.275326215	0.096004546	0.959197722	0.325064775
0.300361052	0.09051357	0.964203347	0.367645516
0.350264414	0.084751055	0.968211387	0.406159682
0.397430307	0.079024279	0.971227909	0.442589597
0.444357218	0.065701624	0.974284858	0.482554865
0.499119607	0.05617235	0.97716619	0.52831973
0.545628253	0.048772463	0.980257502	0.580206769
0.599773802	0.038319149	0.98210705	0.62278026
0.646014554	0.034332163	0.984182748	0.673114247
0.699944799	0.025438595	0.986175247	0.724679314
0.739890788	0.025125464	0.988060047	0.7849591
0.769755713	0.028812679	0.98915215	0.829325916
0.799648913	0.033420917	0.990172776	0.872099738
0.819598017	0.038170854		

**Table B.2 (cont.)**

3000 psi, 40°C (Iso): N <sub>2</sub>		3000 psi, 40°C (Iso): N <sub>2</sub>	
Relative Pressure (P/P <sub>0</sub> )	Quantity Absorbed (mmol/g)	Relative Pressure (P/P <sub>0</sub> )	Quantity Absorbed (mmol/g)
0.098121356	0.127215021	0.839909617	0.087828018
0.120258681	0.128159776	0.859821257	0.104030278
0.125635762	0.127383717	0.874887175	0.118901479
0.140491135	0.127084841	0.889840542	0.136646744
0.14872568	0.126073765	0.904823859	0.163007787
0.157073346	0.126017805	0.914893365	0.187493453
0.173676803	0.126165063	0.924851196	0.216901979
0.180339757	0.125727797	0.932852387	0.244426423
0.200332208	0.123713496	0.939704425	0.276988188
0.224624126	0.123263881	0.946841297	0.310806003
0.250470892	0.123046971	0.952639145	0.346445819
0.274942434	0.120719299	0.958792855	0.390168055
0.299288193	0.117880164	0.963736057	0.432466988
0.347872006	0.110783006	0.968124306	0.47702857
0.395982403	0.104755621	0.97124625	0.511358108
0.450355316	0.092143278	0.974163747	0.549878558
0.500372018	0.082532418	0.9771757	0.593229166
0.548088825	0.074659699	0.980106679	0.648449791
0.595763558	0.068122977	0.982204745	0.697287207
0.643299981	0.060945842	0.984251926	0.748736825
0.700193113	0.058668351	0.986184922	0.799808671
0.739974697	0.062139962	0.988037849	0.857099654
0.770066226	0.064538077	0.989066495	0.902471893
0.799924476	0.069895067	0.99029408	0.953671005
0.819977869	0.07642001		

**Table B.2 (cont.)**

3000 psi, 40°C (DMF): N <sub>2</sub>		3000 psi, 40°C (DMF): N <sub>2</sub>	
Relative Pressure (P/P <sub>0</sub> )	Quantity Absorbed (mmol/g)	Relative Pressure (P/P <sub>0</sub> )	Quantity Absorbed (mmol/g)
0.100964378	0.137599587	0.840280754	0.174646184
0.120291374	0.142400838	0.860146598	0.193299196
0.125111932	0.142444249	0.875179707	0.217251209
0.140665051	0.14216377	0.890390764	0.240778101
0.150569265	0.144600869	0.905055046	0.275227256
0.160404458	0.144368405	0.915298311	0.300611726
0.175292053	0.146406321	0.925157116	0.334630565
0.180338034	0.149362507	0.933377315	0.359484022
0.200366215	0.151601343	0.940075795	0.387614394
0.225463648	0.15030269	0.947202691	0.426379522
0.250589983	0.151378717	0.953245124	0.462793283
0.275516199	0.147982825	0.959045436	0.511308073
0.300397881	0.154079385	0.964150412	0.56036304
0.350633079	0.147401058	0.968165931	0.60886659
0.4004731	0.150831467	0.971222958	0.648513144
0.45051269	0.146312736	0.974203125	0.684441188
0.500578429	0.145610266	0.977208175	0.717022882
0.550517325	0.135605736	0.980012278	0.768316196
0.600408709	0.138171559	0.982149774	0.823503232
0.650501351	0.136217886	0.984209673	0.889674977
0.700508877	0.131692778	0.986231184	0.962043119
0.740442986	0.135119218	0.988171579	1.026930775
0.770296715	0.135427405	0.988900639	1.070688561
0.800181303	0.1439672	0.990530813	1.133893468
0.820138576	0.157848163		

**Table B.2 (cont.)**

Graphite : CO <sub>2</sub>		Graphite : CO <sub>2</sub>	
Relative Pressure (P/P <sub>0</sub> )	Quantity Absorbed (mmol/g)	Relative Pressure (P/P <sub>0</sub> )	Quantity Absorbed (mmol/g)
0.003795029	0.621833226	0.039184276	20.55520768
0.007860901	1.307111913	0.038270742	21.29659011
0.016228289	2.027507145	0.018576905	21.94899613
0.050195556	2.778731958	0.013575861	22.61335107
0.104267201	3.029087031	0.015434324	23.28978969
0.140304726	3.736123465	0.015619044	23.90811612
0.195292702	4.457884322	0.015795821	24.52622969
0.250930203	4.819409681	0.015188462	25.26735989
0.260680497	5.041828334	0.015382067	25.92457158
0.279599253	5.782973414	0.013117235	26.54974031
0.320368387	6.468827377	0.0107283	27.21006062
0.337433528	6.548940806	0.011053905	27.99718826
0.52047158	6.643522628	0.011481089	28.67410684
0.634591781	6.75741771	0.011840919	29.35107214
0.039798904	7.369470834	0.012149334	30.02791286
0.048011876	8.110810796	0.012364837	30.70458696
0.059161588	8.84195169	0.013274922	31.38121407
0.067906237	9.569142942	0.011600813	32.1199962
0.082072402	10.29920324	0.010417121	32.85982386
0.085898843	11.03525924	0.011167036	33.60204614
0.089353483	11.77614352	0.011459181	34.27881021
0.091873568	12.52122962	0.011727996	34.95548473
0.094442689	13.27618507	0.01194452	35.63223005
0.091403502	14.01805652	0.012135371	36.30898142
0.086878675	14.75993178	0.013182849	36.98541647
0.083983271	15.51592371	0.011916484	37.64252247
0.037296262	16.12256953	0.010888416	38.3005149
0.037819542	16.8269716	0.010864024	38.96310633
0.038729147	17.58941633	0.010845839	39.6388805
0.040948053	18.33082256	0.011033074	40.31516272
0.04056105	19.07224225	0.012335123	40.99204904
0.039917806	19.8137147	0.013094685	41.66915993

**Table B.2 (cont.)**

Graphite : CO <sub>2</sub>		Graphite : CO <sub>2</sub>	
Relative Pressure (P/P <sub>0</sub> )	Quantity Absorbed (mmol/g)	Relative Pressure (P/P <sub>0</sub> )	Quantity Absorbed (mmol/g)
0.01390205	42.34620688	0.005781588	64.40994697
0.014789413	43.02307463	0.006455831	65.08623511
0.01557391	43.69999275	0.007134759	65.76256921
0.017809028	44.37678197	0.007781531	66.43867678
0.01475556	45.09140304	0.007507379	67.11476141
0.013703448	45.80427192	0.006957995	67.79038686
0.012948365	46.49881811	0.006433097	68.46570947
0.013503352	47.29886108	0.006035459	69.14091936
0.013783341	47.97622693	0.005725471	69.81559205
0.010297303	48.67140452	0.005372898	70.4901788
0.011431032	49.44827685	0.005254138	71.16469861
0.012352799	50.12566077	0.005212481	71.83896236
0.013258196	50.80303709	0.005167154	72.51301949
0.01414986	51.48034109	0.005118662	73.18723161
0.016477919	52.15725261	0.005070222	73.8614379
0.01419108	52.82134894	0.005022278	74.53576032
0.013778092	53.47147078	0.004899708	75.21036141
0.01328737	54.09196595	0.004839408	75.88515279
0.015131126	54.89693253	0.004776986	76.56042381
0.016354994	55.57445802	0.004714202	77.2358179
0.017551498	56.25173665	0.004652833	77.91163465
0.018598519	56.88379561	0.004596425	78.58743682
0.019649152	57.51546221	0.00448795	79.26351278
0.021908177	58.25660866	0.004424656	79.93972564
0.023132862	58.91098965	0.004366605	80.61616971
0.024332263	59.56519017	0.004311558	81.2927965
0.025022143	60.30621769	0.004302626	81.96926501
0.012189722	61.01898681	0.004247497	82.64589893
0.008262405	61.63938632	0.004135336	83.32251854
0.006273512	62.25130979	0.004070019	83.99874877
0.0057646	62.99222584	0.003989267	84.67512454
0.005138118	63.73357875	0.003929408	85.35108374

**Table B.2 (cont.)**

Graphite : CO <sub>2</sub>		Graphite : CO <sub>2</sub>	
Relative Pressure (P/P <sub>0</sub> )	Quantity Absorbed (mmol/g)	Relative Pressure (P/P <sub>0</sub> )	Quantity Absorbed (mmol/g)
0.003854295	86.02717496	0.002868676	112.5715467
0.003772943	86.70298126	0.00277727	113.2143477
0.00370655	87.37871954	0.002796244	114.3391546
0.003640094	88.05423418	0.002758056	115.4649582
0.003579122	88.72998456	0.002701597	116.1241055
0.003522549	89.40542752	0.002698486	117.2497456
0.003464903	90.08075529	0.002643629	117.893682
0.003412337	90.75629537	0.002648123	119.0189992
0.003369937	91.43182968	0.00258022	119.6784575
0.003317982	92.10721286	0.002596968	120.8045421
0.003267488	92.78272452	0.002610214	121.9301243
0.003223955	93.45807905	0.002579728	123.0558239
0.003179262	94.13336649	0.002502399	123.6993275
0.003138756	94.80868943	0.002519254	124.8265523
0.003140422	95.67138985	0.002559227	125.9512469
0.003202573	97.03395946	0.002546867	127.0200842
0.0032585	98.52435436	0.00236026	127.8552298
0.003178799	99.37693118	0.002377803	128.9227784
0.003123145	100.2859226	0.002368614	130.0444568
0.003075812	101.1943256	0.002223314	130.8961455
0.003030571	102.0639453	0.002146905	132.0089359
0.002990107	102.9330727	0.002128633	132.6130627
0.002969154	103.8409783	0.002079555	133.7891952
0.002944604	104.7486237	0.00201306	134.9654333
0.002928094	105.6175649	0.001995034	135.6241561
0.00290525	106.5424424	0.001989707	136.2275163
0.002902968	107.4663156	0.001948339	137.0621024
0.002872615	108.3197054	0.001998043	138.0501065
0.002858269	109.1732259	0.002020518	139.0972312
0.002843839	110.027515	0.002033362	140.0908306
0.002979087	110.8809903	0.002070705	141.1390295
0.00289873	111.5234906	0.002378828	142.3122642

**Table B.2 (cont.)**

Graphite : CO <sub>2</sub>		3000 psi, 40°C (NMP): CO <sub>2</sub>	
Relative Pressure (P/P <sub>0</sub> )	Quantity Absorbed (mmol/g)	Relative Pressure (P/P <sub>0</sub> )	Quantity Absorbed (mmol/g)
0.002228036	143.4873468	0.11205	0.123618261
0.002165128	144.0898607	0.15412	0.164869327
0.00205422	145.2660178	0.16312	0.175197281
0.00196234	146.440916	0.17727	0.199638035
0.001938656	147.0437079	0.17874	0.209978528
0.001857983	148.2189932	0.19386	0.221534895
0.001823717	148.8212745	0.20574	0.2865073
0.001855695	149.4251471	0.21809	0.940637178
0.001847172	150.2807786	0.26302	1.344356599
0.001816759	151.1982625	0.30898	1.67214164
0.001689003	152.246267	0.31987	1.798200678
0.001700946	153.2400801	0.05358	2.404243266
0.001687534	154.2322341	0.06352	3.058842208
0.001667254	155.1544013	0.07985	3.684172224
0.001527198	155.9942326	0.10402	4.308384692
0.001545596	156.9152682	0.10596	5.049406675
0.00154229	157.8531414	0.11097	5.750511756
0.001560259	158.7889951	0.11685	6.43875449
0.001540437	159.8426148	0.12385	7.106269999
0.001884055	160.6667962	0.11773	7.751131314
0.00327275	161.6615929	0.11262	8.38968647
0.006596328	162.7864972	0.10943	9.00761978
0.008861375	163.626342	0.04362	9.613417869
0.012341385	164.7390046	0.01741	10.22075843
0.018545489	165.794449	0.02955	10.84112486
0.032126712	166.8595451	0.0359	11.46482829
0.08082192	167.9994466	0.04181	12.09081061
0.185397084	169.0227174	0.05309	12.71763798
0.412912043	169.8526699	0.05787	13.4586891
0.698299716	170.3190161	0.06261	14.18762317
0.834067064	170.3319186	0.07104	14.91586645
1.046212205	170.3923617	0.0751	15.63156171

**Table B.2 (cont.)**

3000 psi, 40°C (NMP): CO <sub>2</sub>		3000 psi, 40°C (NMP): CO <sub>2</sub>	
Relative Pressure (P/P <sub>0</sub> )	Quantity Absorbed (mmol/g)	Relative Pressure (P/P <sub>0</sub> )	Quantity Absorbed (mmol/g)
0.07559762	16.3390299	0.002594277	38.47759965
0.075929848	17.0427302	0.002551709	39.12204297
0.078786348	17.73925244	0.002489188	39.7330281
0.003065791	18.4427967	0.002472974	40.41129087
0.002935195	19.18504265	0.00252593	41.08946945
0.00302039	19.86298828	0.002463817	41.74371119
0.003226125	20.54088784	0.002420716	42.40986045
0.003524583	21.21874314	0.002377781	43.07587509
0.003670688	21.89658285	0.002369757	43.74184234
0.003790698	22.57450042	0.00232955	44.41945868
0.003888951	23.25226849	0.002371943	45.09692277
0.003841316	23.93006156	0.002327032	45.77426418
0.003961947	24.60769606	0.002283007	46.45159975
0.003690467	25.28472793	0.002242917	47.12880576
0.00345907	25.96204222	0.002218031	47.80600402
0.003261878	26.63958037	0.00227063	48.4831852
0.003260071	27.38062525	0.002223127	49.16012458
0.003276927	28.05890331	0.002187183	49.83717243
0.003283965	28.73706931	0.002151013	50.51436442
0.003284304	29.41507658	0.002144701	51.1914921
0.003272927	30.09325754	0.002112096	51.86885873
0.003232111	30.77138974	0.002155353	52.54609971
0.00327414	31.44943702	0.002116102	53.22349845
0.003090514	32.24229563	0.002078261	53.9010686
0.002961381	33.03521242	0.002051453	54.57863045
0.002909914	33.6385676	0.002019699	55.25641133
0.002810834	34.37981749	0.002055512	55.93422796
0.002774454	35.05768146	0.002006351	56.61204384
0.002610172	35.79888361	0.001961941	57.29000004
0.002611024	36.47702988	0.001919921	57.96788874
0.002582243	37.15514422	0.001913022	58.64582656
0.002639329	37.83319902	0.001895585	59.32387908



**Table B.2 (cont.)**

3000 psi, 40°C (NMP): CO <sub>2</sub>		3000 psi, 40°C (NMP): CO <sub>2</sub>	
Relative Pressure (P/P <sub>0</sub> )	Quantity Absorbed (mmol/g)	Relative Pressure (P/P <sub>0</sub> )	Quantity Absorbed (mmol/g)
0.00195104	60.0019765	0.000668361	81.70468757
0.001941632	60.67996595	0.000711779	82.38229776
0.001924752	61.35818404	0.000678064	83.05984316
0.001937803	62.03619311	0.000634589	83.73744419
0.002005009	62.71430378	0.00059677	84.41492029
0.002675969	63.39186143	0.000558601	85.09247708
0.002522292	64.06951084	0.000522824	85.76991044
0.002496147	64.74724797	0.000547675	86.44725462
0.002349001	65.42507508	0.00051586	87.12452789
0.002220152	66.10317422	0.000480096	87.80188434
0.002108323	66.78141749	0.000452557	88.47912584
0.001946706	67.45954186	0.000430784	89.15660919
0.00178193	68.13784261	0.000413708	89.83389917
0.001636702	68.81607988	0.000458396	90.51094548
0.001600697	69.49433216	0.000427615	91.18803183
0.001474791	70.1727666	0.000405589	91.86520435
0.001366627	70.85115704	0.000389233	92.54239126
0.00127173	71.52967992	0.000378705	93.21938976
0.001189651	72.20837887	0.000405377	93.89627782
0.00112148	72.88695935	0.000727653	94.57254172
0.001138956	73.56558054	0.002110931	95.24551155
0.00106724	74.24422659	0.008695085	95.9026475
0.001002879	74.92274204	0.058471727	96.74742798
0.00094802	75.60129819	0.131400039	97.00054863
0.000899718	76.28006836	0.190325644	96.9770901
0.000856424	76.95853027	0.276076011	97.068927
0.000818613	77.63687494	0.412673704	99.09029499
0.000849091	78.31509989	0.764144777	100.0616416
0.000800335	78.99302215	0.89414135	100.3565492
0.000758634	79.67113775	1.49831055	99.68340406
0.000722114	80.34907394		
0.000701881	81.02683088		

## **Appendix C. AFM section analysis**

## C.1 Section analysis of the treated flakes at 60°C and 3000 psi

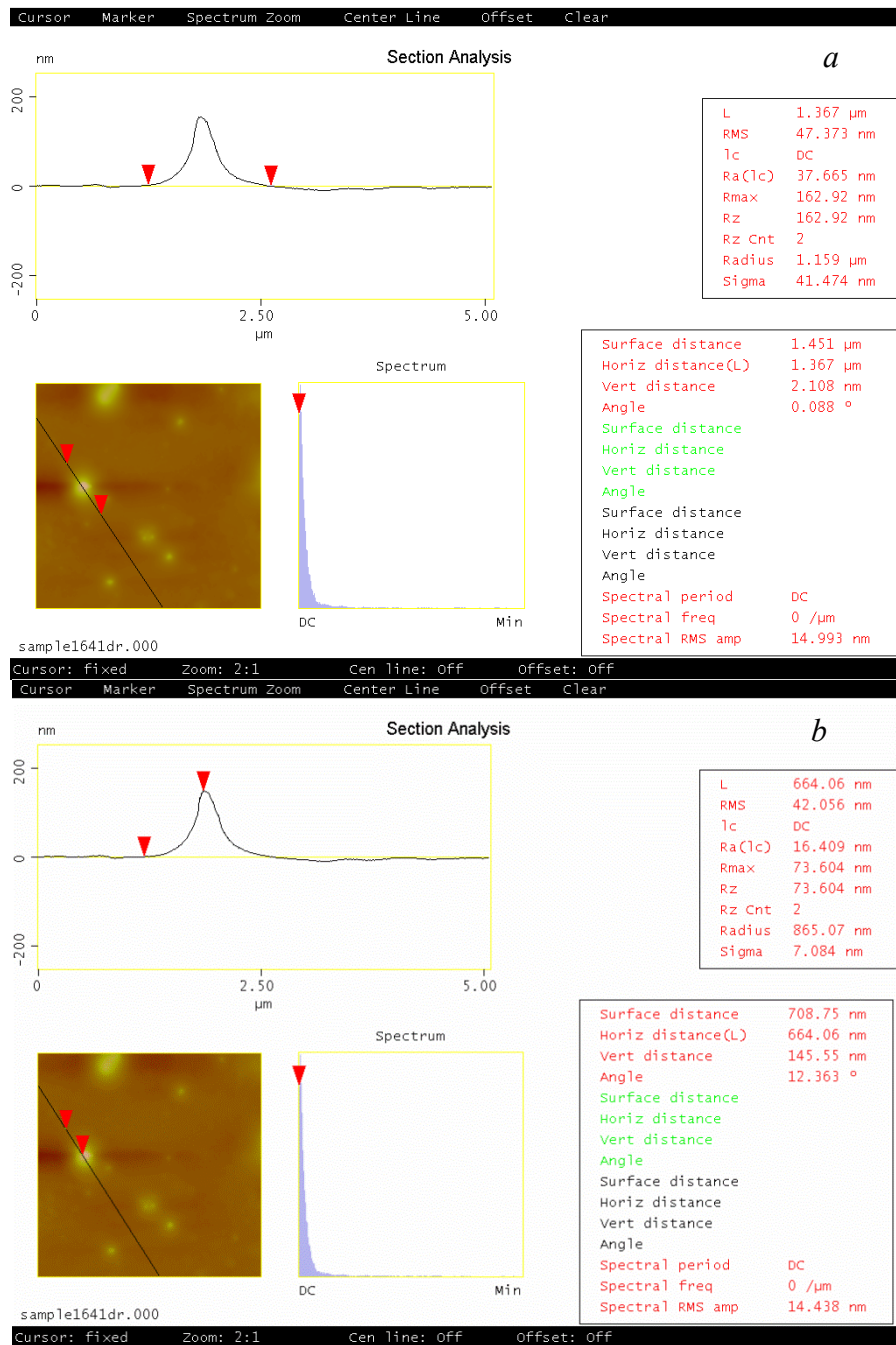


Figure C.1 Horizontal (a) and vertical section analysis (b) of the flake 1.2 of Figure 4.51 (60°C, 3000 psi). The image was constructed at a 5.00 μm scan size, a 1.387 Hz scan rate, 512 numbers per line, and a 500.0 nm data scale.

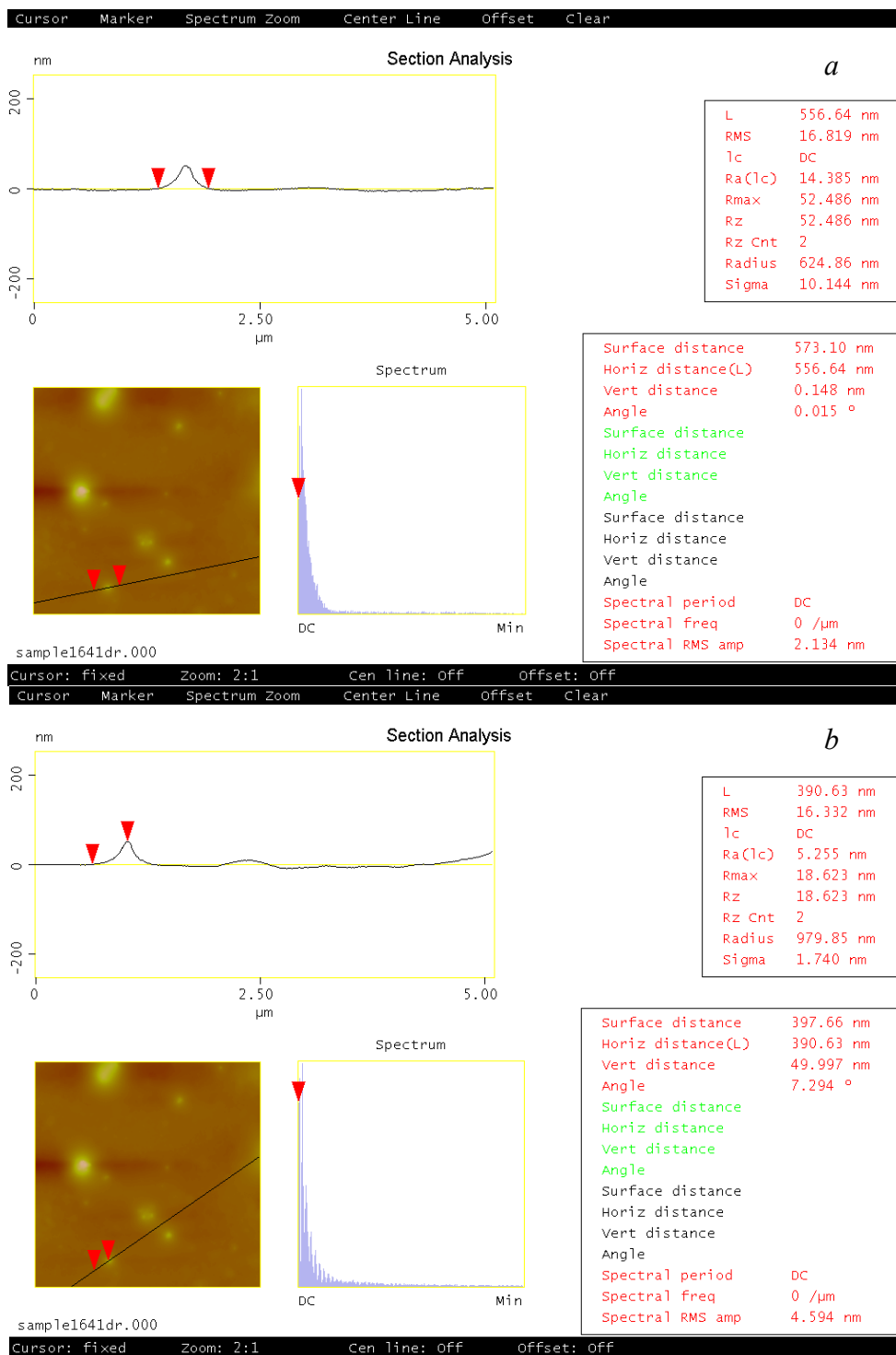


Figure C.2 Horizontal (a) and vertical section analysis (b) of the flake 1.3 of Figure 4.51 (60°C, 3000 psi). The image was constructed at a 5.00 μm scan size, a 1.387 Hz scan rate, 512 numbers per line, and a 500.0 nm data scale.

## C.2 Section analysis of the treated flakes at 60°C and 2500 psi

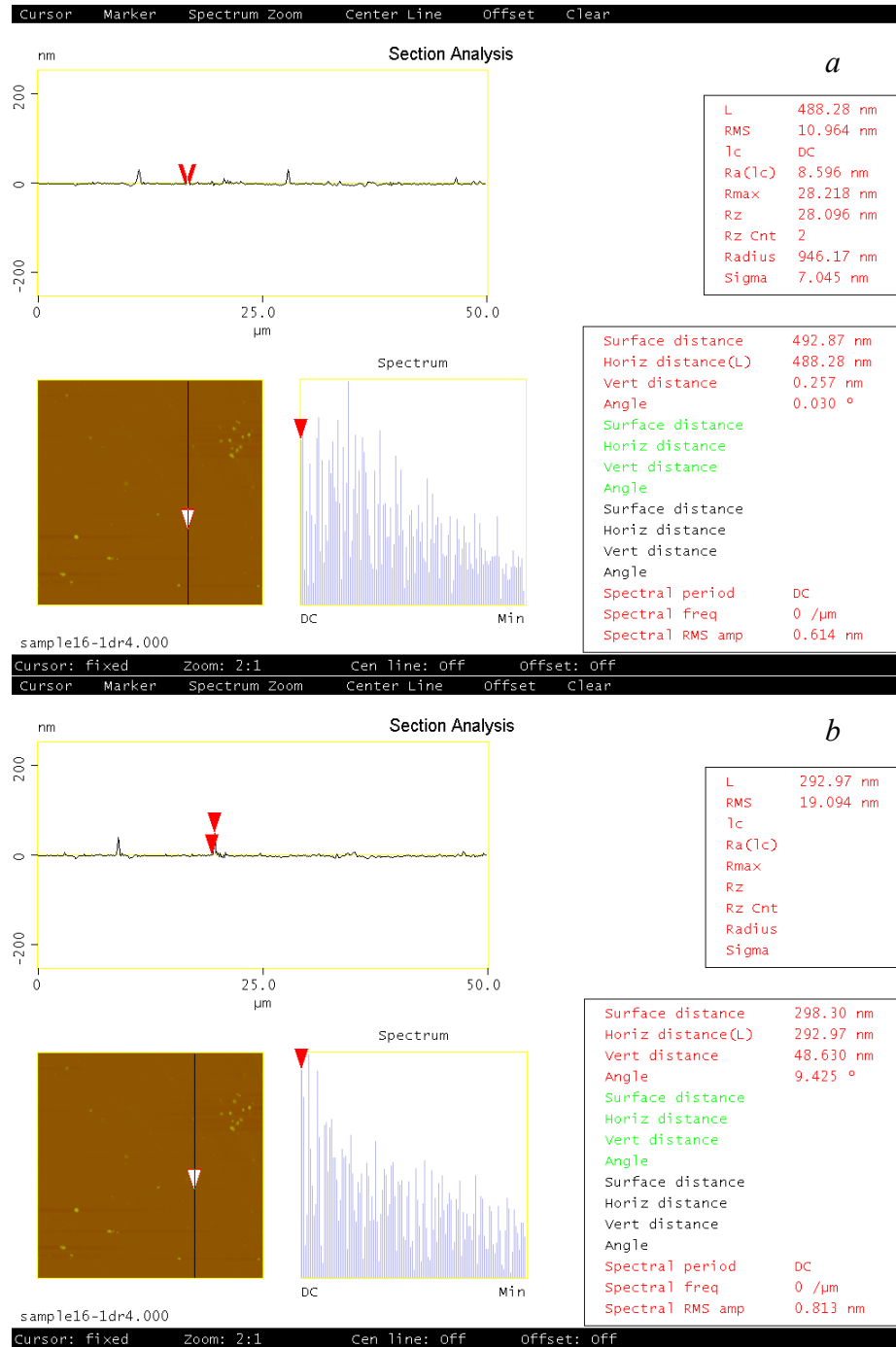


Figure C.3 Horizontal (a) and vertical section analysis (b) of the flake 2.2 (60°C, 2500 psi). The image was constructed at a 50.00  $\mu\text{m}$  scan size, a 0.1001 Hz scan rate, 512 numbers per line, and a 500.0 nm data scale.

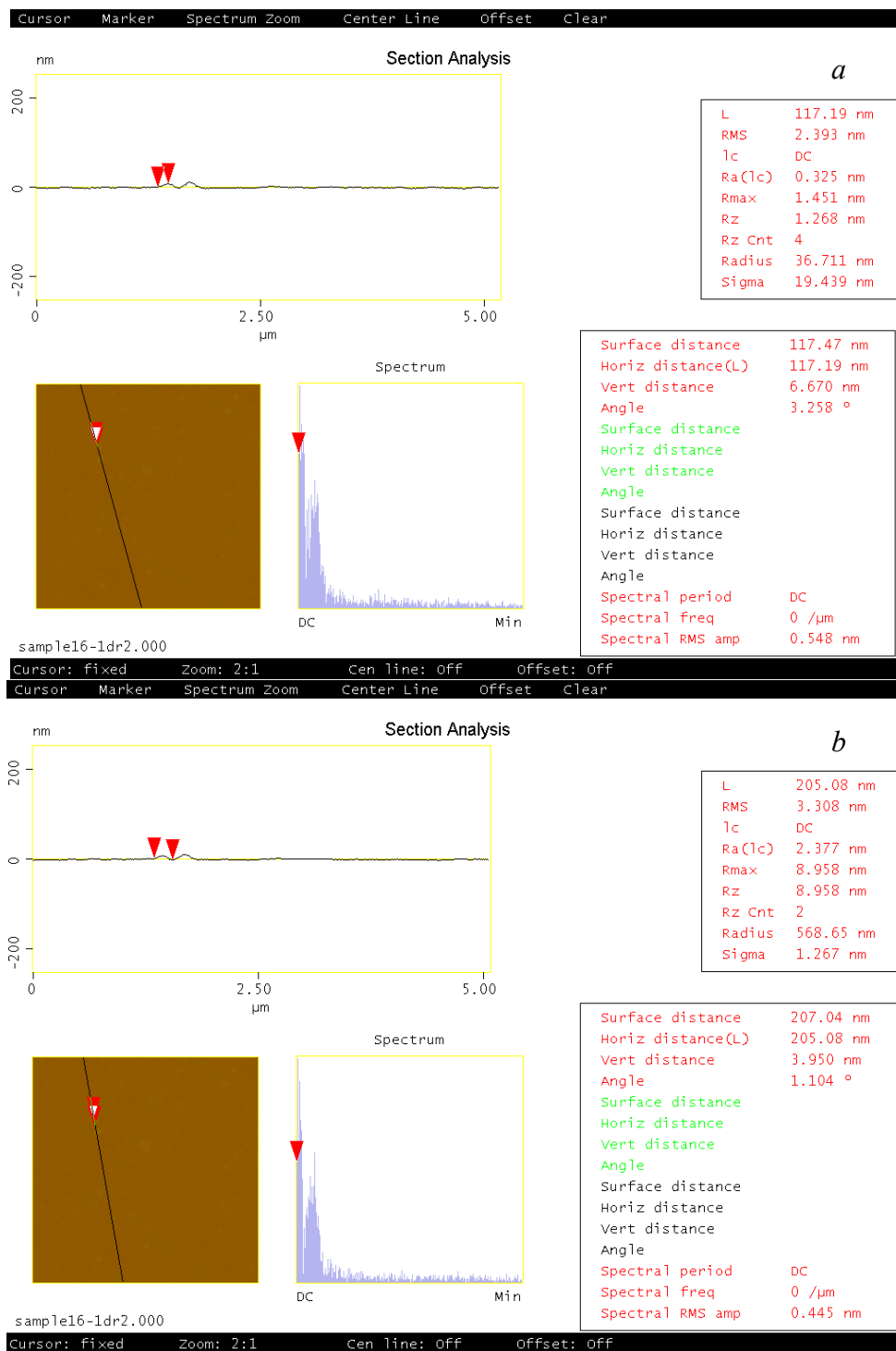


Figure C.4 Horizontal (a) and vertical section analysis (b) of the flake 2.4 of Figure 4.53 (60°C, 2500 psi). The image was constructed at a 5.00  $\mu\text{m}$  scan size, a 1.387 Hz scan rate, 512 numbers per line, and a 500.0 nm data scale.

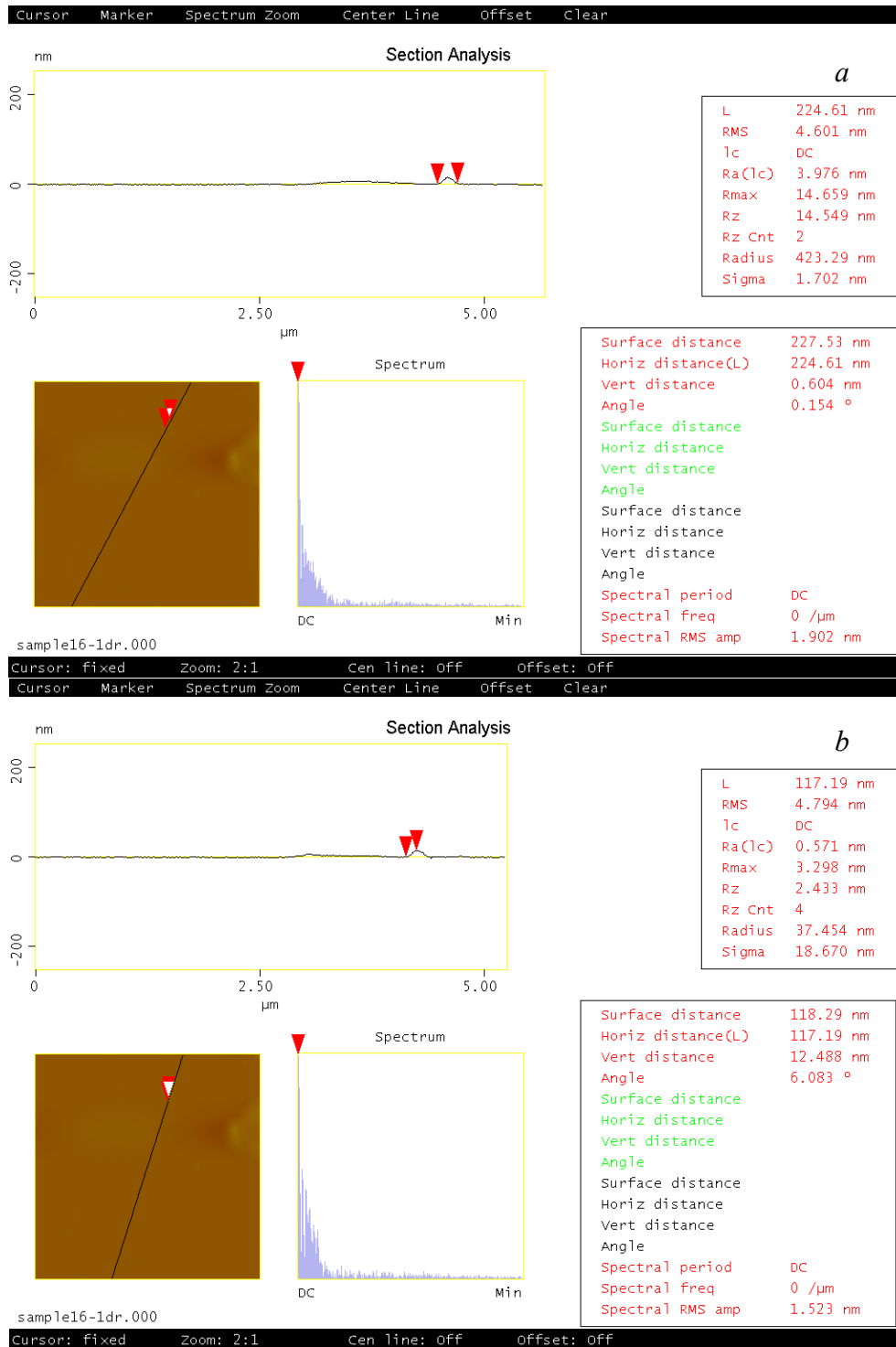


Figure C.5 Horizontal (a) and vertical section analysis (b) of the flake 2.6 of (60°C, 2500 psi). The image was constructed at a 5.00 μm scan size, a 1.387 Hz scan rate, 512 numbers per line, and a 500.0 nm data scale.

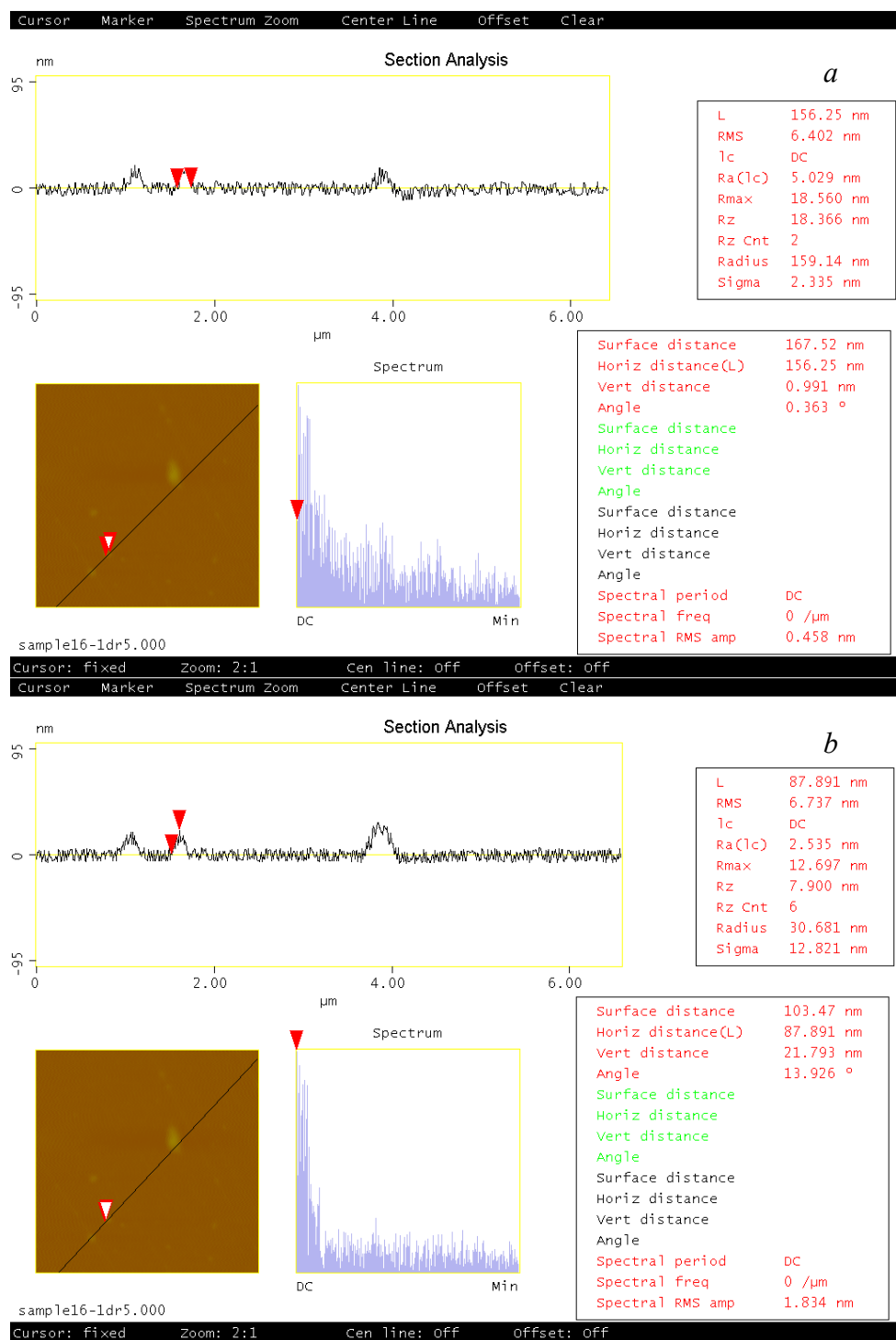


Figure C.6 Horizontal (a) and vertical section analysis (b) of the flake 2.8 of (60°C, 2500 psi). The image was constructed at a 5.00  $\mu\text{m}$  scan size, a 1.001 Hz scan rate, 512 numbers per line, and a 200.0 nm data scale.



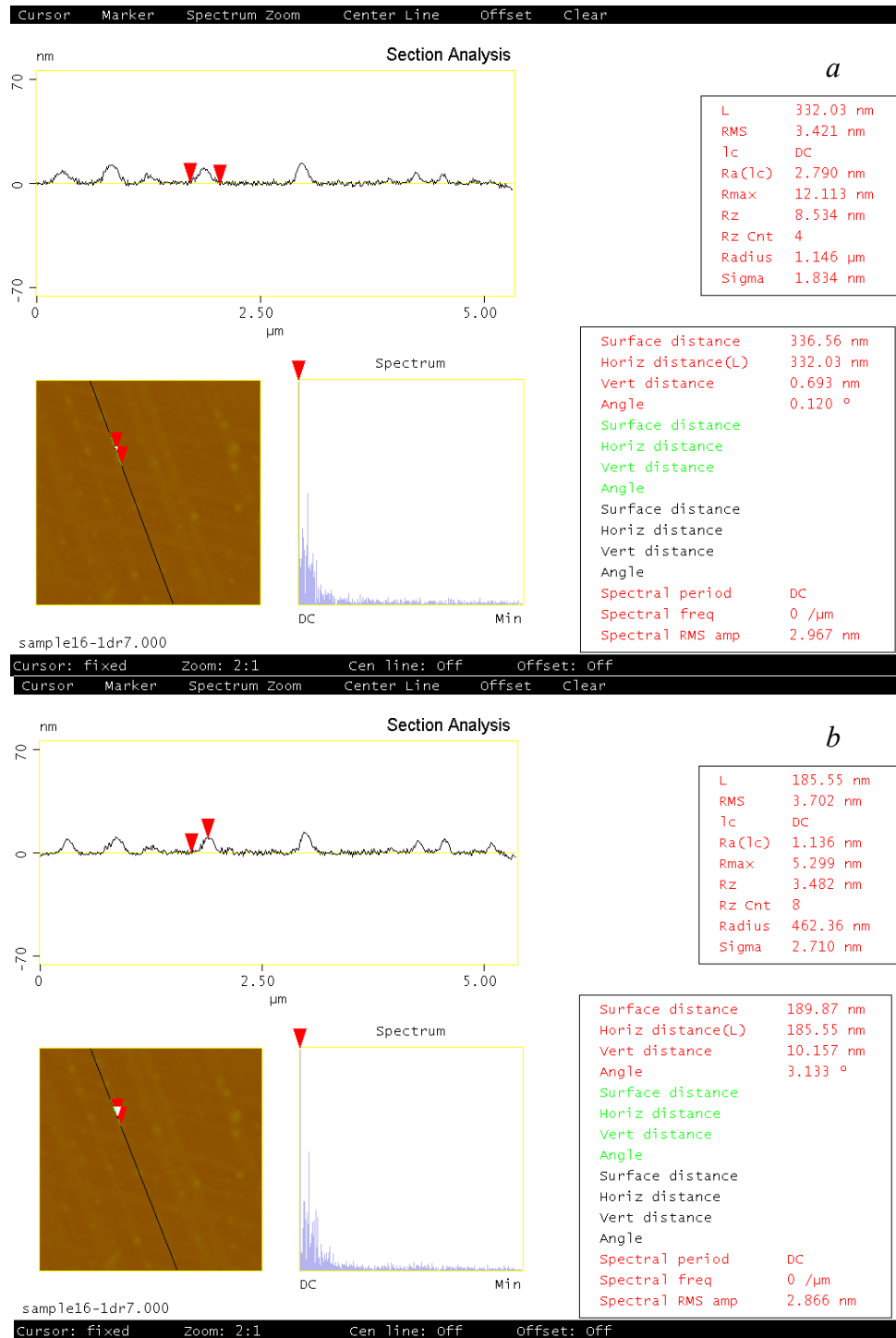


Figure C.7 Horizontal (a) and vertical section analysis (b) of the flake 2.9 (60°C, 2500 psi). The image was constructed at a 5.00 μm scan size, a 1.001 Hz scan rate, 512 numbers per line, and a 150.0 nm data scale.

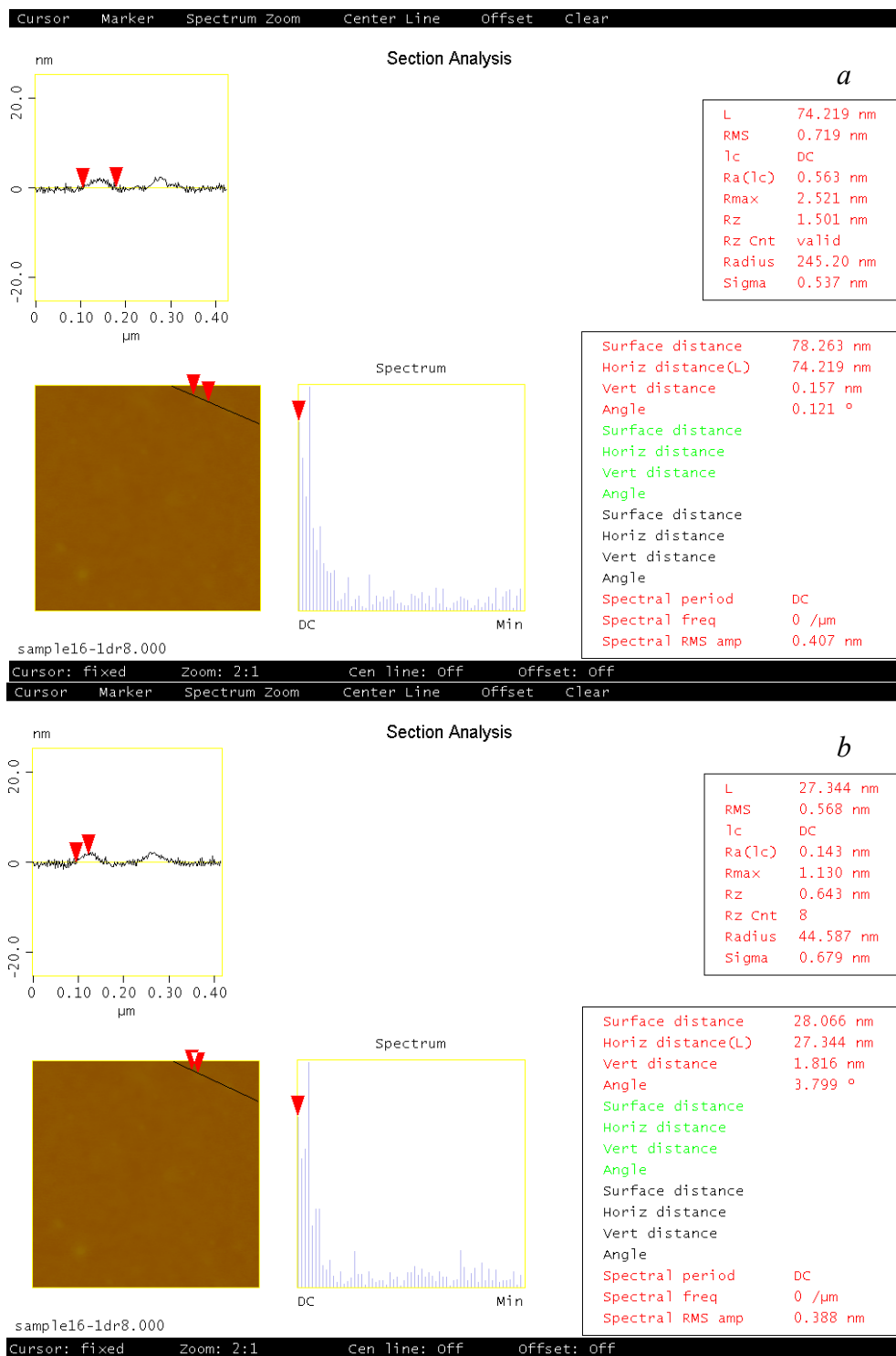


Figure C.8 Horizontal (a) and vertical section analysis (b) of the flake 2.13 (60°C, 2500 psi). The image was constructed at a 1.00  $\mu\text{m}$  scan size, a 1.001 Hz scan rate, 512 numbers per line, and a 50.0 nm data scale.

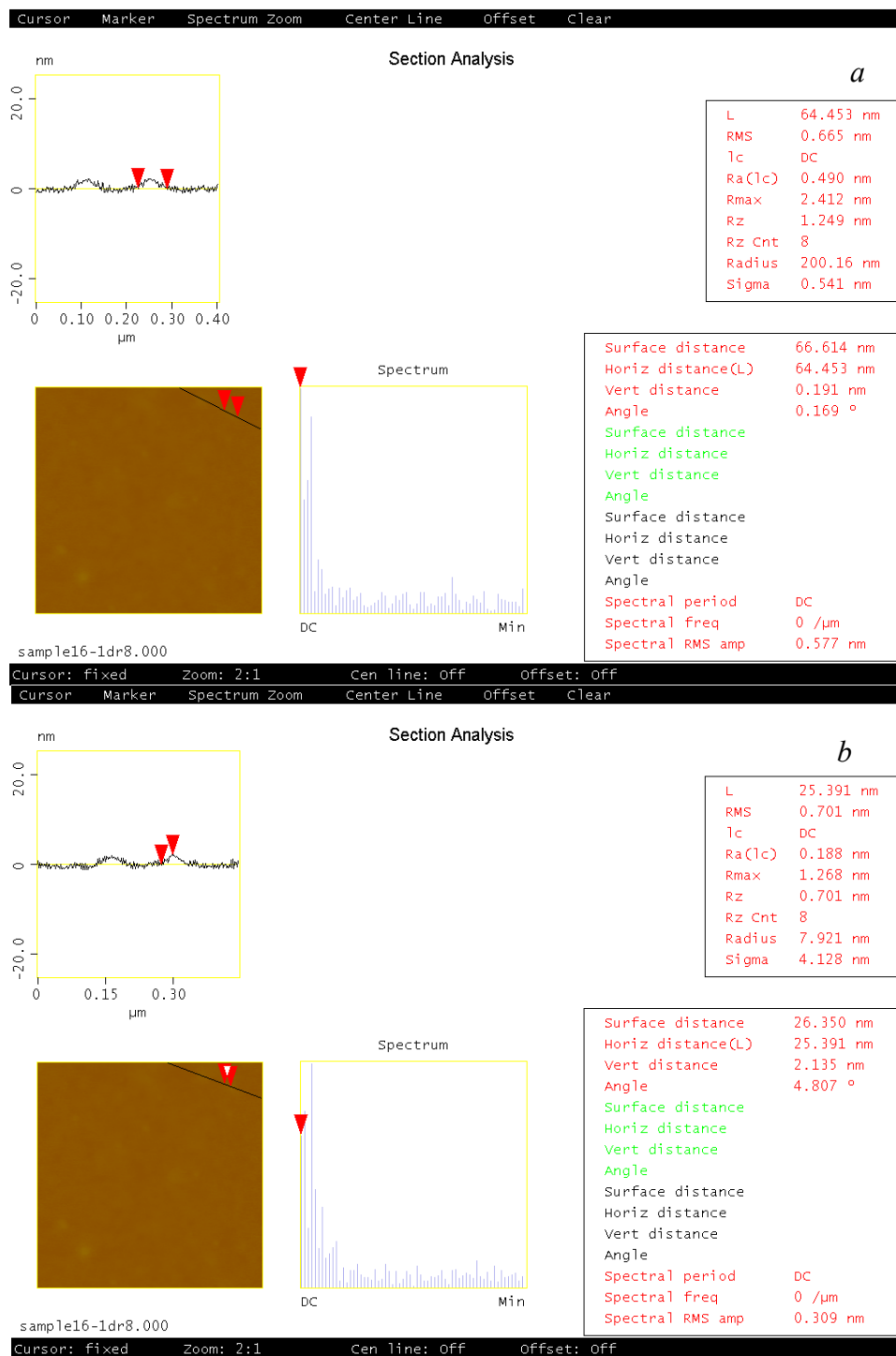


Figure C.9 Horizontal (a) and vertical section analysis (b) of the flake 2.14 (60°C, 2500 psi). The image was constructed at a 1.00 μm scan size, a 1.001 Hz scan rate, 512 numbers per line, and a 50.0 nm data scale.

### D.3 Section analysis of the treated flakes at 60°C and 2000 psi

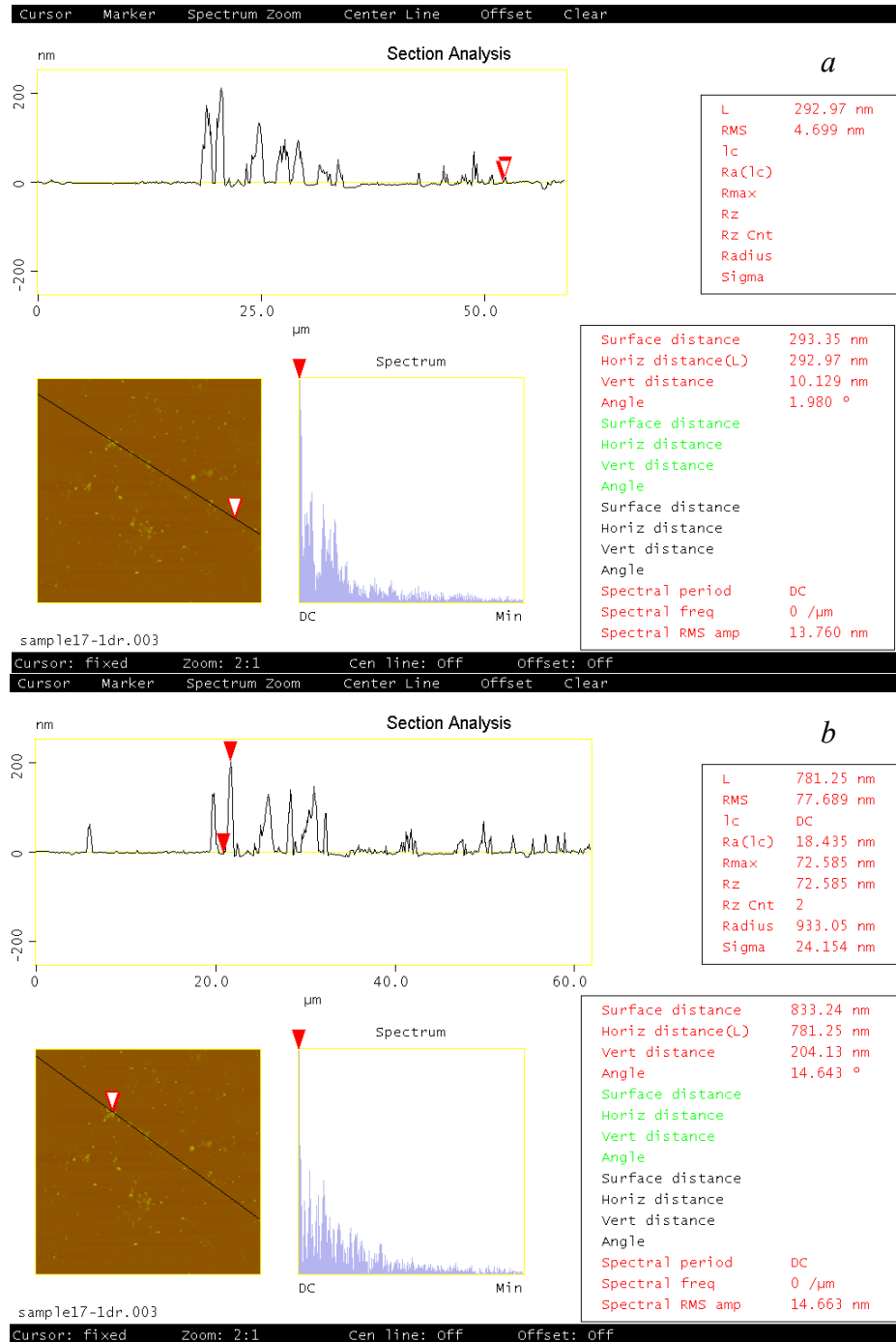


Figure C.10 Vertical section analysis of the flake 3.1 (a) and 3.2 (b) (60°C, 2000 psi). The image was constructed at a 50.00 μm scan size, a 0.1001 Hz scan rate, 512 numbers per line, and a 500.0 nm data scale.

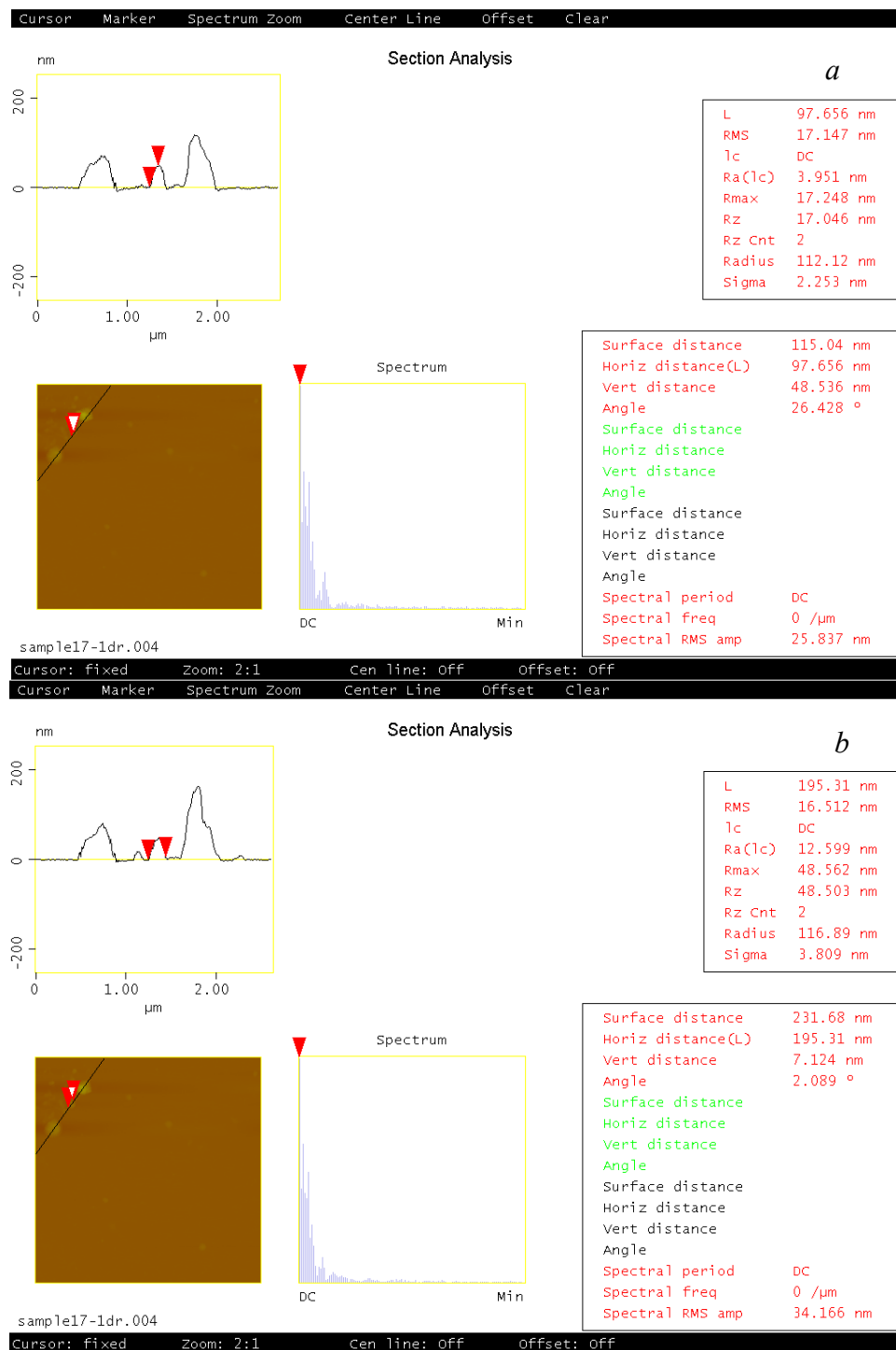


Figure C.11 Horizontal (a) and vertical section analysis (b) of the flake 3.3 (60°C, 2000 psi). The image was constructed at a 5.00 μm scan size, a 1.001 Hz scan rate, 512 numbers per line, and a 500.0 nm data scale.

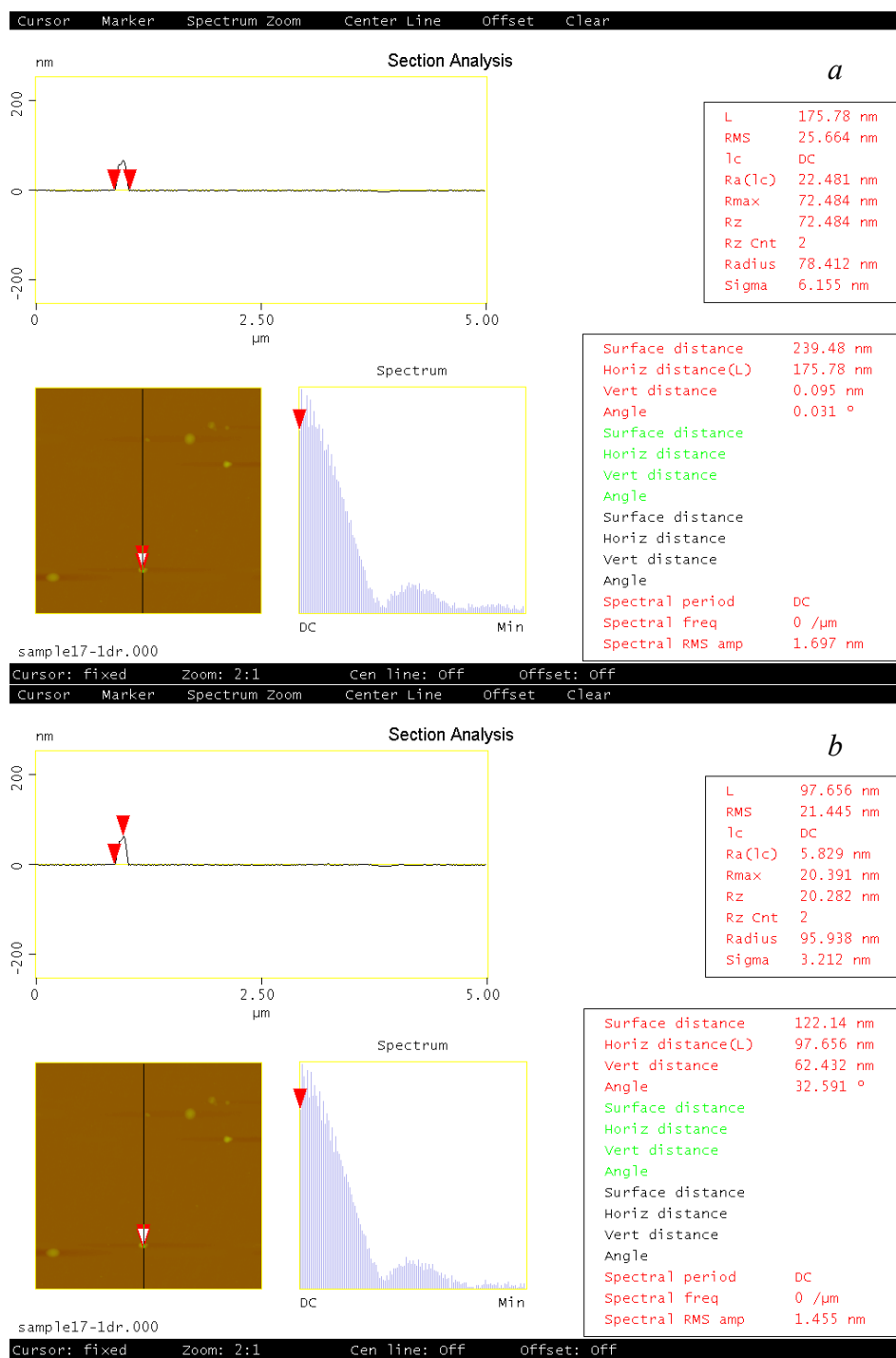


Figure C.12 Horizontal (a) and vertical section analysis (b) of the flake 3.8 (60°C, 2000 psi). The image was constructed at a 5.00  $\mu\text{m}$  scan size, a 1.387 Hz scan rate, 512 numbers per line, and a 500.0 nm data scale.

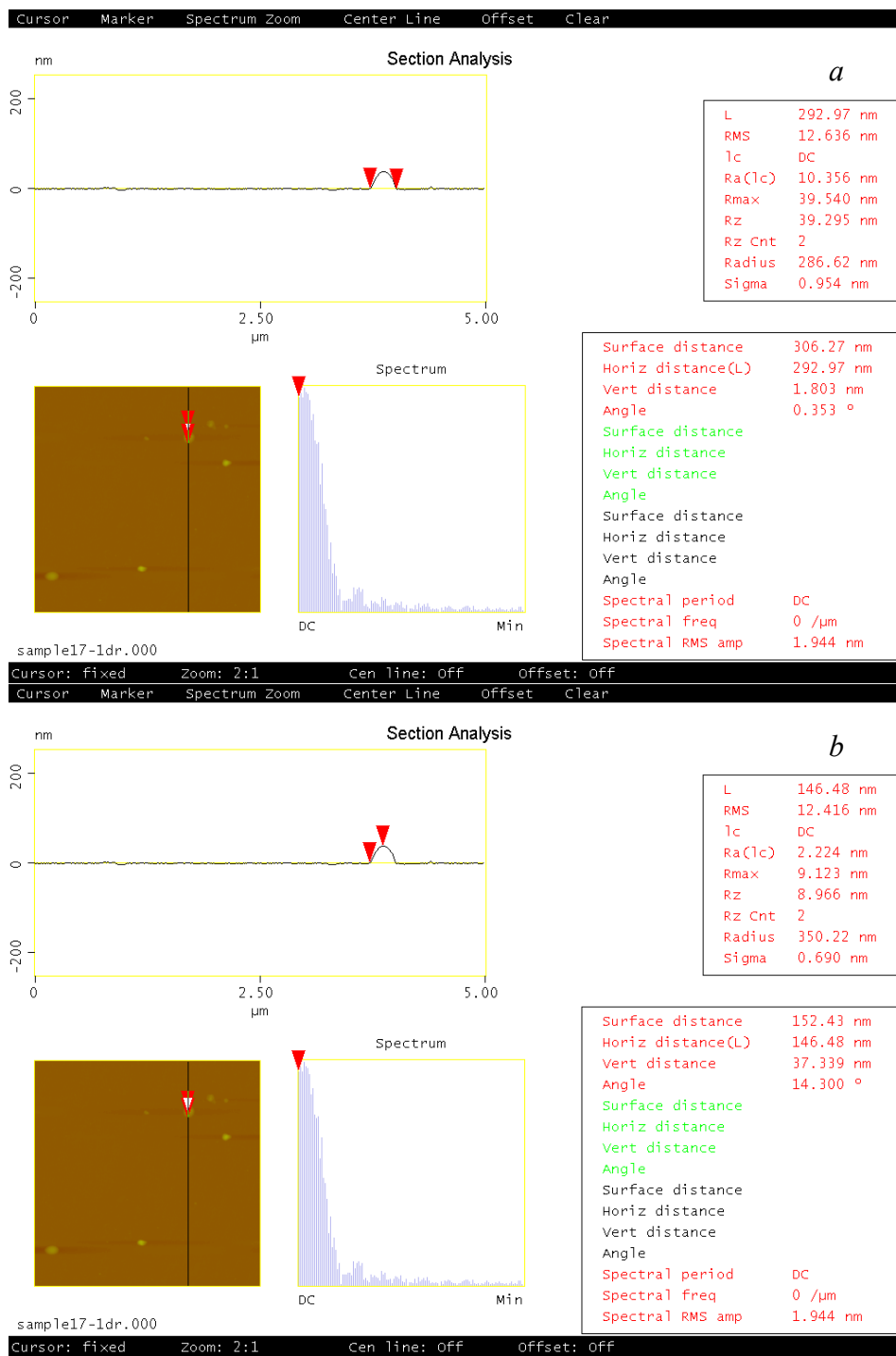


Figure C.13 Horizontal (a) and vertical section analysis (b) of the flake 3.9 (60°C, 2000 psi). The image was constructed at a 5.00  $\mu\text{m}$  scan size, a 1.387 Hz scan rate, 512 numbers per line, and a 500.0 nm data scale.

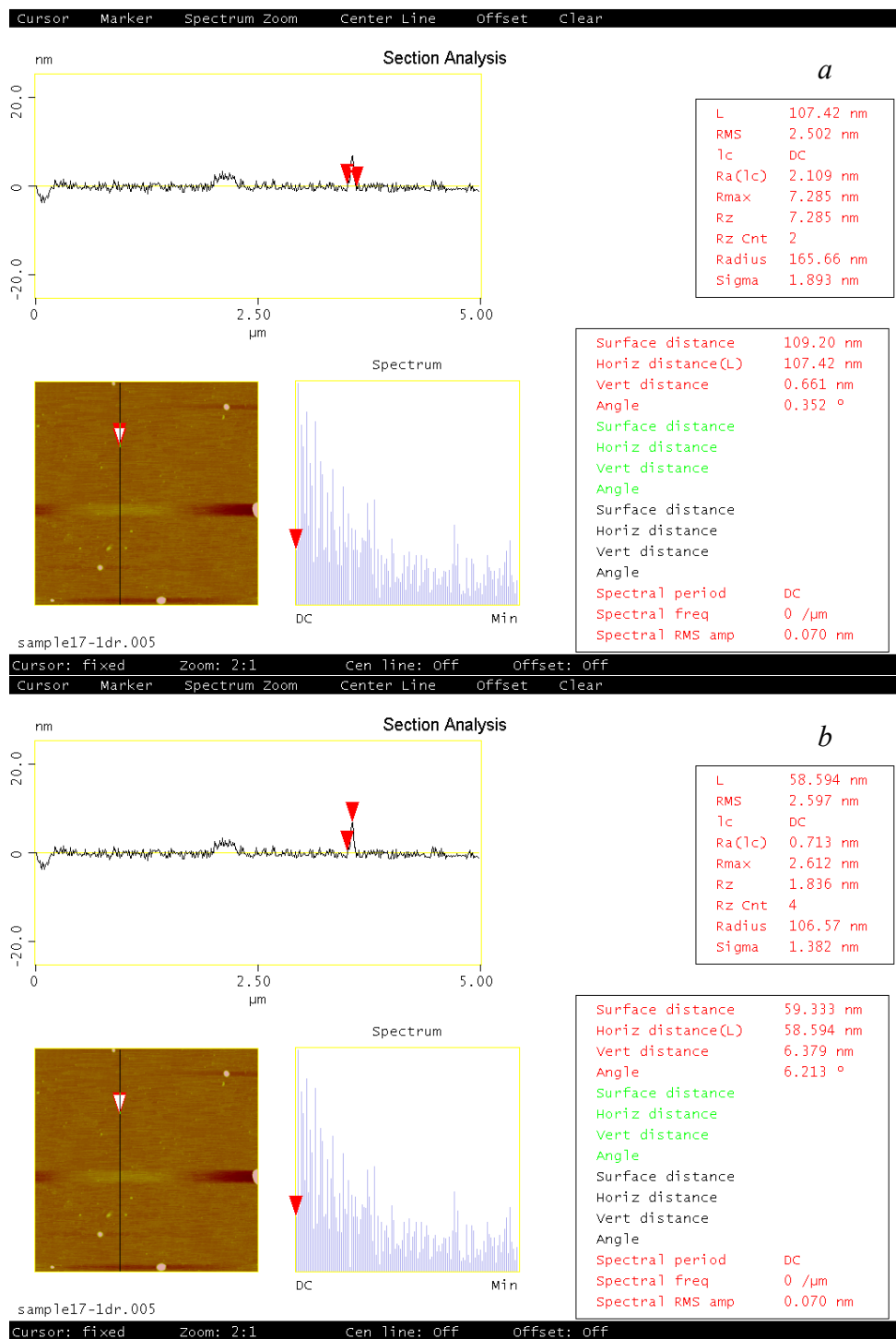


Figure C.14 Horizontal (a) and vertical section analysis (b) of the flake 3.11 (60°C, 2000 psi). The image was constructed at a 5.00  $\mu\text{m}$  scan size, a 1.001 Hz scan rate, 512 numbers per line, and a 50.0 nm data scale.



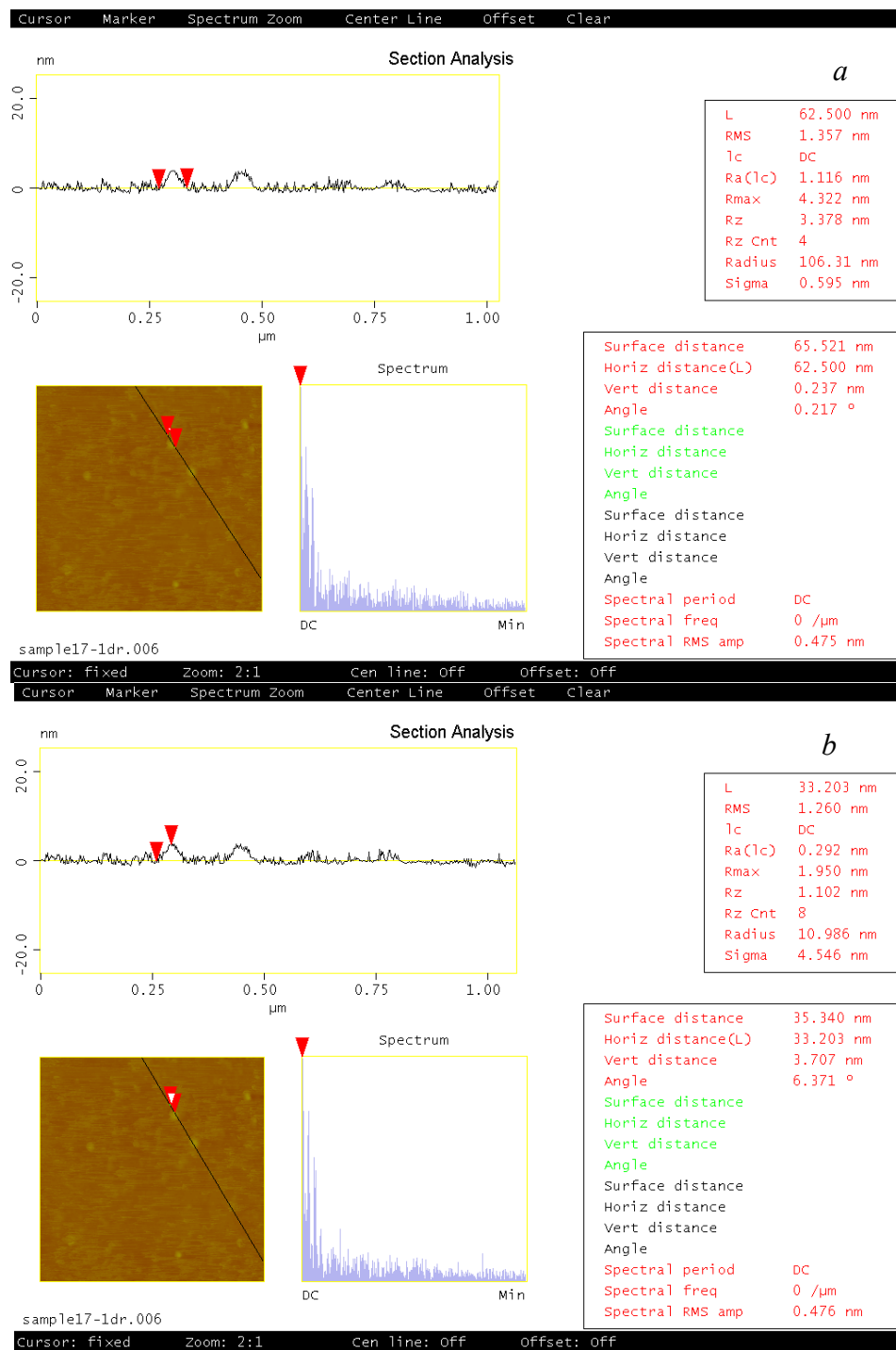


Figure C.15 Horizontal (a) and vertical section analysis (b) of the flake 3.12 of Figure 4.55 (60°C, 2000 psi). The image was constructed at a 1.00 μm scan size, a 1.001 Hz scan rate, 512 numbers per line, and a 50.0 nm data scale.